

MODELING AND COMPARISON OF DYNAMICS  
OF AC AND DC COUPLED REMOTE HYBRID  
POWER SYSTEMS

TANJILA HAQUE







**Modeling and Comparison of Dynamics of AC and DC Coupled Remote  
Hybrid Power Systems**

by

© Tanjila Haque

A thesis submitted to the

School of Graduate Studies

in partial fulfillment of the requirements for the degree of

Master of Engineering

Faculty of Engineering and Applied Science

Memorial University of Newfoundland

**October 2011**

St. John's

Newfoundland

**To**

**Omit Mehfuz and Zarif Ahanaf Ovro**

## ABSTRACT

In this research two different types of remote hybrid power systems are designed using solar, wind and diesel power sources. In both designs load and renewable resources data of an isolated site in St.John's, Newfoundland Canada is considered. The sizing and steady-state performance of the systems are analyzed by the HOMER software tool. While maintaining the same renewable fraction a comparison is made between an AC coupled and a DC coupled hybrid power systems. In first case a 100% AC load is considered. Most of the load in North America is heating type of load, so for the second case a 70% DC and a 30 % AC load is considered. Detailed comparison indicates that the DC coupled hybrid system is better than the AC Coupled hybrid system. Comparison is made based on diesel saving, component required, system cost and environmental impact. The dynamic and transient analysis of two hybrid systems are analyzed by using the Matlab/Simulink software tool. Each component is individually simulated in Simulink, and then the models are combined to form a system.

## ACKNOWLEDGEMENTS

Firstly I want to gratefully remember the Almighty for being accorded all the encouragement, patience and optimism throughout the research.

This work has been carried out at the Faculty of Engineering and Applied Science at Memorial University of Newfoundland, Canada. It has been funded by National Science and Engineering Research Council (NSERC), Wind Energy strategic Network (WESNet), and School of Graduate Studies (SGS) of Memorial University. I am obliged to express my gratitude to those organizations providing me financial support during my course program.

I would earnestly like to show my gratitude to my supervisor, Dr. Tariq Iqbal for his supervision, advice and guidance from the very early stage of this research. Above all and the most needed, he provided me unflinching encouragement and support in various ways. His positive attitude and scientific reviewing made me more confident to carry out my research successfully. I am really grateful and admirable to him.

I would like also to thank all the fellow members of the Centre for Instrumentation, Control and Automation (INCA), at Memorial University for providing a good working environment. I also want to thank Razzaqul Ahasan for his constructive comments on this thesis. Furthermore, the administrative cooperation from Moya Crocker is highly acknowledged.

I am also grateful to my father Md. Shamsul Haque Khan and my mother Maksuda Begum, who sincerely raised me with their caring and gently loves, deserve special

mention for their inseparable support and prayers. Also thanks to my all brothers and sisters for their encouragements. I am extraordinary fortunate in having such a nice mother-in-law Ismat Ara Mostafa who is beside me with encouragement, support and love. I am also blessed to have a nice, cute, and lovely son Zarif Ahanaf.

At last, but not the least, I would like to express my thanks to my understanding beloved husband Omit Mehruz who is not only a good husband but also a best friend of mine. His supports, sacrifices, and encouragements can't be expressed by few words. He was always with me to give me inspiration. Without his mental support this research would not be done properly.

I would like to express my apology that I could not mention everybody one by one who was important to the successful realization of thesis.

## Table of Contents

<b>Abstract</b>	iii
<b>Acknowledgement</b>	iv
<b>Table of Contents</b>	vi
<b>List of Tables</b>	xi
<b>List of Figures</b>	xiii
<b>List of Abbreviations</b>	xx
<b>List of Symbols</b>	xxiii
<b>List of appendix</b>	xxvii
<b>Chapter 1 Introduction</b>	1
1.1 Background	1
1.2 Hybrid Power System	2
1.2.1 DC Coupled Hybrid System	4
1.2.2 AC Coupled Hybrid System	6
1.3 Related Works	7
1.3.1 DC Distribution System	7
1.3.2 Optimization methods of Hybrid Power System	9
1.3.3 Operation and performance of hybrid Power System	12
1.3.4 Wind Energy Conversion System With Different Generators	16
1.4 Motivation	18

1.5 Outline of Thesis	20
<b>Chapter 2 Analysis of AC and DC Coupled Hybrid Power system</b>	<b>21</b>
2.1 Introduction	21
2.2 Energy Planning	22
2.3 System Design Inputs	22
2.3.1 Load Profile	22
2.3.2 Photovoltaic System and Pricing	24
2.3.3 Solar Radiation for St. John's	26
2.3.4 Selection of Wind Generator and Pricing	27
2.3.5 Calculation of wind Potential of St. John's	29
2.3.6 Selection of Diesel Generator and Pricing	31
2.3.7 Energy Storage and Pricing	34
2.3.8 Selection of Inverter/Charger and pricing	35
2.4 Hybrid System Design	37
2.4.1 AC bus-based Hybrid System	37
2.4.1.1 Simulation Results	37
2.4.1.2 Electrical production	39
2.4.2 DC bus-based Hybrid System	42
2.4.2.1 Simulation results for DC System	42
2.4.2.2 Electric production	44

2.5 Comparison between PV-Wind-Diesel AC bus-based System and PV Wind-Diesel DC bus-based System	47
2.5.1 The Cost Summary	47
2.5.2 Electrical Factor	50
2.5.3 Emission	52
2.6 Summary	57
<b>Chapter 3 Modeling of Wind Turbine</b>	59
3.1 Wind Energy conversion system	59
3.2 Components of wind Power plant	63
3.2.1 Electrical Generation System	64
3.2.1.1 Squirrel cage induction generator	64
3.2.1.2 Permanent magnet synchronous generator	68
3.2.2 Transformer	71
3.2.3 Capacitor Bank	75
3.3 Power Extraction From the wind	76
3.4 Modeling and Simulation of FD-13-50 wind Turbine for AC Coupled Hybrid System	78
3.5 Summary	87
<b>Chapter 4 Modeling of Photovoltaic System, Battery and Diesel Generator</b>	89
4.1 Photovoltaic Modules	89
4.1.1 Introduction	89

4.1.2 Photovoltaic Cell	90
4.1.3 Modeling a PV Cell	91
4.1.3.1 The Simplest Model	91
4.1.3.2 Two Diode Solar Cell Model	95
4.1.4 Photovoltaic Module	97
4.1.5 Modeling a PV Module by MATLAB	98
4.1.6 Maximum Power Point Tracker	102
4.1.7 DC-DC Converter	107
4.1.7.1 Boost Converter Analysis	107
4.2 Battery Bank	110
4.3 Diesel Engine	114
4.3.1 Speed Control of Diesel Engine	115
4.3.1.1 Modeling of Diesel Engines	115
4.3.2 Diesel Generators	116
4.3.2.1 Modeling of Diesel Generator	116
4.4 Summary	122
<b>Chapter 5 Simulation and Results of the Hybrid Power System</b>	123
5.1 Simulation for AC coupled Hybrid Power System	123
5.1.1 Case Study 1: Simulation of AC system with the fixed wind speed and variable load	125

5.1.2 Case Study II: Simulation of AC system with Fixed Load	128
Variable Wind Speed	
5.1.3 Case Study III: Simulation of AC system with diesel generators	134
and Photovoltaic system in operation	
5.2 DC coupled system simulation and its results	138
5.2.1 Case Study I: Simulation of DC system with the fixed wind	140
speed and variable load	
5.2.2 Case Study II: Simulation of DC system with Fixed Load	142
Variable Wind Speed	
5.2.3 Case Study III: Simulation of DC system with diesel generators	145
and Photovoltaic system in operation	
5.3 Summary	147
<b>Chapter 6 Conclusions and Recommendations</b>	151
6.1 Summary of Research	151
6.2 Future Work	154
<b>Publications</b>	156
<b>References</b>	158
<b>Appendix A MATLAB/SIMULINK Subsystem Blocks</b>	166

## List of Tables

Table 2.1	Monthly Average Solar Data from HOMER simulation	27
Table 2.2	Monthly Average Wind Speed of St. John's	30
Table 2.3	Optimization results for AC bus-based System	38
Table 2.4	Optimization results for DC bus-based System	43
Table 2.5	Total Cost of AC System	49
Table 2.6	Total Cost of DC System	49
Table 2.7	Energy Production of DC System	51
Table 2.8	Energy Production of AC System	51
Table 2.9	Excess Energy of AC System	52
Table 2.10	Excess Energy of DC System	52
Table 2.11	Emissions in AC Systems	53
Table 2.12	Emissions in DC Systems	53
Table 2.13	Comparison based on Component Required for 100% AC load	53
Table 2.14	Comparison based on Component Required for 30% AC load and 70% DC load	54
Table 2.15	Comparison based on cost for 100% AC load	54
Table 2.16	Comparison based on cost for 30% AC and 70% DC load	55
Table 2.17	Comparison based on Diesel Use and corresponding emission for 100% AC load	55

Table 2.18	Comparison based on Diesel Use and corresponding emission for 30% AC and 70% DC load	56
Table 2.19	Comparison Based On Renewable Fraction for 100 % AC load	57
Table 2.20	Comparison Based On Renewable Fraction for 30 % AC and 70 % DC load	57
Table 3.1	Specification of 50 kW Wind Turbine	81
Table 3.2	Parameters of 50 kW WECS Used for Simulation	82
Table 4.1	Specification of solar panel	99
Table 4.2	Specification of battery	114
Table 4.3	Diesel generator system parameters for 150 kW generator.	120
Table 4.4	Diesel generator system parameters for 75 kW generator.	120
Table 4.5	Diesel Engine System Parameters	121
Table 4.6	Diesel Excitation System Parameters	121
Table 5.1	Summary of Three Case Studies.	148

## List of Figures

Figure 1.1	Hybrid Power System	3
Figure 1.2	DC Coupled Hybrid Power System	5
Figure 1.3	Centralized AC Coupled Hybrid Power System	6
Figure 2.1	HOMER software tool plot of monthly load variations	23
Figure 2.2	HOMER software tool formed daily load profile	24
Figure 2.3	HOMER software tool formed Cost curve of Solar Panel	25
Figure 2.4	HOMER software tool formed Monthly Solar Radiation	26
Figure 2.5	Power Curve of Wind Turbine	28
Figure 2.6	Cost Curve of Wind Turbine from HOMER	29
Figure 2.7	Wind resource of St. John's Plotted in HOMER	30
Figure 2.8	Efficiency Curve of 75 kW diesel Generator and 150 kW diesel Generator	32
Figure 2.9	Fuel Consumption Curve of 75 kW diesel Generator and 150 kW diesel Generator	33
Figure 2.10	Cost Curve of 75 kW diesel Generator and 150 kW diesel Generator	33
Figure 2.11	Cost curve of Surrette 12-Cs-11-Ps 12 volts battery	34
Figure 2.12	(a) Capacity curve (b) Lifetime curve of Surrette 12-Cs-11-Ps 12 volt battery	35
Figure 2.13	Cost curve of Solectria PVI60kW-480V, 60kW Inverter 480 V AC	36

Figure 2.14	AC bus-based Electrical System	37
Figure 2.15	Monthly Average Electric Production for AC bus-based System	39
Figure 2.16	PV Array Power Output	40
Figure 2.17	Wind Turbine Power Output	40
Figure 2.18	75 kW Diesel Generator Output	41
Figure 2.19	150 kW Diesel Generator Output	41
Figure 2.20	DC bus-based Hybrid System	42
Figure 2.21	Monthly Average Electric Production for DC bus-based System	44
Figure 2.22	PV Array Power Output	45
Figure 2.23	Wind Turbine Power Output	45
Figure 2.24	75 kW Diesel Generator Output	46
Figure 2.25	150 kW Diesel Generator Output	46
Figure 2.26	Cash Flow Summary of PV-wind-diesel AC System	47
Figure 2.27	Cash Flow Summary of PV-wind-diesel DC System	48
Figure 2.28	Average Energy Production of AC System	50
Figure 2.29	Average Energy Production of DC System	50
Figure 3.1	World Electricity Generation in 1999	60
Figure 3.2	Average annual growth rate from 2001 to 2010 of the world installed capacity of wind power	60
Figure 3.3	Wind Energy conversion system	61
Figure 3.4	Components of wind Turbine	62

Figure 3.5	Asynchronous generator representations in d-q axis frame	68
Figure 3.6	Change of line inductance with rotor positions	70
Figure 3.7	Ideal Transformer	72
Figure 3.8	A Two winding Transformer	73
Figure 3.9	Equivalent Circuit referred to primary	74
Figure 3.10	Equivalent Circuit referred to secondary	74
Figure 3.11	The 50kW wind generator and control using PMG	79
Figure 3.12	The 50kW wind generator and control using Synchronous generator in Simulink	80
Figure 3.13	Power generated by the 50kW generator at different wind speeds	84
Figure 3.14	Generator speed in per unit value	87
Figure 3.15	Power versus Wind Speed Curve of 50kW Wind Turbine	88
Figure 4.1.1	Illustration of the p-n junction of PV cell	91
Figure 4.1.2	PV cell with a load and its simple equivalent circuit	92
Figure 4.1.3	Diagrams showing a short-circuit and an open-circuit condition	93
Figure 4.1.4	I-V plot of ideal PV cell under five different levels of irradiance	95
Figure 4.1.5	More accurate equivalent	96
Figure 4.1.6	PV cells are connected in series to make up a PV module	97
Figure 4.1.7	Picture of SG17524 (175W) PV module	98
Figure 4.1.8	Equivalent circuit used in the MATLAB simulations	100
Figure 4.1.9	PV module is directly connected to a (variable) resistive load	103

Figure4.1.10	Solar panel model in Simulink	104
Figure4.1.11	Power generation in solar panel at different solar irradiance.	105
Figure4.1.12	Circuit diagram of boost converter	108
Figure4.1.13	Mode 1-Circuit diagram of boost converter during $T_{on}$	108
Figure4.1.14	Mode 2-Circuit diagram of boost converter during $T_{off}$	108
Figure4.1.15	Waveforms for boost converter operating under CCM	109
Figure 4.2.1	Model of a battery	111
Figure 4.2.2	Discharge characteristics of Lead-Acid battery	111
Figure 4.2.3	Charge characteristics of Li-Ion and lead acid battery	112
Figure 4.3.1	Diesel generator equivalent circuit	117
Figure 4.3.2	Simulink model of Diesel Generator	119
Figure 4.3.3	Engine and excitation system of Diesel generator.	122
Figure 5.1	Overall block diagram of the AC coupled Hybrid System	124
Figure 5.2	Simulink Model for the AC coupled Hybrid System	125
Figure 5.3	Simulation result for fixed wind speed variable load	126
Figure 5.4	Effect of change of load on voltage	127
Figure 5.5	Effect of change of load on frequency	127
Figure 5.6	Simulation results for 300kW load and two step changes in the wind speed	129
Figure 5.7	Effect of two step changes in the wind speed on voltage	130
Figure 5.8	Effect of two step changes in the wind speed on frequency	130

Figure 5.9	Simulation Results for 200kW load and wind speed drop from 7 to 9m/s	131
Figure 5.10	Voltage curve for 200kW load and wind speed drop from 7 to 9m/s	131
Figure 5.11	Frequency curve for 200kW load and wind speed drop from 7 to 9m/s	132
Figure 5.12	Simulation results for fixed load and wind speed 14ms to 15 m/s variation.	133
Figure 5.13	Voltage curve for fixed load and wind speed 14ms to 15 m/s variation.	133
Figure 5.14	Frequency curve for fixed load and wind speed 14ms to 15 m/s variation.	134
Figure 5.15	Simulation results for 200kW load with zero wind speed	135
Figure 5.16	Voltage at 200kW load with zero wind speed	135
Figure 5.17	Frequency at 200kW load with zero wind speed	136
Figure 5.18	Simulation results for Variable load with Zero wind speed	137
Figure 5.19	Voltage at Variable load with Zero wind speed	137
Figure 5.20	Frequency at Variable load with Zero wind speed	138
Figure 5.21	Complete block diagram of DC coupled hybrid system	139
Figure 5.22	Simulink model for DC coupled hybrid system	140
Figure 5.23	Simulation result for fixed wind speed variable load	141
Figure 5.24	Simulation results of DC system for 300kW load and two step	142

	changes in the wind speed	
Figure 5.25	Simulation Results of DC coupled system for 200kW load and wind speed drop from 7 to 9m/s	143
Figure 5.26	Simulation Results of DC coupled system for 350kW load and wind speed drop from 14 to 15m/s	144
Figure 5.27	Simulation results of DC based system for 200kW load with zero wind speed	145
Figure 5.28	Simulation results of DC based system for Variable load with Zero wind speed	146
Figure A-1	Subsystem of Wind Turbine	166
Figure A-2	Subsystem Model of PMG based WECS for AC System	167
Figure A-3	Subsystem of induction generator based WECS.	167
Figure A-4	Subsystem model of PMG based WECS	168
Figure A-5	Subsystem model of Solar cell.	169
Figure A-6	Subsystem model of PV system.	170
Figure A-7	Simulink Model of Excitation System	170
Figure A-8	Simulink Model of Governor and Diesel Engine	171
Figure A-9	Diesel generator Subsystem model for DC system.	171
Figure A-10	Battery Subsystem Model.	172

## **List of Abbreviations**

APU

Auxiliary Power Unit

CanWEA	Canadian Wind Energy Association
CCM	Continuous Conduction Mode
CCT	Critical Clearing Time
COE	Cost of Energy
C-Pt	Carbon-Platinum Catalyst
CSPM	Constant Speed Prime Mover
DDPMSG	Direct Drive Permanent Magnet Synchronous Generator
DSP	Digital Signal Processing
DVR	Dynamic Voltage Regulator
ECS	Energy Conversion System
EMTDC	Electromagnetic Transients including <b>DC</b>
FC	Fuel cell
FLC	Fuzzy Logic Controller
FRM	Fuzzy Regression Model
GHG	Green House Gas
HRI	Hydrogen Research Institute
KCL	Kirchoff's Current Law
KOH	Potassium Hydroxide
MOEA	Multi objective evolutionary algorithm
MPPT	Maximum Power Point Tracker

NiO	Nickel Oxide
NLH	Newfoundland and Labrador Hydro
NN	Neural-Net
NPC <sup>1</sup>	Neutral point Clamped
NPC <sup>2</sup>	Net Present Cost
NRCan	Natural Resources Canada
P&O	Perturbation and Observation
PEMFC	Proton Exchange Membrane Fuel Cell
PMSG	Permanent Magnet Synchronous Generator
PSCAD	<b>Power Systems Computer Aided Design</b>
PV	Photovoltaic
PWM	Pulse Width Modulation
RES	Renewable Energy System
SCIG	Squirrel Cage Induction Generator
SOC	State of Charge
TCR	Thyristor Controlled Reactor
THD	Total Harmonic Distortion
TSC	Thyristor Switched Capacitor
UC	Ultra Capacitor
UPFC	Unified Power Flow Control
VSPM	Variable Speed Prime Mover

WDICS	Wind Diesel Integrated Control System
WECS	Wind Energy Conversion System
WT	Wind Turbine

## List of Symbols

### *Wind Energy Conversion Systems*

Symbols	Parameters	Units
$\lambda$	Flux induced by the permanent magnets of the rotor	V-s
$\varphi_{ds}, \varphi_{qs}$	Stator d and q axis fluxes	Wb
$\varphi'_{dr}, \varphi'_{qr}$	Rotor d and q axis fluxes	Wb
$\omega_m$	Rotor angular velocity	rad/s
$\omega_r$	Electrical angular velocity	rad/s
$\theta_m$	Rotor angular position	rad
$\theta_r$	Electrical rotor angular position	rad
$E_b$	Induced back EMF	V
$f$	Frequency	Hz
$F$	Combined rotor and viscous friction coefficient	N.m.s
$H$	Combined rotor and load inertia constant	s
$I_l$	Stator current	A
$i_{ds}, i'_{dr}$	d-axis stator and rotor currents	A
$i_{qs}, i'_{qr}$	q-axis stator and rotor currents	A
$I_g, I_d$	Generator current and dc link current	A
$J$	Combined rotor and load inertia coefficient	kg.m <sup>2</sup>
$L_{ab}$	Line-line inductance	H
$L_{ls}, L'_{lr}$	Stator and rotor leakage inductances	H

$L_m$	Magnetizing inductance	H
$L_s, L'_r$	Total stator and rotor inductance	H
$L_d, L_q$	D and q axis inductances	H
$n_s$	Field rotation in the air-gap	rad/s
$p$	Number of pole pair	-
$R_s, R'_r$	Stator and rotor resistances	$\Omega$
$T_e$	Electromagnetic torque	N.m
$T_m$	Shaft mechanical torque	N.m
$V_1$	Stator terminal voltage	V
$V_{ds}, V'_{dr}$	d-axis stator and rotor voltages	V
$V_{qs}, V'_{qr}$	q-axis stator and rotor voltages	V
$V_g, V_d$	Generator terminal voltage and dc link voltage	V
$X_{ls}$	Stator reactance	$\Omega$

### Wind Turbines

<b>Symbols</b>	<b>Parameters</b>	<b>Units</b>
$\beta$	Pitch angle	Deg.
$\lambda$	Tip speed ratio	-
$\omega$	Turbine rotational speed	rad/s
$\rho$	Air density	kg/m <sup>3</sup>
$A$	Turbine swept area	m <sup>2</sup>

$c_1-c_6$	Turbine coefficients	-
$C_p$	Performance coefficient of the turbine	-
$C_q$	Torque coefficient of the turbine	-
$P_t$	Mechanical power generated by the turbine	W
$R$	Radius of the turbine	m
$T_t$	Turbine torque	N.m
$v_w$	Wind speed	m/s

#### Transformer

<b>Symbols</b>	<b>Parameters</b>	<b>Units</b>
A	Turns ratio	-
$I_{1tr}, I_{2tr}$	Primary and Secondary side currents	A
$N_1, N_2$	No. of turns of primary and secondary side coils	-
$R_{1tr}, R_{2tr}$	Primary and secondary side resistances	$\Omega$
$X_{1tr}, X_{2tr}$	Primary and Secondary side reactances	$\Omega$

#### Photovoltaic

<b>Symbols</b>	<b>Parameters</b>	<b>Units</b>
D	Duty Cycle	-
G	Solar irradiance	(W/m <sup>2</sup> )
$I_d$	Diode current	A

$I_{mp}$	Current at $P_{max}$	A
$I_o$	reverse saturation current of diode	A
$I_{sc}$	short-circuit current	A
$k$	Boltzmann's constant	J/K
$P_{max}$	Maximum power	W
$q$	electron charge	C
$R_p$	parallel resistor	$\Omega$
$R_s$	Series resistor	$\Omega$
$T$	junction temperature	<i>Kelvin</i>
$V_d$	voltage across the diode	V
$V_{mp}$	Voltage at $P_{max}$	V
$V_{oc}$	open circuit voltage	V

#### Battery

<b>Symbols</b>	<b>Parameters</b>	<b>Units</b>
$E_0$	Constant voltage	V
$i$	Battery current	A
$it$	Extracted capacity	Ah
$i^*$	Low frequency current dynamics	A
$K$	Polarization constant	Ah <sup>-1</sup>
$Q$	Maximum battery capacity	Ah

## List of Appendix

Appendix A

MATLAB/Simulink sub-system blocks

# Chapter 1

## Introduction

### 1.1 Background

As the world population grows, energy consumption is increasing. One of the major challenges for the world's future is linked to the continuous supply of energy. Global energy demand is continuously increasing. Billions of people who live in rural and remote places or small islands around the world do not have access to an electricity grid. It is not economical to connect to the national grid, especially in the developing countries [1]. To supply electricity to the people of remote areas, stand-alone power systems are used. A stand-alone system becomes economical at some point depending upon the size of load and the distance to the national grid [2]. A stand-alone system can have lower investment costs due to the reduced infrastructure requirements.

The majority of stand-alone power systems use diesel generators. There are increasing economic and environmental problems with dependence upon this fossil fuel resource [29]. In addition, the population of the world grows more than the average 2% a year and the need for energy is increasing. The richest 25% of world's population consumes 75% of the world's energy supply [1]. The uses of energy are related to global warming and the use of fossil fuels is not environmentally safe. It causes many environmental problems such as air pollution by carbon emission. A better solution is to use renewable energy resources and technologies [3]. Using renewable energy may have

a higher cost/kWh but it will be compensated for by the reduction or even the absence of expenditure on fuel.

At any rate, future environmental constraints will require a massive exploitation of solar energy, in all its conventional and new forms, namely: biomass, thermal energy, and photovoltaic energy. The expansion process of renewable electricity is deemed to have an important and growing share of power markets, starting from the present situation of remote village electrification, roof-top applications and grid-tied supporting and peaking systems until reaching the bulk power market. Renewable electricity is judged to be a real energy option, capable of supplying a significant contribution to the energy balance and, as a consequence, of mitigating the environmental crisis. However it is not possible to use only renewable energy to produce electricity. Solar energy, wind energy, hydro energy etc. are mainly used as renewable energy; but the wind, sun and tide etc. cannot produce the same amount of energy for the whole year. Because the use of this renewable energy will not give continuous power, the use of a hybrid power system gives the best performance.

## **1.2 Hybrid Power System**

A hybrid energy system usually consists of two or more energy sources combined to provide increased system efficiency as well as greater balance in the energy supply. A hybrid system may be a combination of renewable sources and non-renewable sources. Many hybrid systems are stand-alone systems, which operate off-grid, not connected to an electricity distribution system. For the times when neither the wind nor the solar system are producing, most hybrid systems provide power through batteries and/or an

engine generator powered by conventional fuels, such as diesel. If the batteries run low, the engine generator can provide power and recharge the batteries. Figure 1.1 shows an example of a hybrid power system [32]

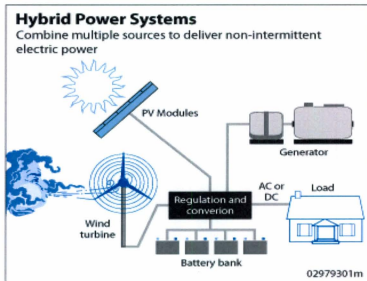


Figure 1.1: Hybrid Power System [32]

Hybrid energy systems often yield greater economic and environmental returns than wind, solar, geothermal or tri-generation stand-alone systems by themselves.

Potential hybrid combinations include generators (e.g. fuel cells that use hydrogen; and natural gas-powered turbines, micro-turbines, and diesel engines) that work in conjunction with renewable energy (e.g. solar concentrators, photovoltaic, wind turbines, or geothermal technologies). The cost and environmental advantages of these advanced power generation technologies can be improved by using "opportunity" fuels, such as bio-generated gases and biomass, to supplement or replace conventional natural gas.

The Center for Energy Efficiency and Renewable Energy (CEERE) of University of Massachusetts Amherst describes hybrid power systems as a way to provide power to the many remote communities in the developing world where the costs for large-scale expansion of electrical grids are prohibitive and the transportation costs of diesel fuel are also very high. The use of renewable power generation systems reduces the use of expensive fuels, allows for the cleaner generation of electrical power and also improves the standard of living for many people in remote areas.

Hybrid energy systems can be used in commercial power parks, industrial plants, renewable energy integrated buildings and remote (off-grid) power sites. Hybrid power systems can also provide electricity to a national grid. The hybrid system reduces fuel consumption, as well as the need for diesel storage [6]. Hybrid systems can be designed to maximize the use of renewables, resulting in a system with lower emissions than those of traditional fossil fuel technologies.

There are various different options for constructing hybrid systems. Mainly two system types are distinguished. They are the DC coupled hybrid power systems and the AC coupled hybrid systems. In the DC coupled hybrid power systems, various power sources and storage is connected on the DC side, while in the AC coupled hybrid systems the connection is on the AC side [32].

### **1.2.1 DC Coupled Hybrid Systems**

Nowadays DC coupled hybrid systems are used mostly for smaller hybrid systems, depending on various external parameters. In these kinds of systems, all the AC energy

sources such as wind generators and genset outputs are rectified to DC and coupled at a battery. Figure 1.2 shows an example of the DC coupled hybrid power system [32].

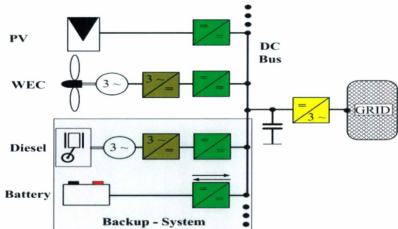


Figure1.2: DC Coupled Hybrid power System [32]

DC consumers are also coupled to the DC side whereas AC consumers are connected through the converters. The power range for DC coupled hybrid systems is extremely broad and can be used cost-effectively for various off-grid applications [33]. The design of the stand-alone system evolves with a growing power demand. If a larger power or energy demand is to be satisfied and cannot be met in a cost-effective manner by PV only, several generators must be implemented in the system. Additional generators are typically wind, hydro or diesel generators. Introducing additional components can thus lower the overall electricity costs but also increase the need for energy management and maintenance skills. Energy management considers the profile of electricity generation from PV or other renewable energy sources, the battery characteristics and the profile of

energy demand of the appliances. To optimize energy and battery management economically, prediction for the fluctuating sources (PV, wind, and hydro) can be helpful [33]. The appliances can either be DC or AC. In the latter case, an inverter is used to provide AC electricity.

### 1.2.2 AC Coupled Hybrid Systems

In general, when systems increase in size they are implemented as an AC coupled hybrid system. AC-coupled hybrid power systems are either centralized or decentralized. An AC-coupled hybrid power system is centralized when all the energy conversion systems (ECSs) constituting it are connected to a main AC-bus before being connected to the grid. An AC-coupled HPS is decentralized when the different ECSs constituting it are not connected to a main AC-bus; otherwise, some or all of them are individually connected to the grid. Figure 1.3 shows an example of a centralized AC coupled hybrid power system [32].

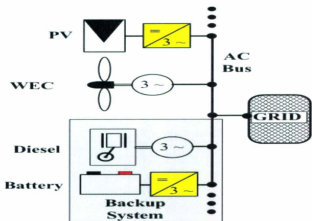


Figure 1.3: Centralized AC coupled hybrid power system. [32]

### **1.3 Related Works**

Before designing an AC coupled hybrid power system and a DC coupled hybrid couple system, several works are reviewed. According to past research work, in the last few years the advantages and disadvantages of the individual network have been worked out and compared very carefully. The complete literature review has been split into several parts. Recent research works related to AC based systems, DC based systems, optimization methods of hybrid power systems, certain control mechanisms, and wind energy conversion systems have been reviewed carefully in this section. Some of the related recent research works will be highlighted next.

#### **1.3.1 DC Distribution System**

In [3,4] it is said the DC coupled distributed system has more advantages such as providing a high power quality, the least expensive extendibility and maintainability over an AC coupled distributed system. In [3] a low voltage DC isolated network is proposed as an alternative to an AC network. The network is fed with distributed generation from renewable sources and cogeneration units. To keep the voltage within a defined range and to ensure the required power flow, the sources are connected to the network via DC/DC converters. The program PSCAD/EMTDC which includes the basic component of power electronics was used to carry out the digital simulation. The simulation analysis shows that it is possible to operate a DC network with standard elements used for the generation side as well as for the consumption side. According to this paper [3] control of a DC network is much easier, and isolated DC networks with distributed generation from a

renewable source could be one of the promising alternatives for the electrification of a developing country. The presented comparison concludes that the DC voltage has several technical and economic advantages over AC voltage but the authors [3] made the comparison for a few aspects, not overall.

In [5], a DC isolated network which is fed by PV unit, to supply unbalanced AC loads is demonstrated. Here the battery and the PV units are connected to the DC network via DC/DC converter. The battery is used to control the network voltage and optimize the operation of the PV generation units, and the PV units ensure the required power flow. The unbalanced AC loads are connected to the DC network via its own DC/AC converter. The simulation results using PSCAD/EMTDC software in this paper [5] show that a DC network with distributed generation is very realistic, and can supply the unbalanced AC load with balanced voltages. Finally, it can be said that the isolated DC network with distributed generation from renewable sources could be one of the most promising alternatives for supplying stand-alone loads.

In order to increase the penetration of renewable energy into a stand-alone power system a DC interconnection has been developed, with the load and generators connected through power electronic converters [12]. The main aim of this project was to implement and demonstrate such a renewable energy based power system, supplying a domestic dwelling. The equipment installed at West Beacon farm was connected through power electronic converters to a DC bus bar and loads supplied from this through a power electronic inverter. Power electronic converters separate the voltage and frequency requirements of the devices and give a reasonable power quality to the load.

### 1.3.2 Optimization Methods of the Hybrid Power System

For power generation in an optimal sustainable island scheme, it is possible to ensure the use of 100% renewable energy resources [6]. It is a scheme that ensures a self-fulfilling energy system based on indigenous renewable resources. This paper presents a plan for a renewable-based energy system to fulfill the electric needs of Karpathos Island, Greece, by replacing the existing diesel generator with new wind farms, photovoltaic installations and hydrogen production systems. Here hydrogen production covers storage and transportation needs. HOMER, NREL's "Micro power Optimization model" was considered in planning the energy systems. First they made a plan using 20% renewable energy. After that they developed a 100% renewable layout. In this paper [6] they also calculated the carbon emission and it is found that 20% renewable energy system scheme would shave off 3500t CO<sub>2</sub> compared to present values. The 100% renewable energy system is a diesel-free scheme and evidently produces zero emissions. This design [6] ensures that it is possible to use 100% renewable energy for power production, and the use of 100% renewable energy is environmental friendly due to 0 % carbon emission. A Wind-PV-Fuel Cell based hybrid power system is simulated for optimization in HOMER in [14]. The authors also designed a control scheme of power flow. The results showed that the fractions of power generation from PV array, WT and the FC system were 29.29%, 70.15% and 0.56%. Unmet load and capacity shortage are expected to be as low as possible for a well designed system and the values found from their design were only 254kWh/yr and 368 kWh/yr.

The main problem of the renewable energy source is that it cannot cover the demand completely because of its dependency on weather patterns. Adding a storage component solves this problem significantly [7]. In this paper [7] the optimal sizing of a wind-fuel cell hybrid system is considered. The main aim was to minimize the total cost of the system such that the demand was met. They considered three situations: generation meets the demand, over generation and over demand for the system. The particle Swarm Optimization (PSO) algorithm was used for optimal sizing of the system's components. In simulation they used weekly mean input data. The data are the wind velocity and the demand in every hour in a day. The average of the input data in each hour is calculated during a week. The PSO algorithm is initialized with two random vectors  $X_0$ ,  $X_1$  which are the size of the system. They calculated the objective function in  $X_0$ ,  $X_1$  and chose one of them. In each iteration, the objective function is determined for each particle and is compared with the previous values. Thus, the best position of each particle is evaluated. This method is not dependent on the system costs; it also depends on the performance of the system. That is, if the obtained sizes do not satisfy the constraints, they are not selected as optimum sizes. Optimum sizing and adding storage elements are the important things for designing a hybrid power system [7].

Different methodologies for optimal sizing of the stand-alone system are presented in different papers [9, 10, and 11]. In [9] the authors proposed a methodology which suggests using commercially available devices for their design. This methodology [9] determined the optimal number and type of units for stand-alone photovoltaic/wind-generator systems. It ensures that the 20-year round total system cost is minimized,

subject to the constraint that the load energy requirements are completely covered. Genetic algorithms (GA) are used to implement the cost function minimization and these algorithms have the ability to attain the global optimum with relative computational simplicity. The results [9] that they have obtained from simulation verify that hybrid PV/WG systems feature a lower system cost compared to the cases where either exclusively WG or exclusively PV sources are used. In their proposed optimal sizing methodology [9], first they examined whether a system configuration, comprising a certain number of system devices and installation details, fulfills the load power supply requirements during the year. The authors [9] used the hourly mean values of ambient temperature and wind speed and the consumed power requirements for a one year time period. In the second step authors [9] employed GAs method, which dynamically searches for the system configuration, which, subject to the criterion set in the first step, minimizes the system total cost. For each combination of system device types [9], the optimal sizing procedure is performed computing the corresponding optimal total system cost and devices configuration. After all device type combinations have been optimally sized, the combination with the lowest cost and the corresponding devices mixture are displayed as the overall optimal system configuration. The methodology used here is perfect for optimal sizing of the hybrid power system where either exclusively WG or exclusively PV sources are used.

A multi objective evolutionary algorithm (MOEA) and genetic algorithm (GA) have been used for a triple multi-objective design of isolated hybrid power systems [10]. Using these algorithms [10] the authors simultaneously tried to minimize the total cost of

the installation, pollutant emissions ( $\text{CO}_2$ ), and unmet load [10]. They designed a complex PV-Wind-diesel-hydrogen battery system. One of the most important characteristics of the MOEA algorithm is the concept of Pareto Optimality [11]. As a result of the optimization process, a set of possible solutions is obtained after a searching process, and thus, the objectives involved in the design are evaluated independently. From the obtained solutions, the designer can choose which are more appropriate depending on the values of the objectives considered. This complex PV-Wind-diesel-hydrogen battery system [11] is a good one, considering the total cost throughout the useful life of the installation, pollutant emissions ( $\text{CO}_2$ ), and unmet load.

### **1.3.3 Operation and Performance of Hybrid Power System**

The performance of the hybrid energy storage system was investigated with a model comprising a photovoltaic electric generation system with combined hydrogen and battery storage [13]. In this work a comparison was made between a battery and a hydrogen based storage system. System performance with individual and combined storage technique has also been illustrated. A battery state of charge (SOC) and a neural-net (NN) based control system have been adopted in this research. The control system was programmed to use system resources more efficiently by adjusting the energy store strategy with the variation in power demand and production. It has been proved that combining a battery with hydrogen energy storage in the proposed system using NN control can significantly reduce the storage cost even lower than either a hydrogen only- or battery only storage device.

Available power from PV energy sources is highly dependent on environmental conditions. To overcome this deficiency of the PV technology a new topology PV system with the fuel cell/ultra-capacitor system is integrated [8]. In this system, during adequate insolation, the PV system feeds the electrolyzer to produce hydrogen for future use and transfers energy to the load side. This work is mainly for the hybridization of alternate energy sources with fuel cell (FC) systems using long and short-term storage strategies with appropriate power controllers. Whenever the PV system cannot completely meet the load demands, the FC system provides power to meet the remaining load. If the load demand exceeds the limits of FC capability, the UC bank meets the load demand. Primarily, a dynamic model is proposed for a PV/ FC/ UC hybrid power generation system. The model is developed and used in the Matlab/Simulink/Simpower Systems environment, based on the mathematical and electrical models developed for the proposed system. This design is a better choice as the availability of solar energy is not the same for the whole year.

More research is being executed in wind-diesel hybrid systems due to the high energy conversion efficiency and low installation and operational (\$/kWh) cost. In [15] the authors have worked on the decentralized controllers to reduce the fluctuation of frequency and terminal voltage. In the proposed system a 20 MW diesel generator and a 4 MW WT supply power to a 10 MW load. The authors modeled a centralized controller beside of decentralized controllers and showed that when the communication delay is ignored, both the controllers provide the same stability to the system. However, in another

instance, an 18ms time delay was considered for a centralized controller, resulting in an unstable condition. The voltage exceeded the maximum allowable range (5%) and the frequency also lost its consistency. Since the decentralized controllers had been placed near each facility, there was no time delay for them, and they retained stability.

In [16] a Fuzzy Logic controller based wind-solar-hydrogen-battery based hybrid power system has been proposed. The first objective of the work was the reduction of energy transfer from the short-term storage (battery) to long-term storage (hydrogen) or vice versa, and the second was limiting the use of batteries. The input variables of the FLC are the net power flow and battery state of charge (SOC), and the output variable is the power set point. The FLC is designed in such a way that when the output is positive, the set point is sent to the boost converter causing the fuel cell to start. On the other hand, when the output is negative, the set point is sent to the buck converter to start the electrolyzer. The simulation results [16] described that the FLC was functioning well by switching the electrolyzer and fuel cell appropriately and keeping the SOC of battery more than 50 % all the time.

A small 500 W wind/fuel cell hybrid energy system has been presented in [17]. Dynamic modeling of wind turbine, Proton exchange Membrane Fuel cell (PEMFC) and Electrolyzer have been presented in this paper [17]. The system responses have been analyzed by employing different loads and wind speeds. The Voltage variations found from the simulation results of this 48 V system is high (43 V- 65 V). The transient's duration of the system is between 1 to 5 s and in most of the transient situations system behaves like an over damped system.

Another thought has come out in [18] regarding the generation of the hybrid power system. Besides modeling the WT, FC, UC, electrolyzer and hydrogen tank, a robust and extensive control strategy has been discussed in this research. Wind generator output voltage and frequency are of a fluctuating nature. In order to get the fixed DC voltage, power conditioning is essential. A 12-pulse AC/DC thyristor controlled double bridge rectifier was used with the WT output and a boost DC/DC converter was used with a FC/UC system output. The DC bus voltage was maintained at 400V and the generated power was further fed to the load through 5 kHz IGBT PWM inverters. The simulation results showed that the load demand had been met by the combined system appropriately.

A stand-alone photovoltaic (PV) system with a hybrid energy storage technique is illustrated in [19]. In addition to observing the dynamic behaviours, sizing optimization and cost analysis has also been explained in this work. The proposed system comprises a solar cell, Fuel cell (FC), electrolyzer, hydrogen compressor, storage and battery. Three different combinations of components have been chosen for performing a comprehensive comparison. Of the PV/battery, PV/FC and PV/FC/battery hybrid systems, the last system provides more potential in terms of cost and efficiency.

A comprehensive control scheme for a two generating unit power plant system has been developed in [20]. The PV served as the primary source whereas the FC ran as the secondary source. The control strategy is of key importance in this literature. Depending on the electricity cost, grid capacity, hydrogen storage capacity and desired solar radiation, a two-level control algorithm was proposed. In order to reduce the complexity of the nonlinear model, power conditioning devices have been overlooked. It has been

proved that the outputs followed the reference inputs as expected with two reference power levels.

In [21] a small wind-fuel cell hybrid energy system has been proposed. In this work [21] a dynamic simulation model of each component has been generated by Matlab/Simulink. The simulation results showed how the voltage, current, power and pressure were deviating with the corresponding input change. In order to maintain stability, suitable controllers and a power electronics mechanism have been suggested. Although such a system is feasible, the final cost of this project does not make it economically viable in the majority of situations. It was hoped that, through standardization and mass manufacture, the costs could be greatly reduced.

#### **1.3.4 Wind Energy Conversion System with Different Generators**

A variable speed wind turbine equivalent circuit approach has been modeled in [22]. The authors [22] were dealing with a 1.5 kW BWC permanent magnet synchronous generator based WT, 1kW Stuart Electrolyzer and 1 kW PEM Fuel cell. The average approximated load was 80 W and the wind speed was considered to vary from 10 m/s to 25 m/s. The wind turbine was modeled based on a power coefficient versus tip speed ratio curve and the generator was designed with the help of park transformation. Component currents, hydrogen production and consumption of power generation and demand have been analyzed by simulation results. The amount of unmet load in certain periods was unexpectedly high, though the proposed system configuration was quite simple.

An output power maximization process for a permanent magnet synchronous generator (PMSG) based WT has been illustrated in [23]. The perturbation and Observation (P&O)

technique was used for simulation and a buck-boost converter was suggested to connect between the rectifier and the DC bus. This buck-boost converter ensures that wind energy is captured for a wide range of wind speeds and hence provides the maximum power output.

Research on DC-link voltage control for a Permanent Magnet Synchronous Generator (PMSG) based WT connected to a weak grid system has been performed in [24]. The vector control method was used for generator side converters. The objective was to determine by simulation results how the capacitor voltage was changing with the load variation. The proposed method has been explained with a flow chart. Finally a prototype was built and verified by laboratory experiments.

In [25], the authors presented a horizontal furling control method for small PMSG based WT. For capturing maximum power from the wind, the tip-speed ratio control method and hill climbing control method were examined. Information about the instantaneous wind speed is required for tip-speed ratio control method. But measuring the wind speed accurately is quite tough because wind turbine experiences a different force on their rotor. On the other hand hill-climbing method is based on the measurement of power. They concluded with comparative simulation results using Matlab/Simulink™.

In [26], it has been recognized that during generation of active power, the SCIG based WT cannot produce reactive power for self-excitation and as a result a capacitor bank is necessary between the generator and the load. An alternative approach that has been proposed by the authors is, instead of using a capacitor bank, a PWM inverter can be used, which can provide leading or lagging reactive power, and at the same time can keep

the system stable when the wind speed and load vary. Load current, output voltage, active and reactive powers were compared in no load and loaded conditions by simulation results and laboratory experiments.

In [27], adaptive interfacing and control strategies for three mostly used WT generators (DFIG, PMSG and SCIG) have been proposed. The proposed configuration is resistant to fault condition and it is possible to monitor hundreds of feeder nodes of the distribution systems.

An approach for terminal voltage regulation of a self excited induction generator has been devised in [28]. A feasible prototype using a fixed excitation capacitor, a thyristor, switched capacitor, a thyristor controlled reactor and some controllers have been built and tested in the laboratory, comparing the experimental results with the simulation results. The terminal voltage and frequency have been characterized with the change of excitation capacitance. The authors also were keen to show the change of voltage and thyristor triggering angle with inductive load disparity.

#### **1.4 Motivation**

There are still many communities around the world with no access to an electric grid. To supply power to these people, a stand-alone hybrid power system is used. Rising fuel costs and environmental concerns make the use of renewable energy in standalone systems increasingly attractive. From the above literature review it can be concluded that use of renewable energy is more economical and environmentally safe [6, 7]. In some papers [3,4] they made a comparison between these two systems but this comparison does not satisfy all the factors; that is, they did not broadly describe all the possible factors

based on which the comparison can be made [3, 4]. Power generated from most renewable sources is DC power and also most of the load is a heating type DC load. In general, 70 % of the load is DC type and 30 % is AC type. The previous works that were reviewed in this chapter did not design any system by splitting the load according to use. Most of the load is a DC load, a DC coupled hybrid system can be an option for power generation. However before selecting a DC coupled system as a power system option, it is necessary to perform the steady state and transient analysis and observe power quality. It is also necessary to make a generalized comparison with a conventional AC coupled system. The results from the comparison of these two systems are important for design of a stand-alone hybrid power system. Keeping all of the above mentioned issues in mind the author embarked on the research.

The main objective of this research is to design and compare an off grid DC based hybrid power system with an AC based hybrid power system for a remote community to supply electricity economically. A detailed comparison will be made between these two systems.

The following are some of the main engineering challenges faced here:

1. Choice of an economical and feasible system component to minimize system cost.
2. Collection and study of wind data, solar data and load data.
3. Design of a DC coupled hybrid system and an AC coupled hybrid system.
4. Dynamic modeling and simulation of two hybrid power systems
5. Study transient and dynamic analysis of DC and AC coupled systems, and make a comparison between them.

All of the above discussed challenges are an urgent motivation for this research.

## **1.5 Outline of thesis**

This thesis is comprised of six chapters. The introduction, literature review and motivation of the thesis have been discussed in Chapter 1. In Chapter 2, the author tried to select economic and feasible system components to minimize the system cost. Collection and study of wind data, solar data and load data has been included in this chapter. Chapter 2 also anticipates the electrical performance of an AC and a DC coupled hybrid power system based on HOMER simulations and sensitivity analysis. After that, the steady state models of both AC and DC coupled wind energy conversion systems are generated and determine the generated power corresponding to each wind speed in Chapter 3. Modeling of a photovoltaic system (PV), battery and diesel generator are described in Chapter 4. In this chapter the power generated from the PV corresponding to solar irradiance is also determined. Finally, the WECS, PV, diesel generators, and batteries are combined according to the AC and DC coupled system and their dynamic responses are analyzed in Chapter 5. In Chapter 6, the culminating remarks, the contribution and direction for future experimentations are delineated.

In the reference section, sources of information with the available web links are given.

For easier understanding, the Matlab subsystem models are presented in Appendix A.

## Chapter 2

### Analysis of AC and DC Coupled Hybrid Power System

#### 2.1 Introduction

Hybrid systems are strong and reliable power sources. Nowadays, they are operated cost-effectively worldwide in rural electrification in both developing and industrial countries [35]. Hybrid systems by definition contain a number of power generation devices such as wind turbines, photovoltaic, micro-hydro and/or fossil fuel generators. The use of renewable power generation systems reduces the use of expensive fuels. The electrical output of generators for the exploitation of renewable sources is either direct current (DC), or alternating current (AC) of variable frequency. If the network operates as a DC system, then many of the converters are not needed as the electrical storage elements are of DC type. To supply AC loads by a DC network, an inverter is required. In this study I designed an isolated DC electrical power system and also an isolated AC power system to supply the required amount of AC loads using standard elements (PV system, wind turbine diesel generators, battery). After that a comparison is made between these two systems. The same types of standard elements are used for both systems. We emphasized wind and solar energy systems of St. John's, Newfoundland, Canada.

## **2.2 Energy Planning**

Energy planning is an important issue. This sustainable energy planning scheme considered various scenarios which vary in the level of intervention in the current energy system. The main challenge was to design a DC and AC coupled hybrid power system using renewable sources, keeping in mind any technical limitations in their integration into the system, as well as their economic viability. Homer, NREL's "Micropower Optimization Model" (<http://www.nrel.gov/docs/fy04osti/35406.pdf>) is used for sizing hybrid energy systems. The National Renewable Energy Laboratory (NREL) has developed this software. The model can deal with various types of energy mixtures; from simple conventional or renewable energy power systems to complicated hybrid systems.

## **2.3 System Design Inputs**

This section includes all gathered information required to run the HOMER model; network load, wind and solar resource input, diesel generators and finally, project costs and system constraints.

### **2.3.1 Load Profile**

The load considered in the design is the electrical load of Grey River. It is located on the south-west coast of Newfoundland. It is a small fishing community of about 160-180 residents where power loads peak at 207 kW and the average daily demands reach 2500 kWh. The network load factor is considered as 0.503. The hourly load data was obtained from Newfoundland hydro (<http://www.nlh.nl.ca>).

By analyzing the hourly load data, HOMER software tool formed load curves in daily and monthly profiles. The most representative load profile is shown in Figure. 2.1 depicts the variation in demand on a monthly basis, indicating maximum and minimum recorded loads. The daily load variation is shown in Figure 2.2.

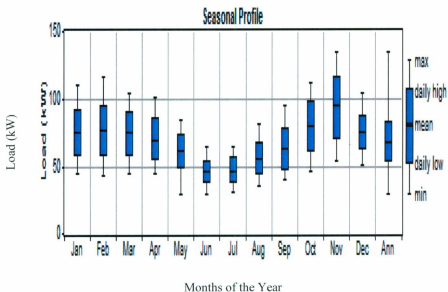


Figure 2.1: HOMER software tool plot of monthly load variations.

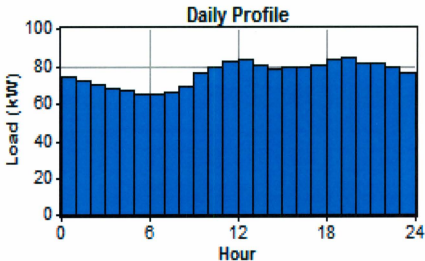


Figure 2.2: HOMER software tool formed daily load profile based on the load data

### 2.3.2 Photovoltaic System and Pricing

The operation of photovoltaic system depends on solar energy. Solar energy has two significant advantages compared to wind applications:

1. Solar energy typically keeps pace with electricity demands; solar stations deliver energy to a grid during medium and high load hours. This allows for the solar output to be directly consumed by the nearby end users. [64]
2. Solar energy resources, for the greatest part of the year, vary distinctly during the day. An island's solar output is more homogenous if photovoltaic packs have been diligently scattered in numerous locations. [64]

Therefore, in order to guarantee system stability in peak load hours, photovoltaic must form a large portion of the system capacity. As cost optimization is one of the most

important factors, it is necessary to select a solar panel with a reasonable cost. We chose to use 175W, 24 V Solar panels (<http://www.solardesigntool.com/components/module-panel-solar/BP/BP4175B/>). The cost for one panel is \$830. As the output of the solar panel is DC voltage, it is connected to the DC bus. As the DC bus voltage is chosen as 648V, the number of panels required per string is 27 and the amount of power delivered by each string is 4.725KW. After analyzing the capital and replacement cost, the HOMER software tool formed the cost curve of the solar panel based on the size of solar panel required. Figure 2.3 shows the cost curve of solar panel.

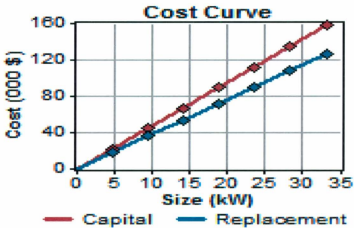


Figure 2.3: HOMER software tool formed the cost curve of a solar panel.

### 2.3.3 Solar Radiation for St. John's

Calculation of solar radiation for a specific location is done by the HOMER software tool. The model calculates theoretical solar radiation, assuming the actual weather conditions, direct and diffused solar radiation values. We imported solar irradiation data from NASA for the latitude of  $47^{\circ}$  on an hourly basis. The annual average value of the solar energy for St. John's is about  $3.15\text{kWh}/\text{m}^2\text{-d}$ . The maximum solar energy occurs during the months of May, June and July. The input solar data in HOMER is given below.

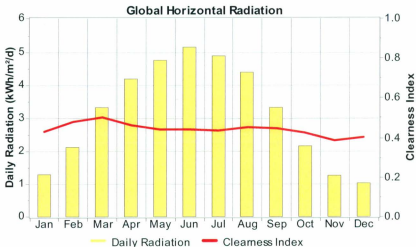


Figure 2.4: HOMER software tool formed monthly solar radiation chart based on the data collected from NASA.

Table2.1: Monthly average solar data from HOMER simulation.

Month	Clearness Index	Daily Radiation
		kWh/m <sup>2</sup> -d
January	0.433	1.280
February	0.479	2.110
March	0.501	3.310
April	0.465	4.180
May	0.439	4.740
June	0.444	5.140
July	0.437	4.880
August	0.455	4.390
September	0.447	3.310
October	0.426	2.150
November	0.388	1.270
December	0.402	1.020
Yearly Average	0.448	3.153

### 2.3.4 Selection of Wind Generator and Pricing

Wind turbines have been added to many diesel-based systems in order to reduce fuel consumption. Choosing a wind turbine that fits the need of an island depends on various

conditions such as target capacity, observed wind time series, as well as the ease of integration into the natural environment. As the load is 207 kW peak, small-sized unit wind turbine is considered. In order to adapt output to bus voltage and frequency in an optimal way, it is necessary to select modern technology. Based on these considerations the FD13-50/12 wind turbine of 50 kW is selected (<http://ghrepower.en.alibaba.com>). The FD13-50/12 wind turbine is a low-speed permanent magnet generator with a hub height of 25m and a rotor diameter of 13 m. It has high efficiency and low torque ripple, contributing to good reliability. Also, the FD13-50/12 has a low cut in speed (3 m/s), increasing operating time and thus the capacity factor. The working range of this wind turbine is 3 m/s~ 25 m/s. The power curve of the wind turbine is given below.

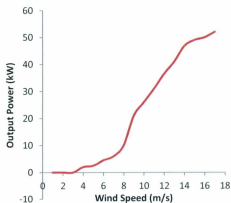


Figure 2.5: Power Curve of Wind Turbine

The cost of one 50 kW wind turbine is about \$265000 (2009), and the replacement cost is about \$165000. The cost includes the price of the turbine and installation costs. Figure 2.6 shows the cost curve of the wind turbine

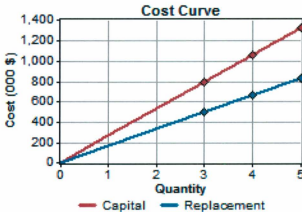


Figure 2.6: Cost curve of wind turbine from HOMER Simulation.

### 2.3.5 Calculation of the Wind Potential of St. John's

St. John's is considered one of the ideal locations for wind applications. Its mountainous nature provides many alternative locations for efficient wind installations. Historical data of recorded wind speeds for St. John's were collected from National Climate Data and the Information Archive ([www.climate.weatheroffice.gc.ca](http://www.climate.weatheroffice.gc.ca)) of Canada. Wind speeds were collected at an elevation of 50 m above sea level and scaled for 10 m height. Monthly average wind values are specifically considered in order to suit the wind generator's profile. Average annual wind speed is 6.04 m/s. Input of wind data in HOMER resulted in the comprehensive Figure 2.7.

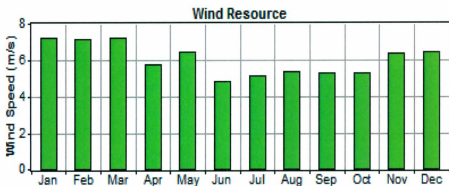


Figure 2.7: Wind resource of St. John's plotted in HOMER

Table 2.2: Monthly average wind speed of St. John's from HOMER simulation.

Month	Wind Speed
	(m/s)
January	7.228
February	7.170
March	7.190
April	5.738
May	6.464
June	4.787
July	5.132
August	5.333
September	5.310
October	5.316
November	6.390
December	6.479
Annual average:	6.041

From the monthly average wind data in Table 2.2 it can be said that the average values are higher in winter months than in summer months, which is correlated with the higher loads in the winter months. The model calculated the maximum, minimum, daily high and daily low values.

### **2.3.6 Selection of Diesel Generators and Pricing**

Small power systems based on diesel generator sets are by far the most common [31]. They require a ready supply of diesel fuel and are run whenever power is required. The task of choosing diesel generators depends on the target capacity, fuel consumption of the generators, the efficiency of the generators and the carbon emission. Diesel generators are generally sized to supply at least the peak load on the system and are commonly available with power outputs, from a few to hundreds of kilowatts. Using diesel generators causes many problems. Problems with the use of diesel generators include:

1. Cost of fuel and its transportation [59, 60].
2. Local environmental effects, such as the reduction of local air quality [61].
3. Global environmental effects, such as climate change [61].
4. Security of fuel supply [62].
5. Inefficiency when partially loaded [59, 60].
6. Start-up response time [63].
7. Noise [62].
8. Require a high level of maintenance [59].

Although diesel generators have problems, they are used extensively as they provide acceptable reliability at very low initial cost.

In the design two diesel generators are selected. The total capacity of the two generators is 225 kW. Generator one has a capacity of 75 kW; generator two has a capacity of 150 kW. Analyzing the data HOMER formed the efficiency curve and the fuel curve of the generators. Fig. 2.8.a & fig 2.8.b show the efficiency curve of the two generators respectively.

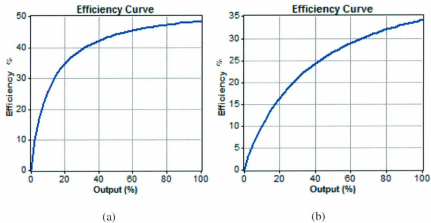


Figure 2.8: Efficiency curve in Percentage of output from HOMER simulation. (a) 75 kW diesel generator (b) 150 kW diesel generator

The fuel curves of the two generators are drawn in HOMER by entering the manufacturer's provided fuel consumption data. HOMER software tool used fuel consumption data for a 50%, 75%, and 100% load. HOMER also calculates the fuel curve parameters, intercept and slope.

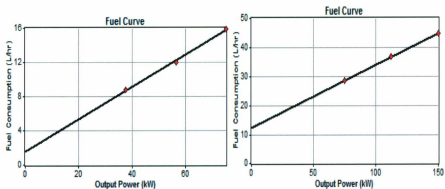


Figure 2.9: Fuel consumption curve of 75 kW and 150 kW diesel generators from HOMER simulation based on the manufacturer’s data.

The capital cost of the first diesel generator is about \$30,000 (2009) and it is considered that the replacement cost of the generator is \$20,000 (2009). The capital cost and the replacement cost of 150 kW diesel generators is \$40,000 (2009) and \$30,000 (2009) respectively. The cost curves of the two generators are given in figures below.

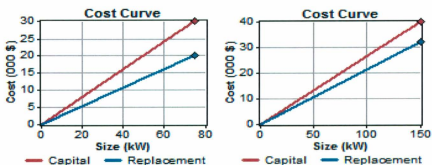


Figure 2.10: The cost curve of 75kW generator and the 150 kW generators from HOMER simulation.

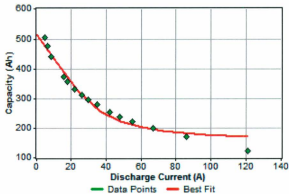
### 2.3.7 Energy Storage and Pricing

A high level of renewable energy penetration into a small power system is desirable for local self-sufficiency. However, due to the high variability and low aggregation of loads and generators, this cannot be achieved directly. Therefore, incorporating renewable energy into standalone power supplies usually requires some form of energy storage. The store must be able to supply the short-term variations to cope with wind turbulence. The energy store may also be required to cover inter-seasonal variation. In this design a Surrette 12-Cs-11-Ps 12V battery is used for an energy storage system (<http://www.rollsbattery.com/>). Taking into consideration the 648V DC bus, then the number of batteries per string is 54. The price of each battery is \$1070 (2009) and replacement cost for each battery is \$856. The cost curve of the battery is shown in figure 2.11.

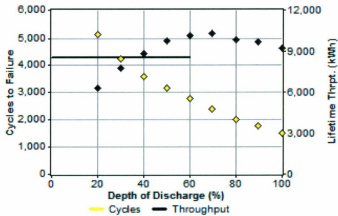


Figure 2.11: Cost curve of Surrette 12-Cs-11-Ps 12V battery from HOMER simulation.

The nominal capacity of the battery is 503 Ah, and the capacity ratio is 0.287. The capacity curve and the lifetime curve of the battery are shown in figure 2.12.



(a)



(b)

Figure 2.12: (a) Capacity curve (b) Lifetime curve of Surrette 12-Cs-11-Ps 12V battery from HOMER simulation.

### 2.3.8 Selection of Inverter / Charger and Pricing

An inverter is required for the system in which DC components serve an AC load and vice-versa. Also, a rectifier can convert AC to DC. Therefore, selection of an inverter / charger is an important thing. For the design Solectria PVI60kW-480V, a 60kw Inverter 480 VAC is selected [<http://www.rollsbattery.com>]. The core of the inverter, a 600VDC version of Solectria's proven DMG 660 distributed generation inverter, uses state-of-the-art control techniques and devices including the space vector PWM, a precision MPT algorithm, and low-loss IGBTs. With peak inverter power electronics efficiency up to 98% (over 96% including the transformer and filters) and fully integrated packaging, this inverter sets a new industry standard for efficiency, ease of installation and use, reliability, and installed cost. Multiple inverters can be used together in any combination for larger systems. The cost for a 60 kW inverter is about \$35,000 (2009). The cost curve of the inverter is shown in figure 2.13.

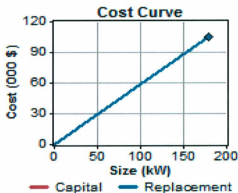


Figure 2.13: Cost curve of Solectria PVI60kW-480V, 60kw Inverter 480 VAC from HOMER simulation.

## 2.4 Hybrid System Design

Using HOMER, an AC bus-based hybrid power system and a DC bus based Hybrid power system are designed. Here these two designs are described.

### 2.4.1 AC- Bus-Based Hybrid System

The optimal AC bus-based hybrid system is determined (Figure 2.14) and simulated using HOMER software.

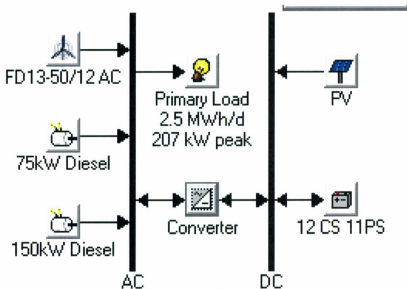


Figure 2.14: AC bus-based electrical system from HOMER simulation.

#### 2.4.1.1 Simulation Results

The design is simulated in HOMER and sensitivity analysis is performed for various wind speed, solar radiations and diesel prices. Table 2.3 shows the optimization result for current wind speed, price of diesel and the solar radiation of St. John's.

Table 2.3: Optimization result for the AC bus-based system from HOMER simulation.

FV (kW)	WT D75 (kW)	WT D150 (kW)	Battery	Converter (kW)	Initial Capital (\$)	Operating Cost (\$/yr)	Total NPC (\$)	COE (\$/kWh)	Ren.Frac	Diesel (L)	D-75 (hrs)	D-150 (hrs)	
4.725	4	75	150	108	180	1392970	182424	3704959	0.318	0.55	121925	4892	1346
4.725	4	75	150	0	180	1257410	229212	4187509	0.359	0.54	162441	3425	4102

### 2.4.1.2 Electrical Production

The AC bus based system produced 1,081,269 kWh/yr. It was found that 54% of energy production was from the wind turbine (584,789 kWh/yr). From the chart of the monthly average energy production, it was found that the energy production is less for the months of June and July.

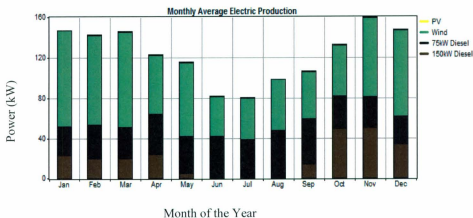


Figure 2.15: Monthly average electric production for the AC bus-based system from HOMER simulation.

The selected PV capacity for the design is 4.725 kW. Figure 2.16 analyzes the array's expected power output on a 24-h basis.

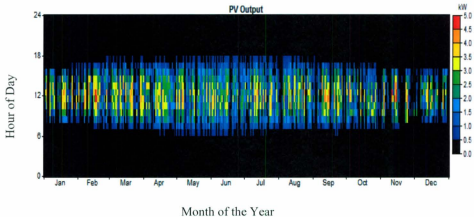


Figure 2.16: Yearly PV array output power spectrum from HOMER simulation.

Four wind turbines are enough to meet the load. These wind turbines provide the power output that is depicted in figure 2.17.

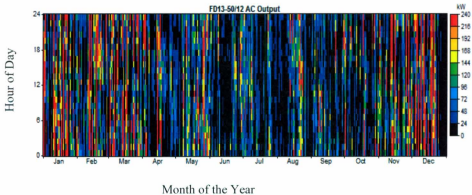


Figure 2.17: Yearly Wind turbine output power spectrum from HOMER simulation.

The diesel power output of the two diesel generators is shown in Figures 2.18 and 2.19. It was found that 150 kW diesel generator was not in an operating condition during the period from May to August.

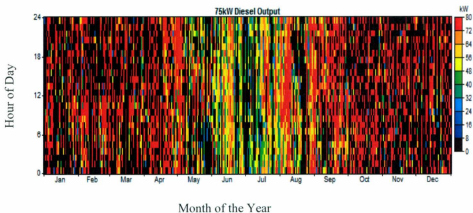


Figure 2.18: Yearly 75 kW diesel generator output power spectrum from HOMER simulation.

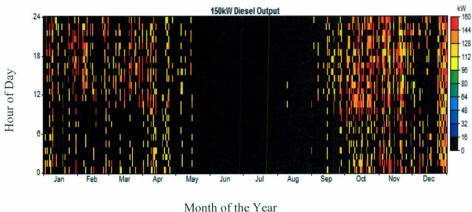


Figure 2.19: Yearly 150 kW diesel generator output power spectrum from HOMER simulation.

## 2.4.2 DC Bus-Based Hybrid System

In the DC bus based system all the components are connected to the DC bus and the loads are connected to the AC bus (figure 2.20).

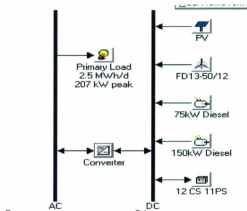


Figure 2.20: DC bus based Hybrid system from HOMER simulation.

### 2.4.2.1 Simulation Results for DC system

The optimization results for the DC bus based system are obtained using HOMER. Sensitivity for different inputs is also analyzed.

Table 2.4: Optimization results for the DC bus based system from HOMER simulation.

PV (kW)	WT (kW)	D-75 (kW)	D150 (kW)	Battery (kW)	Converter (kW)	Initial Capital (\$)	Operating Cost (\$/yr)	Total NPC (\$)	COE (\$/kWh)	Ren.Frac.	Diesel (L)	D-75 (hrs)	D-150 (hrs)
4.725	4	75	150	108	180	1372970	187054	3764154	0.323	0.54	125659	4877	1432
4.725	4	75	150	0	180	1257410	235564	4268711	0.366	0.53	167467	3321	4273

### 2.4.2.2 Electrical Production

In the DC system about 1,093,858 kWh energy is produced per year. 53% of this electricity comes from the wind turbine (584,789kWh/yr). The monthly average electricity production is shown in the chart below.

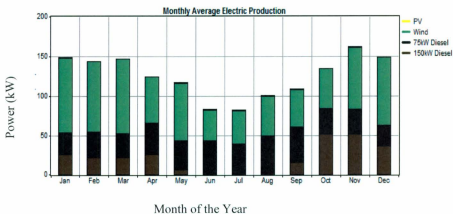


Figure 2.21: Monthly average electric production for the DC bus-based system from HOMER simulation.

The selected PV capacity for the design is 4,725 kW. Figure 2.22 analyzes the array's expected power output on a 24-h basis.

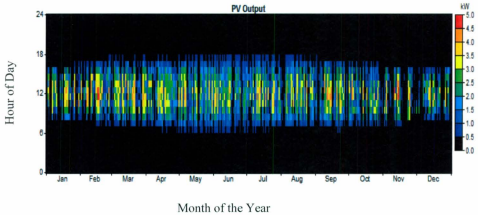


Figure 2.22: Yearly PV array output power spectrum from HOMER simulation.

Four wind turbines are enough to meet the load. These wind turbines provide the power output that is depicted in figure 2.23

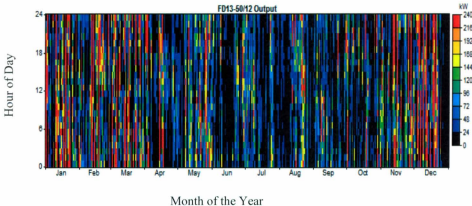


Figure 2.23: Yearly Wind turbine output Power spectrum from HOMER simulation.

The diesel power output of the two diesel generators are shown in Figure 2.24 and 2.25. It was found that the 150 kW diesel generator was not operating during the period from May to August.

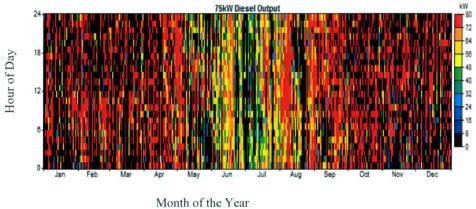


Figure 2.24: Yearly 75 kW diesel generator output power spectrum from HOMER simulation.

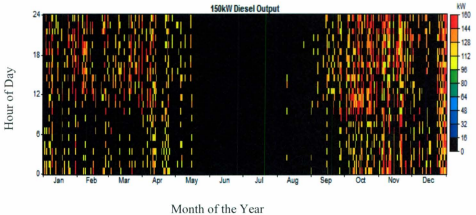


Figure 2.25: Yearly 150 kW diesel generator output power spectrum from HOMER simulation.

## 2.5 Comparison between a PV-wind-diesel AC bus-based system and a PV-wind-diesel DC bus based system

The main aspect of this research was to design an AC system and a DC system and to make a comparison between these two systems. The HOMER, NREL software tool was used to design these systems. The PV system, the wind turbine, the diesel generators, the converters and the batteries that are used in both designs are the same model. The simulation is run using a number of sensitivity parameters. Comparison can be made depending on different factors. Two case studies have been considered for comparison: firstly, a 100% AC load and secondly, a 70% DC load and a 30% AC load, as most of the load is a heating type DC load. The following sections will describe all factors based on which the comparison is made for the 100% AC load. Then the overall comparison for the 100% AC load and the 70% DC and 30% load will be given.

### 2.5.1 The Cost Summary

Although the equipment used in both AC and DC systems are the same model, and the prices of them are the same, the total cost of these two systems is different.

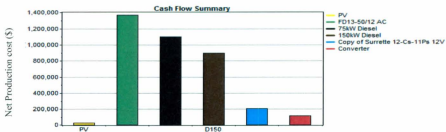


Figure 2.26: Cash flow summary of a PV-Wind-Diesel AC system from HOMER simulation.

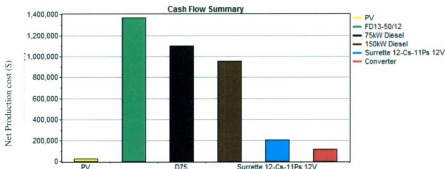


Figure 2.27: Cash flow summary of a PV-Wind- Diesel DC system from HOMER simulation.

Figure 2.26 and figure 2.27 show the cash flow summary for the AC and DC system respectively. From the charts it can be said that the net present cost of PV in the DC system is the same as the cost of the AC system because the DC system used same number of solar panels as the AC system, and the kW from PV at the DC system and the AC system is 4.725 kW. The costs of the wind turbine for both systems are the same and both systems use the same number of wind turbines. The net present cost of two diesel generators in the AC system is lower than the cost for the DC system. The capital costs of the two systems are the same for both systems but the operation and maintenance cost; the fuel cost and the operation and maintenance cost are larger for the DC system than for the AC system. The fuel cost is large for the DC system because both generators are in operation for more hours throughout the year than for the AC system. The cost of batteries for the DC system and the AC system are the same as both systems use 108

batteries. The cost of the converter for both systems is the same. The total cost of the AC system and the DC system is given in the following two tables. The diesel cost of the DC system is a bit higher, since 75kW diesel operates for more hours.

Table 2.5: Total cost of the AC system from HOMER simulation.

Component	Capital (\$)	Replacement (\$)	O&M (\$)	Fuel (\$)	Salvage (\$)	Total (\$)
PV	22,410	0	639	0	0	23,049
FD13-50/12 AC	1,060,000	0	306,801	0	0	1,366,801
75kW Diesel	30,000	27,596	4,630	1,036,951	-2,357	1,096,822
150kW Diesel	40,000	0	25,810	833,389	-1,184	898,015
Copy of Sunette 12-Cs-1	115,560	68,777	41,418	0	-19,745	206,009
Converter	105,000	0	9,204	0	0	114,204
System	1,372,970	96,373	388,562	1,870,341	-23,286	3,704,960

Table 2.6: Total cost of the DC system from HOMER simulation.

Component	Capital (\$)	Replacement (\$)	O&M (\$)	Fuel (\$)	Salvage (\$)	Total (\$)
PV	22,410	0	639	0	0	23,049
FD13-50/12	1,060,000	0	306,801	0	0	1,366,801
75kW Diesel	30,000	27,535	4,676	1,039,232	-2,407	1,099,037
150kW Diesel	40,000	0	27,459	888,379	-783	955,055
Surette 12-Cs-11Ps 12k	115,560	68,777	41,418	0	-19,745	206,009
Converter	105,000	0	9,204	0	0	114,204
System	1,372,970	96,312	390,197	1,927,611	-22,935	3,764,155

### 2.5.2 Electrical Factor

Both the AC and DC system met the same amount and the same type of AC load. However, their production of electricity using the same components is different. The total production of electricity for the AC system is lower than the electricity production of the DC system.

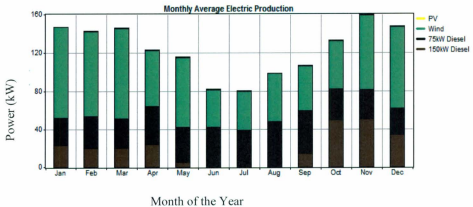


Figure 2.28: Average Energy Production of the AC system from HOMER simulation.

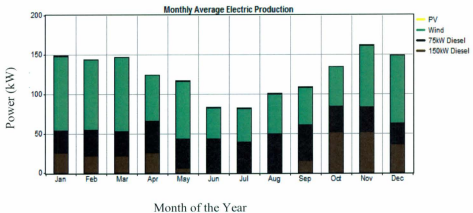


Figure 2.29: Average Energy Production of the DC system from HOMER simulation.

The energy production of the AC system per year is 1,081,269 kWh. In the case of the DC system it is 1,093,858 kWh. However, the excess electricity produced in the AC system is larger than for the DC system. The percentage contribution of excess electricity in the AC system is 14% where as the DC system, it is 13.9 %. The contribution of PV in total energy production is almost the same in both DC system and AC system. The wind turbine produced the same amount of electricity for both systems, but if we calculated it as a percentage of total production, then the percentage contribution of electricity from wind turbine is larger in the AC system than in the DC system. The two diesel generators produced more electricity in the DC system than in the AC system. The production of electricity of all components of these two systems is given in tabular form below.

Table2.7: Energy production of DC system from HOMER simulation.

Production	kWh/yr	%
PV array	5,213	0
Wind turbines	584,789	53
75kW Diesel	317,632	29
150kW Diesel	186,224	17
Total	1,093,858	100

Table2.8: Energy production of AC system from HOMER simulation.

Production	kWh/yr	%
PV array	5,209	0
Wind turbines	584,789	54
75kW Diesel	316,721	29
150kW Diesel	174,549	16
Total	1,081,269	100

Table2.9: Excess Energy of AC system.

from HOMER simulation.

Quantity	kWh/yr	%
Excess electricity	156,037	14.4
Unmet electric load	0.000946	0.0
Capacity shortage	0.00	0.0

Quantity	Value
Renewable fraction	0.546

Table2.10: Excess Energy of DC system

from HOMER simulation.

Quantity	kWh/yr	%
Excess electricity	151,645	13.9
Unmet electric load	264	0.0
Capacity shortage	779	0.1

Quantity	Value
Renewable fraction	0.539

The renewable fraction of the AC system is 0.546, but for the DC system the value of the renewable fraction is 0.539. This difference is mainly due to the losses in the main inverter used in the DC system. The inverter required for the DC system is larger, hence there are more losses.

### 2.5.3 Emissions

The system in which carbon emission is less can be said to be a better system as regards to environmental pollution. Emission of more carbon is responsible for environmental pollutions. In that sense, the AC system is better than the DC system because in the AC system the carbon emission is less than for the DC system. The emissions of carbon dioxide in the AC system are 321,070 kg/yr, where as for the DC system, the value is 330,901 kg/yr. The emissions of the other gases are given in the following two tables.

Table2.11: Emissions in AC system

from HOMER simulation.

Pollutant	Emissions (kg/yr)
Carbon dioxide	321,070
Carbon monoxide	793
Unburned hydrocarbons	87.8
Particulate matter	59.7
Sulfur dioxide	645
Nitrogen oxides	7,072

Table2.12: Emissions in DC system

from HOMER simulation.

Pollutant	Emissions (kg/yr)
Carbon dioxide	330,901
Carbon monoxide	817
Unburned hydrocarbons	90.5
Particulate matter	61.6
Sulfur dioxide	665
Nitrogen oxides	7,288

The summary of the overall comparisons is given in the following tables; 2.13, 2.14, 2.15, 2.16, 2.17 and 2.18.

Table -2.13: Comparison based on components required for 100% AC load

Component	AC Based System	DC Based System
PV	4,725 kW	4,725 kW
W.T	4 X 50 kW	4 X 50 kW
D-75 kW	1 X 75 kW	1 X 75 kW
D-150 kW	1 X 150kW	1 X 150kW
Batteries required	108	108
Converter	180 kW	180 kW

Table -2.14: Comparison based on components required for 30% AC and 70% DC load

Component	AC Based System	DC Based System
PV	33 kW	4.725 kW
W.T	5 X 50 kW	5 X 50 kW
D-75 kW	1 X 75 kW	1 X 75 kW
D-150 kW	1 X 150kW	1 X 150kW
Batteries required	108	108
Converter	120 kW	60 kW

Table -2.15: Comparison based on cost for 100% AC load.

Cost Type	AC Based System	DC Based System
Initial Capital cost(\$)	13,72,970	13,72,970
Operating cost (\$/Y)	182,424	187,054
Total NPC (\$)	3,704,959	3,764,154
COE (%/kWh)	0.318	0.323

Table -2.16: Comparison based on cost for 30% AC and 70% DC load

Cost Type	AC Based System	DC Based System
Initial Capital cost(\$)	17,38,260	15,67,970
Operating cost (\$/Y)	180,033	174,044
Total NPC (\$)	4,039,688	3,792,835
COE (%/kWh)	0.346	0.326

Table -2.17: Comparison based on diesel use and emission for 100% AC load

	AC Based System	DC Based System
Diesel (L)	121,925	125,659

Pollutant	Emission (Kg/Yr)	Emission (Kg/Yr)
CO <sub>2</sub>	321,070	330,901
CO	793	817
UHCs	87.8	90.5
PM	59.7	61.6
SO <sub>2</sub>	645	665
NO <sub>x</sub>	7,072	7,288

Table -2.18: Comparison based on diesel use and corresponding emission for 30% AC and 70% DC load

	AC based System	DC based System
Diesel (L)	127,057	122,102
Pollutant	Emission (kg/Yr)	Emission (kg/Yr)
CO <sub>2</sub>	334,583	321,536
CO	826	794
UHCs	91.5	87.9
PM	62.3	59.8
SO <sub>2</sub>	672	646
NO <sub>x</sub>	7,369	7,082

Table – 2.19 Comparison Based on Renewable Fraction for 100 % AC load

	AC System	DC System
Renewable Fraction	55 %	54 %

Table – 2.20 Comparison Based on Renewable Fraction for 30 % AC & 70 % DC load

	AC System	DC System
Renewable Fraction	60 %	60 %

The above tables clearly indicate that the DC system would be better when the load is mainly DC. Such a system will lead to a lower cost of electricity and lower emissions. This can easily be achieved since commonly used water and space heaters can directly run on DC. Based on the selected high DC bus voltage it could be achieved with a little modification.

## 2.6 Summary

In this chapter the simulation of an AC based hybrid power system and a DC based hybrid power system is done by using the HOMER software tool. The optimization method of the HOMER software tool can be found at (<https://analysis.nrel.gov/homer/>). Most of the essential data have been obtained from hNewfoundland Hydro, NASA and Weather Network Canada. Capital, replacement and O&M costs are assigned for each component along with their lifetime. In fact these three costs are the primary inputs the

HOMER software tool delineates. In order to establish the internal combustion generator's efficiency curve, a number of associated parameters have been designated. Wind speed, diesel price and consumed energy have been considered as the parameters which are subjected to change over time. A number of sensitivity parameters are used to simulate the system. Hence the effects of changes on other parameters have been highlighted with different plots. The later part of this chapter deals with the hourly transient behaviours of power system components. Results are shown in this chapter for an annual average wind speed of 6.04 m/s, global solar radiation of 3.15 kWh/m<sup>2</sup>-d and diesel price of \$1.2/L. Then a comparison of two systems is done based on two case studies. From the comparison table it can be concluded that there is no significant difference between an AC based hybrid system and a DC based hybrid system when a 100% AC load is considered. But when a 70 % DC and a 30 %AC load is considered, the simulations show different results. In that case the DC based system is better than the AC based system based on components required, cost, diesel required and corresponding emissions.

## Chapter 3

### Modeling of Wind Turbines

#### 3.1 Wind Energy Conversion System

Differential heating of the earth's surface by the sun causes the movement of large air masses on the surface of the earth, i.e., the wind. Wind energy conversion systems convert the kinetic energy of the wind into electricity or other forms of energy. Wind power generation has experienced a tremendous growth in the past decade, and has been recognized as an environmentally friendly and economically competitive means of electric power generation. More countries are ratifying the 1997 Kyoto Protocol, and wind power has become one of the most effective ways to reach its goals. The Kyoto Protocol sets targets for participating countries to reduce greenhouse gas emissions to at least 5% below the 1990 level in the commitment period of 2008 to 2012. According to the U.S. Energy Information Administration, world electricity consumption will increase from 12,833 TWh in 1999 to 22,230 TWh in 2020, mainly driven by developing countries, where two billion people are still without access to electricity [34]. The fuel mix for the world's electricity generation in 2008, as presented in Figure 3.1, indicates that fossil fuels accounted for 62%, while renewable including hydropower, wind and solar etc. accounted for 19% [IEA Electricity information].

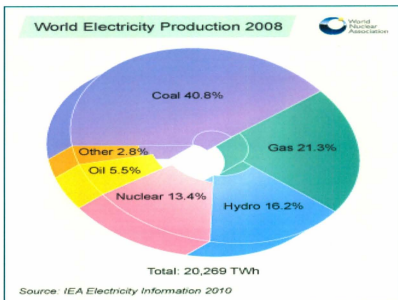


Figure 3.1: World Electricity Generation (IEA Electricity information 2010).



Figure 3.2: World average annual wind energy growth rate from 2001 to 2010 (windfair.net)

Worldwide development of wind energy expanded rapidly starting in the early 1990s. Figure 3.2 shows the average annual growth rate from 2001 to 2010 of the world's installed wind power, making the wind industry one of the fastest growing.

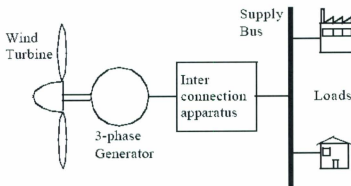


Figure 3.3: Wind Energy conversion system

A modern wind turbine captures the kinetic energy available in the wind through an electro mechanical coupling for generating electricity. Figure 3.3 shows a general wind energy conversion system. In addition to the rotor-generator assembly, a complete wind energy conversion system (WECS) consists of several other mechanisms such as a yaw regulator, speed controller, protection devices and power converter [36]. The components of the wind turbine are shown in figure 3.4.



Figure 3.4: Components of Wind Turbine (<http://www.alternative-energy-news.info/technology/wind-power/wind-turbines/>)

The principal components of a modern wind power plant are the tower, the rotor and the nacelle, which accommodates the transmission mechanisms and generator; and for horizontal-axis devices, the yaw system for steering in response to change in wind direction. Switching and protection systems, lines and maybe also transformers and networks will be required for supplying end users or for storage. In response to the internal influences, a unit for operational control and regulation must adapt the flow of

energy in the system to the demands placed upon it. The following sections provide a model of the components of the wind energy conversion system.

### **3.2 Component of Wind Power Plant**

In this research the dynamic model of a FD13-50/12 wind turbine is included [30]. This is a 50kW Permanent magnet generator based wind turbine. In this research both AC and DC bus based systems are designed and analyzed, and it is found that for a AC bus based system, if we use a permanent magnet generator based system, more power electronics is required, which is not cost effective. Therefore, for the AC bus based system squirrel-case induction generator based wind turbine is used. Before analyzing the dynamic behavior, the steady state behaviours are computed first. The constituents of a wind power plant are given below.

1. Rotor Blade
2. Rotor Shaft and Bearings
3. Rotor Brakes
4. Gearbox
5. Electrical Generation System
6. Transformer

## 7. Capacitor Bank

The mathematical modeling of an electrical generation system and transformer are discussed below.

### 3.2.1 Electrical Generation System

Depending on the manufacturer, different types of generators are used in a wind energy conversion system. The doubly-fed induction generator, permanent magnet synchronous generator and squirrel case induction generator etc. are examples of this kind of generator. All of them perform well and are being used on a number of wind farms. The generator of the wind turbine that we used in the DC system is the permanent magnet synchronous generator. In a dynamic simulation of the AC coupled hybrid system, we used a squirrel cage induction generator. The following sections will explicate the basic principles of these generators.

#### 3.2.1.1 Squirrel Cage Induction Generator

In a three-phase squirrel cage induction generator there are three identical windings that are symmetrically distributed around the inner surface of a laminated cylindrical shell called the stator. The laminated rotor inside carries a winding consisting of bars connected to two shorting rings at both ends. This rotor can be adapted to any number of stator poles. When the balanced stator windings are wound for  $p$  number of pole pairs and displaced in space by 120 electrical degrees, and the applied torque creates a field rotation in the air gap,  $n_s$ , a three phase voltage will be induced in the stator winding having the

frequency,  $f$ . The relationship between pole pairs, frequency and the field rotation can be expressed as follows [42]:

$$n_s = \frac{f}{p} \quad (3.2.1)$$

Here  $n_s$  is expressed in rad/s and is known as the synchronous speed of the induction generator and  $p$  is the number of pole pairs.

The resultant air gap flux  $\varphi_m$  is set up by the combined action of the stator and the rotor magneto-motive force (mmf). This synchronous rotating flux induces a counter emf  $E_l$  in the stator phase winding. The stator terminal voltage  $V_l$  differs from this counter emf  $E_l$  by the stator leakage impedance drop. The stator emf phasor equation is then:

$$\vec{V}_1 = \vec{E}_1 + \vec{I}_1(R_s + jX_{ls}) \quad (3.2.2)$$

The circuit representation of the equation (3.2.2) is shown in figure 3.8. The stator winding current  $I_1$  can be resolved into an exciting component  $I_0$  and a compensating load component current  $I'_2$ . The load component current  $I'_2$  counteracts the rotor emf, thereby demanding power from the source. The exciting component  $I_0$  can be resolved into a core loss component  $I_c$ , in phase with the stator induced emf  $E_l$  and a magnetizing component  $I_m$ , lagging behind the induced emf  $E_l$  by  $90^\circ$ . This is the magnetizing component which sets up the air gap flux  $\varphi_m$ .

The asynchronous machine block in MATLAB/Simpower System/ Machine library operates either in motor or generator mode. The mode of operation is dictated by the sign of the mechanical torque. For positive  $T_m$  the block acts as a motor, and for negative  $T_m$  it operates as a generator. The electric part of the machine is represented by a fourth order state space model and the mechanical part by a second order system. All electrical

parameters and variables are referred to the stator. These are denoted by the prime signs in the machine equations. All stator and rotor quantities are in the arbitrary two axis d-q reference frame.

The expressions related to d-q axis representation of an asynchronous machine are stated below [26, 38].

$$V_{qs} = R_s i_{qs} + \frac{d}{dt} Q_{qs} + \omega \varphi_{ds} \quad (3.2.3)$$

$$V_{ds} = R_s i_{ds} + \frac{d}{dt} Q_{ds} - \omega \varphi_{qs} \quad (3.2.4)$$

$$V'_{qr} = R'_r i'_{qr} + \frac{d}{dt} \varphi'_{qr} + (\omega - \omega_r) \varphi'_{dr} \quad (3.2.5)$$

$$V'_{dr} = R'_r i'_{dr} + \frac{d}{dt} \varphi'_{dr} - (\omega - \omega_r) \varphi'_{qr} \quad (3.2.6)$$

$$T_e = \frac{3}{2} p (\varphi_{ds} i_{qs} - \varphi_{qs} i_{ds}) \quad (3.2.7)$$

where

$$\varphi_{qs} = L_s i_{qs} + L_m i'_{qr} \quad (3.2.8)$$

$$\varphi_{ds} = L_s i_{ds} + L_m i'_{dr} \quad (3.2.9)$$

$$\varphi'_{qr} = L'_r i'_{qr} + L_m i_{qs} \quad (3.2.10)$$

$$\varphi'_{dr} = L'_r i'_{dr} + L_m i_{ds} \quad (3.2.11)$$

$$L_s = L_{ls} + L_m \quad (3.2.12)$$

$$L'_r = L'_{lr} + L_m \quad (3.2.13)$$

$p$  number of pole

$R_s, L_{ls}$  are stator resistance and leakage inductance

$L_m$  is magnetizing inductance

$L_s$  is total stator inductance

$V_{qs}$ ,  $i_{qs}$  are q axis stator voltage and current

$V_{ds}$ ,  $i_{ds}$  are d axis stator voltage and current

$\varphi_{qs}$ ,  $\varphi_{ds}$  are stator q and d axis fluxes

$\omega_r$  is electrical angular velocity

$T_e$  is electromagnetic torque

$L'_r$  is total rotor inductance

$R'_r$ ,  $L'_{lr}$  are rotor resistance and leakage inductance

$V'_{qr}$ ,  $i'_{qr}$  are q axis rotor voltage and current

$V'_{dr}$ ,  $i'_{dr}$  are d axis rotor voltage and current

$\varphi'_{qr}$ ,  $\varphi'_{dr}$  are rotor q and d axis fluxes

The mechanical part can be represented by the following equations

$$\frac{d}{dt} \omega_m = \frac{1}{2H} (T_e - F\omega_m - T_m) \quad (3.2.14)$$

$$\frac{d}{dt} \theta_m = \omega_m \quad (3.2.15)$$

where:

$\omega_m$  is angular velocity of the rotor

$T_m$  is shaft mechanical torque

$F$  is combined rotor and load viscous friction coefficient

The topology of the asynchronous generator in d-q axis frame is depicted as follows, in

Figure 3.5:

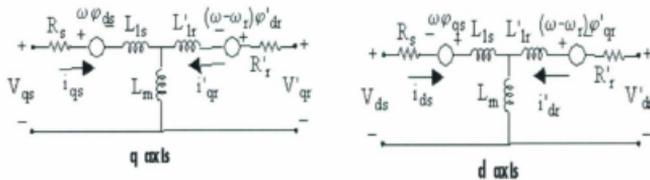


Figure: 3.5: Asynchronous generator representations in d-q axis frame.

### 3.2.1.2 Permanent Magnet Synchronous Generator

The basic wind energy conversion requirements of a variable speed permanent magnet generator are almost the same as those for a wound field synchronous generator. The permanent magnet generator dispenses with the need for external excitation. Therefore, the output voltage under variable speed operation varies both in frequency and in magnitude. As a consequence, the DC link voltage changes in an uncontrolled manner. The control, however, is realized via the DC-AC converter on the grid side.

The turbine shaft speed is controlled by the opposing reaction torque of the generator. The optimum values of the DC voltage and current can be obtained from equation 3.2.16 and 3.2.17. With the diode bridge, assuming the ripple free DC-link current, the generator terminal voltage and currents are as follows [42]:

$$V_g = \frac{\pi}{3\sqrt{6}} V_d \quad (3.2.16)$$

$$I_g = \frac{\sqrt{6}}{\pi} I_d \quad (3.2.17)$$

It is noteworthy that for any particular DC- link voltage, there is a minimum speed below which there is no generation. For any wind speed, there exists an optimum turbine speed at which maximum power can be extracted from the wind.

The permanent magnet synchronous generator block exists in the Matlab/SimPower System/ Machines library. Like the asynchronous machine, these machines have two operating modes. The sign of  $T_m$  determines whether it will run in motor mode or generator mode. Electrically these machines are characterized as sinusoidal models and trapezoidal models. The sinusoidal model assumes that the flux established by the permanent magnets in the stator is sinusoidal, which implies that the electromotive forces are sinusoidal. For the trapezoidal machines, the model assumes that the flux established by the permanent magnets produces three trapezoidal back EMF waveforms. The research is focused on the sinusoidal model only. The electric model of such a generator is implemented by the following equations: [38]

$$\frac{d}{dt} i_d = \frac{1}{L_d} v_d - \frac{R}{L_d} i_d + \frac{L_q}{L_d} p \omega_r i_q \quad (3.2.18)$$

$$\frac{d}{dt} i_q = \frac{1}{L_q} v_q - \frac{R}{L_q} i_q + \frac{L_d}{L_q} p \omega_r i_q - \frac{\lambda p \omega_r}{L_q} \quad (3.2.19)$$

$$T_e = 1.5p[\lambda i_q + (L_d - L_q)i_d i_q] \quad (3.2.20)$$

where

$L_q, L_d$  are q and d axis inductances

$R$  is Resistance of the stator windings

$i_q, i_d$  are q and d axis currents

$v_q, v_d$  are q and d axis voltages

$\omega_r$  is angular velocity of the rotor

$\lambda$  is amplitude of the flux induced by the permanent magnets of the rotor in the stator phases

$p$  is the number of pole pairs

$T_e$  is the electromagnetic torque.

The  $L_q$  and  $L_d$  inductances represent the relation between the phase inductance and the rotor position due to the saliency of the rotor. For example, the inductance measured between phase a and b is given by:

$$L_{ab} = L_d + L_q + (L_q - L_d) \cos\left(2\theta_e + \frac{\pi}{3}\right) \quad (3.2.21)$$

where  $\theta_e$  represents the electrical angle.

The following diagram uncovers how the line-line inductance varies as a function of the electrical angle of the rotor.

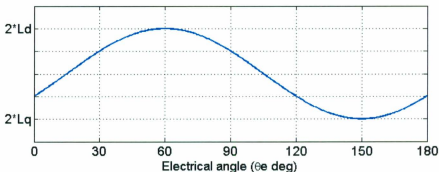


Figure: 3.6 Change of line inductance with rotor positions

For a permanent magnet synchronous generator, the rotor might be either round or a salient-pole type. The relationship between d-q frame inductance and lone inductance will differ according to their types.

Condition for round rotor:

$$L_d = L_q = \frac{L_{ab}}{2} \quad (3.2.22)$$

Condition for salient pole rotor:

$$L_d = \frac{\max(L_{ab})}{2} \quad (3.2.23)$$

and

$$L_q = \frac{\min(L_{ab})}{2} \quad (3.2.24)$$

The mechanical behaviour of this machine is the same as for an induction generator.

The mechanical part can be represented by the following equations:

$$\frac{d}{dt} \omega_m = \frac{1}{2H} (T_e - F\omega_m - T_m) \quad (3.2.25)$$

$$\frac{d}{dt} \theta_m = \omega_m \quad (3.2.26)$$

where

$T_e$  is electromagnetic torque

$T_m$  is shaft mechanical torque

$F$  is combined viscous friction of rotor and load.

### 3.2.2 Transformer

A three-phase transformer is very important to increase or decrease the voltage magnitude. These transformers can be made either by connecting three phase

transformers in a three phase bank, or by three windings wound on a common core. The former one is cheaper, smaller and lighter than the latter one [40].

The primary winding draws a current when it is connected to an alternating voltage source. This current produces a flux in the transformer core. When the flux moves through the magnetic core and cuts it by both the windings, a voltage will be induced in the primary and secondary windings. In the Figure 3.7 the instantaneous emf induced in the primary windings is as follows:

$$e_1 = -N_1 \frac{d\phi}{dt} = N_1 \omega \phi_m \sin(90^\circ + \omega t) \quad (3.2.27)$$

The maximum value of  $e_1$  is

$$E_{m1} = N_1 \omega \phi_m \quad (3.2.28)$$

Now the effective value of the primary emf is,

$$E_1 = \frac{E_{m1}}{\sqrt{2}} = 4.44f\phi_m N_1 \quad (3.2.29)$$

Similarly, the emf of the secondary winding is,

$$E_2 = 4.44f\phi_m N_2 \quad (3.2.30)$$

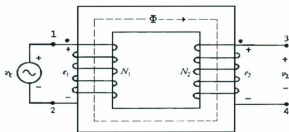


Figure: 3.7 Ideal Transformer.

In a two winding transformer, the windings are magnetically coupled and are hard to analyze. Therefore the ideal transformer is converted to its equivalent circuit for the purpose of easy computation. The parameters such as resistance, reactance, voltage and current can be transferred either from primary to secondary or from secondary to primary in the equivalent circuits. The magnitude of the no-load circuit current is very small and it is less than 5% of the rated primary current. Hence in the equivalent circuit the no load circuit can be neglected without making a serious error. The two windings ideal transformer is shown in the figure 3.8

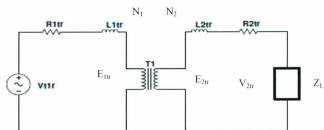


Figure: 3.8 A two winding transformer

The equivalent circuits referred to as primary and secondary are depicted in figure 3.9 and 3.10 respectively. In the case of the former one, all parameters are transferred from secondary to primary. The parameters are:

$$R'_{2tr} = a^2 R_{2tr} \tag{3.2.31}$$

$$X'_{2tr} = a^2 X_{2tr} \tag{3.2.32}$$

$$Z'_L = a^2 Z_L \tag{3.2.33}$$

$$I'_{2tr} = \frac{I_{2tr}}{a} \quad (3.2.34)$$

Combined resistance referred to primary:

$$R_{01} = R_{1tr} + R'_{2tr} = R_{1tr} + a^2 R_{2tr} \quad (3.2.35)$$

Combined reactance referred to primary:

$$X_{01} = X_{1tr} + X'_{2tr} = X_{1tr} + a^2 X_{2tr} \quad (3.2.36)$$

The voltage across load,

$$V'_{2tr} = aV_{L2tr} \quad (3.2.37)$$

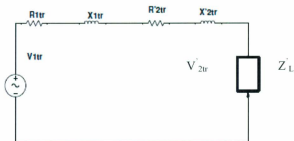


Figure: 3.9 Equivalent circuit referred to primary

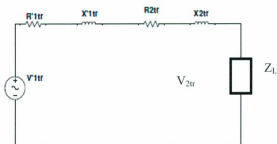


Figure: 3.10 Equivalent circuit referred to secondary

In a similar fashion, it is possible to express all the parameters transferred from the primary to the secondary side to form the equivalent circuit referred to as secondary.

These shifted parameters are:

$$R'_{1tr} = \frac{R_{1tr}}{a^2} \quad (3.2.38)$$

$$X'_{1tr} = \frac{X_{1tr}}{a^2} \quad (3.2.39)$$

$$I'_{1tr} = aI_{1tr} \quad (3.2.40)$$

$$V'_{1tr} = \frac{V_{1tr}}{a} \quad (3.2.41)$$

Total resistance referred to the secondary:

$$R_{02} = R_{2tr} + R'_{1tr} = R_{2tr} + \frac{R_{1tr}}{a^2} \quad (3.2.42)$$

$$X_{02} = X_{2tr} + X'_{1tr} = X_{2tr} + \frac{X_{1tr}}{a^2} \quad (3.2.43)$$

where  $a$  is the turn ratio and expressed as

$$a = \frac{N_1}{N_2} = \frac{V_{1tr}}{V_{2tr}} = \frac{I_{2tr}}{I_{1tr}} \quad (3.2.44)$$

### 3.2.3 Capacitor Bank

Due to being cheap, simple and robust in design, the squirrel cage induction generators based wind turbines have received a great deal of attention for operating in AC coupled stand-alone conditions. Although they are capable of generating active power, their limitation is that they are unable to produce reactive power needed for their own excitation. In order to mitigate this problem, a capacitor bank is connected to this system between the generator and the load or grid. In this simulation a 55 kVAR rated capacitor

bank is used for each 100kW generator. As the three phase capacitor bank is connected to the induction generator, an emf is induced to the machine windings due to the self excitation provided by the capacitors. The magnetizing requirements of the machines are met by these capacitors. In order to create the self-excitation by this capacitor bank, the following two conditions should be fulfilled [26,41].

1. The rotor of the machine should have sufficient residual magnetism and
2. The three-phase capacitor bank should be of sufficient value.

After satisfying the above conditions an emf will be induced in the machine windings due to the excitation provided by the capacitors. The phenomenon is known as "capacitor self excitation". If the induced emf is sufficient, leading currents through the capacitors will circulate.

The model of a linear capacitor block described with the following equation

$$I = C \frac{dV}{dt} \quad (3.2.3.1)$$

where,

$I$  Current

$V$  Voltage

$C$  Capacitance

$t$  Time

### 3.3 Power Extraction from the Wind

Energy conversion takes place on two levels in a wind energy conversion system. First, the WT rotor converts the wind energy into the mechanical energy. Then this mechanical energy is fed to the generator which produces electrical energy. After that, different schemes, composed of inverter converter sets, chopper circuits and power electronic switches are deployed for power shaping or maximum power extraction. Assuming no yaw misalignment, the wind turbine's energy conversion technique is governed by equation (3.3.1) as follows [23, 39]:

$$P_t = \frac{1}{2} \rho A C_p(\lambda, \beta) v_w^3 \quad (3.3.1)$$

where  $P_t$  is the mechanical power generated by the turbine,  $\rho$  is the air density,  $A$  is the Turbine swept area,  $C_p$  is the performance coefficient and  $v_w$  is the wind speed. This equation reveals that  $C_p$  is the function of the tip speed ratio (TSR),  $\lambda$  and the pitch angle  $\beta$ . The pitch angle is fixed for both the turbines and the mechanical power depends on the  $C_p$ - $\lambda$  curve.  $C_p$ - $\lambda$  relationship is characterized by the following two equations:

$$C_p(\lambda, \beta) = c_1 \left( \frac{c_2}{\lambda_1} - c_3\beta - c_4 \right) e^{-\frac{c_5}{\lambda_1}} + c_6\lambda \quad (3.3.2)$$

$$\frac{1}{\lambda_1} = \frac{1}{\lambda + 0.08\beta} - \frac{0.035}{\beta^2 + 1} \quad (3.3.3)$$

where,  $c_1$ - $c_6$  are the coefficients. TSR can be measured by the ratio of the rotor speed at the tip to the wind speed. Mathematically it is expressed by the following equation:

$$\lambda = \frac{\omega R}{v_w} \quad (3.3.4)$$

where,  $\omega$  is the rotational speed and  $R$  is the radius of the turbine. When the wind blows over the cut-in speed, the turbine rotates, and at the same time it produces some torque, which is associated with produced mechanical energy. The behaviour is articulated by :

$$T_t = \frac{P_t}{\omega} \quad (3.3.5)$$

where,  $T_t$  is the turbine torque.

A more generalized equation of turbine torque can be formulated after combining equations (3.3.1), (3.3.4) and (3.3.5) as follows:

$$T_t = \frac{1}{2} \rho A R \frac{C_p(\lambda, \beta)}{\lambda} v_w^2 = \frac{1}{2} \rho A R C_q(\lambda, \beta) v_w^2 \quad (3.3.6)$$

Here  $C_q$  is the torque coefficient and is defined as

$$C_q(\lambda, \beta) = \frac{C_p(\lambda, \beta)}{\lambda} \quad (3.3.7)$$

where,

$\beta$  is pitch angle, Deg.

$\lambda$  is tip speed ratio

$\omega$  is turbine rotational speed, rad/s

$\rho$  is air density, kg/m<sup>3</sup>

$A$  is turbine swept area, m<sup>2</sup>

$c_p$ - $c_b$  are turbine coefficients

$C_p$  is performance coefficient of the turbine

$C_q$  is torque coefficient of the turbine

$P_t$  is mechanical power generated by the turbine, W

$R$  is radius of the turbine, m

$T_t$  is turbine torque, N-m

$v_w$  is wind speed, m/s.

The Simulink block diagram showing the input output relationship is shown in Appendix A (Figure A-1).

### 3.4 Modeling and Simulation of FD-13-50 Wind Turbine for AC Coupled Hybrid System.

The FD-13/50 kW wind turbine is a 50 kW permanent magnet generator based wind turbine. First we have modeled the wind turbine with PMG and the topology is shown in figure 3.11.

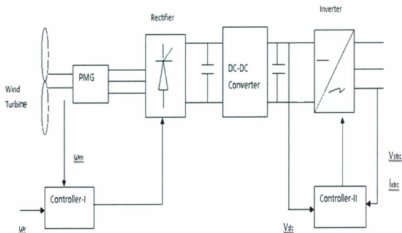


Figure: 3.11 The 50kW wind generator and control using PMG

From the above figure it is clear that if we use a permanent magnet generator based wind turbine for the AC system, we need extra power electronics to convert the DC output to AC. In that case, we decide to use an induction generator based wind turbine. The mechanical components and the electrical characteristics of this WECS have been illustrated thoroughly in section 3.2. The further specifications obtained from [43, 44] are given in table 3.1. Basically a steady state model has been developed here in this section and it is intended to compute how energy is being produced with different levels of wind speed. The following figure 3.12 shows the steady state wind turbine Matlab/ Simulink model using an induction generator based wind turbine.

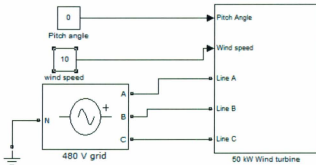


Figure 3.12: The 50kW wind generator and control using Synchronous generator in Simulink.

The above figure includes the turbine, generator and other mechanical accessories as practical systems. The detailed components of this subsystem are given in appendix A

(Figure A-1). Table 3.2 unveils the parameter used in the simulation model. Finally, the power from 50kW WECS at different wind speed levels and speed characteristics of the generator are recorded and shown in Figure (3.13) and Figure (3.14). It has been found that at 5 m/s wind speed the wind turbine generated power is 1.2 kW. At base wind speed and the rated speed, the energy production become 22 kW and 50 kW respectively.

Table 3.1: Specification of 50 kW wind Turbine

Parameters	Specification	Parameters	Specification
Connection		Nacelle	
Frequency	60 Hz	Cover material	Aluminium
Voltage	480 V	Mass	3990 kgs
Performance		Main Bearing	
Cut-in Wind speed	3 m/s	Number	2
Wind Speed for max power	15 m/s		
Cut-out wind speed	25 m/s		
Rated electric power	66 kW		
Tower		Operation Brake	
Type	Galvanized 3 legged, bolted lattice	Type	Disk Brake
Tower Height	24.8 m	Location	Turbine shaft
		Operation	Hydraulic

Foundation		Gear Box	
Type	Concrete	Number of Stage	2
Anchor Bolts	Certified ASTM A - A - 193	Gear Ratio	1:27
	-Grade B7		
Turbine		Generator	
Type	3 blades, Stall Regulated	Type	Asynchronous with Squirrel Cage
Diameter	15 m	Rated Electrical Power	50 kW
Swept Area	177 m <sup>2</sup>	Rated speed	1800 @ 60 Hz
Rotational speed	65 rpm		
Tilt angle	0 Degree		
Cone Angle	6 Degree		
Mass	2420 kgs		
Blades		Aerodynamics Brakes	
Material	Epoxy/ glass Fibre	Type	Spoilers
Length	7.2 m		
Aero foil	NREL, Thick Series, Modified		
Pitch	Fixed		

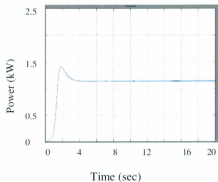
Table 3.2: Parameters of 50 kW WECS Used for Simulation.

Parameters	Value
Turbine	
Nominal Mechanical Output Power	50kW
Base Power of Electrical generator	50 kW
Base Wind Speed	8 m/s
Pitch angle	0 Degree
50 kW generator	
Stator Resistance	0.05963 $\Omega$
Stator Inductance	0.633 mH
Rotor Resistance	0.03281 $\Omega$
Rotor Inductance	0.633 mH
Mutual Inductance	27.42 mH
Inertia	1.3 kg-m <sup>2</sup>
Pole Pair	2

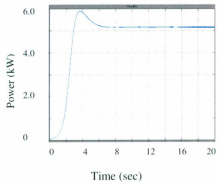
The Simulink models of a PMG based WT and an induction generator based WT are given in Appendix A (Figure A-1 to Figure A-4). The inputs of the WT are the wind speed, pitch angle and the generator speed. The pitch angle is kept as zero in this case and the generator speed is fed back from the PMG or induction generator. The three phase voltage and current are measured using a measurement block at the generator output

terminal. Using voltage and current, the real power has been calculated. The output powers from the WECS for different wind speeds are given below.

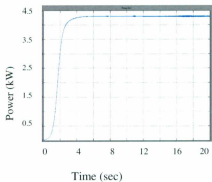
$V_s = 5 \text{ m/s}; P_{out} = 1.2 \text{ kW}$



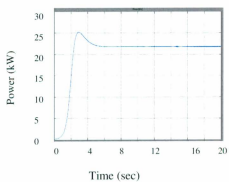
$V_s = 7 \text{ m/s}; P_{out} = 5.1 \text{ kW}$



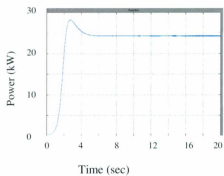
$V_s = 6 \text{ m/s}; P_{out} = 4.3 \text{ kW}$



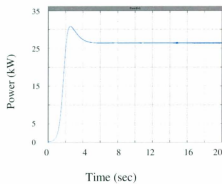
$V_s = 8 \text{ m/s}; P_{out} = 22 \text{ kW}$



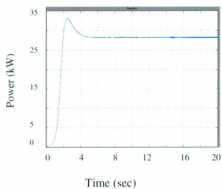
$V_s = 9 \text{ m/s}; P_{out} = 24 \text{ kW}$



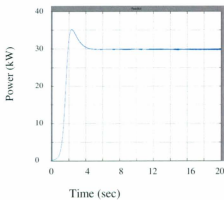
$V_s = 10 \text{ m/s}; P_{out} = 26.2 \text{ kW}$



$V_s = 11 \text{ m/s}; P_{out} = 27.5 \text{ kW}$



$V_s = 12 \text{ m/s}; P_{out} = 30 \text{ kW}$



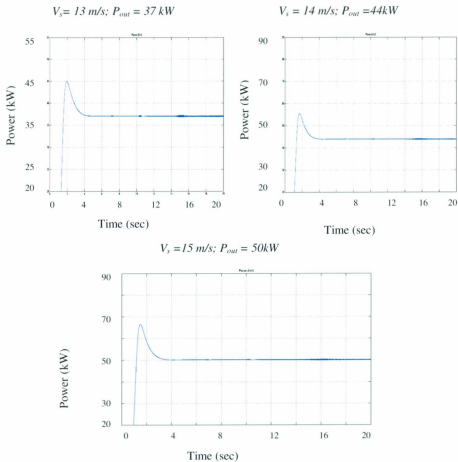


Figure 3.13: Power generated by the 50kW generator at different wind speeds.

It can be said from Figure 3.13 that when the wind speed belongs to the range from the cut-in speed to below 8 m/s, the wind turbine generates a small amount of power but after 8 m/s it generates more power. The generated speed has been recorded as 0.94 pu shown

in Figure 3.14 below. To have the generator speed in pu, the generator speed from the generator is divided by the rated generator speed and the gear box ratio.

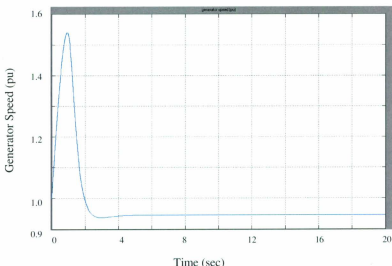


Figure: 3.14 Generator speed in per unit value

### 3.5 Summary

This chapter illustrates all the wind energy conversion systems that we have used in our design. The mechanical parts of the WECS, the machines, transformer and capacitor bank have been explained with their working principles and their indispensabilities for being used in this system. It is intended to develop the steady state models of the WECS and to determine how those models react with different wind speeds, aiming to compare the power curves found from simulation results and the same provided by the manufacturers. Figure 3.15 elucidates this comparison.

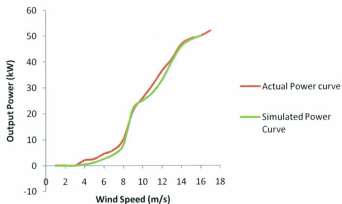


Figure 3.15: Power versus Wind Speed Curve of 50kW Wind Turbine.

It is quite clear from the figure 3.15 that the generated WECS model almost resembles the actual wind turbine, and exhibits almost identical characteristics corresponding to those the manufacturer has provided. Wind speed below 8 m/s generates a small amount power and after that a higher amount of power is produced.

## Chapter 4

### **Modeling of Photovoltaic System, Battery and Diesel Generator**

A Wind-PV-Diesel system has greater reliability for electricity production than a Wind-only system. Diesel engine production is independent of atmospheric conditions. This fact provides greater flexibility, higher efficiency and lower costs for the same energy quantity produced [45]. Also, Wind-PV-Diesel systems, compared with Diesel-only systems, provide a reduction of the operation costs and air pollutants emitted to the atmosphere [46]. Though St. John's is not considered an ideal location for a photovoltaic system (PV) installation, it has been decided to perform modeling and simulation of a PV system so that we can use this model later for another suitable location by changing only the solar irradiance. As the wind speed and solar irradiance are not constant throughout the year, it is necessary to have diesel generators to provide a constant power supply to the load. To store excess energy produced by renewable sources, a storage component (battery) is also necessary. The following sections provide details and models of PV, battery and diesel generators.

#### **4.1 Photovoltaic Modules**

##### **4.1.1 Introduction**

The history of PV starts when a French physicist, Edmund Becquerel, discovered the first photovoltaic effect in 1839, when he illuminated a metal electrode in an electrolytic

solution [47]. Thirty-seven years later the British physicist, William Adams, with his student, Richard Day, discovered a photovoltaic material, selenium, and made solid cells with 1~2% efficiency, which were soon widely adopted in the exposure meters of cameras [47]. In 1954 the first generation of semiconductor silicon-based PV cells was born, with an efficiency of 6% [48], and adopted in space applications. Today, the production of PV cells follows an exponential growth curve since technological advancement of the late '80s which has started to rapidly improve efficiency and reduce cost.

This chapter discusses the fundamentals of PV cells and modeling of a PV cell using an equivalent electrical circuit. Models of a battery and diesel generator are also presented. The models are implemented using Matlab to study characteristics and system dynamics.

#### **4.1.2 Photovoltaic Cell**

Light photons with energy higher than the band-gap energy of PV material can make electrons in the material break free from atoms that hold them and create hole-electron pairs, as shown in Figure 4.1.1. These electrons, however, will soon fall back into holes, causing charge carriers to disappear. If a nearby electric field is provided, those in the conduction band can be continuously swept away from holes toward a metallic contact where they will emerge as an electric current. The electric field within the semiconductor itself at the junction between two regions of crystals of different type is called a p-n junction [47].

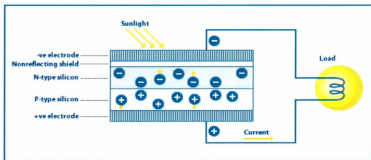


Figure 4.1.1: Illustration of the p-n junction of PV cell [47]

The PV cell has electrical contacts on its top and bottom to capture the electrons, as shown in Figure 4.1.1. When the PV cell delivers power to the load, the electrons flow out of the n-side into the connecting wire, through the load, and back to the p-side where they recombine with holes [47]. Note that conventional current flows in the opposite direction from electrons.

#### 4.1.3 Modeling a PV Cell

The use of equivalent electric circuits makes it possible to model characteristics of a PV cell. The method used here is implemented in Matlab programs for simulations. The same modeling technique is also applicable for modeling a PV module.

##### 4.1.3.1 The Simplest Model

The simplest model of a PV cell is shown as an equivalent circuit below, that consists of an ideal current source in parallel with an ideal diode. The current source represents the

current generated by photons (often denoted as  $I_{ph}$  or  $I_L$ ), and its output is constant under constant temperature and constant incident radiation of light.

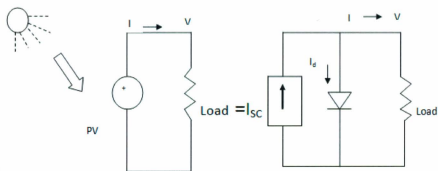


Figure 4.1.2: PV cell with a load and its simple equivalent circuit [47]

There are two key parameters frequently used to characterize a PV cell. Shorting together the terminals of the cell, as shown in Figure 4.1.3 (a), the photon generated current will follow out of the cell as a short-circuit current ( $I_{sc}$ ). Thus,  $I_{ph} = I_{sc}$ . As shown in Figure 4.1.3 (b), when there is no connection to the PV cell (open-circuit), the photon generated current is shunted internally by the intrinsic p-n junction diode. This gives the open circuit voltage ( $V_{oc}$ ). The PV module or cell manufacturers usually provide the values of these parameters in the datasheets.

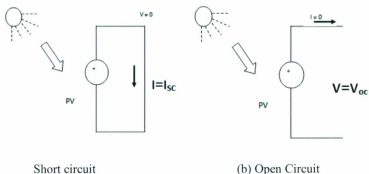


Figure 4.1.3: Diagrams showing a short-circuit and an open-circuit condition [47]

The output current ( $I$ ) from the PV cell is found by applying the Kirchoff's current law (KCL) on the equivalent circuit shown in Figure 4.13:

$$I = I_{sc} - I_d \quad (4.1.1)$$

where,  $I_{sc}$  is the short-circuit current that is equal to the photon generated current, and  $I_d$  is the current shunted through the intrinsic diode. The diode current  $I_d$  is given by Shockley's diode equation:

$$I_d = I_o (e^{qV_d/kT} - 1) \quad (4.1.2)$$

where,  $I_o$  is the reverse saturation current of diode ( $A$ ),

$q$  is the electron charge ( $1.602 \times 10^{-19} C$ ),

$V_d$  is the voltage across the diode ( $V$ ),

$k$  is the Boltzmann's constant ( $1.381 \times 10^{-23} J/K$ ),

$T$  is the junction temperature in Kelvin ( $K$ ).

Replacing  $I_d$  of the equation (4.1.1) by the equation (4.1.2) gives the current-voltage relationship of the PV cell.

$$I = I_{sc} - I_o(e^{qV_d/kt} - 1) \quad (4.1.3)$$

where  $V$  is the voltage across the PV cell, and  $I$  is the output current from the cell. The reverse saturation current of diode ( $I_o$ ) is constant under a constant temperature, and is found by setting the open-circuit condition as shown in Figure 4.1-4 (b). Using the equation (4.1.3), let  $I = 0$  (no output current) and solve for  $I_o$ .

$$0 = I_{sc} - I_o(e^{qV_d/kt} - 1) \quad (4.1.4)$$

$$I_{sc} = I_o(e^{qV_d/kt} - 1) \quad (4.1.5)$$

$$I_o = \frac{I_{sc}}{(e^{qV_d/kt} - 1)} \quad (4.1.6)$$

To a very good approximation, the photon generated current, which is equal to  $I_{sc}$ , is directly proportional to the irradiance, and the intensity of illumination on the PV cell [49]. Thus, if the value  $I_{sc}$  is known from the datasheet, under standard test conditions,  $G_o=1000W/m^2$  at the air mass ( $AM$ ) = 1.5, then the photon generated current at any other irradiance,  $G$  ( $W/m^2$ ), is given by:

$$I_{sc}I_G = \left(\frac{G}{G_o}\right) I_{sc}I_{G_o} \quad (4.1.7)$$

Figure 4.1.4 shows the current and voltage relationship (often called an  $I$ - $V$  curve) of an ideal PV cell simulated by Matlab using the simplest equivalent circuit model. The discussion of Matlab simulations is presented in Section 4.1.4. The PV cell output is both limited by the cell current and the cell voltage, and it can only produce power with any combination of current and voltage on the  $I$ - $V$  curve. It also shows that the cell current is proportional to the irradiance.

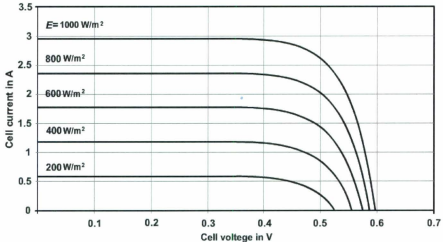


Figure 4.1.4: I-V plot of ideal PV cell under five different levels of irradiance (25°C)

#### 4.1.3.2 Two Diode Solar Cell Model

There are a few things that have not been taken into account in the simple model that will affect the performance of a PV cell in practice.

##### a) Series Resistance

In a practical PV cell, there is a series of resistance in a current path through the semiconductor material, the metal grid, contacts, and current collecting bus [50]. These resistive losses are lumped together as a series resistor ( $R_s$ ). Its effect becomes very conspicuous in a PV module that consists of many series-connected cells, and the value of resistance is multiplied by the number of cells.

##### b) Parallel Resistance

This is also called shunt resistance. It is a loss associated with a small leakage of current through a resistive path parallel to the intrinsic device [50]. This can be represented by a

parallel resistor ( $R_p$ ). Its effect is much less conspicuous in a PV module compared to the series resistance, and it will only become noticeable when a number of PV modules are connected in parallel for a larger system.

### c) Recombination

Recombination in the depletion region of PV cells provides non-ohmic current paths parallel to the intrinsic PV cell [50] [51]. As shown in Figure 4.1.5, this can be represented by the second diode ( $D2$ ) in the equivalent circuit.

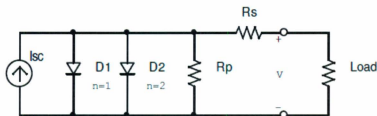


Figure 4.1.5: More accurate equivalent

Summarizing these effects, the current-voltage relationship of the PV cell is written as:

$$I = I_{sc} - I_{01} \left[ e^{q \left( \frac{V+I R_s}{kT} \right)} - 1 \right] - I_{02} \left[ e^{q \left( \frac{V+I R_s}{2kT} \right)} - 1 \right] - \left( \frac{V+I R_s}{R_p} \right) \quad (4.1.8)$$

It is possible to combine the first diode ( $D1$ ) and the second diode ( $D2$ ) and rewrite the equation (4.1.8) in the following form:

$$I = I_{sc} - I_0 \left[ e^{q \left( \frac{V+I R_s}{n k T} \right)} - 1 \right] - \left( \frac{V+I R_s}{R_p} \right) \quad (4.1.9)$$

where,  $n$  is known as the "ideality factor" (" $n$ " is sometimes denoted as " $A$ ") and takes the value between one and two [51].

#### 4.1.4 Photovoltaic Module

A single PV cell produces an output voltage of less than 1V, about 0.6V for crystalline silicon (Si) cells. Thus, a number of PV cells are connected in series to achieve a desired output voltage. When series-connected cells are placed in a frame, it is called a module. Most commercially available PV modules with crystalline-Si cells have either 36 or 72 series-connected cells. A 36-cell module provides a voltage suitable for charging a 12V battery, and similarly a 72-cell module is appropriate for a 24V battery. This is because most PV systems used to have backup batteries; however, today many PV systems do not use batteries; for example, grid-tied systems. Furthermore, the advent of high efficiency DC-DC converters has alleviated the need for modules with specific voltages. When the PV cells are wired together in series, the current output is the same as the single cell, but the voltage output is the sum of each cell voltage, as shown in Figure 4.1.6.

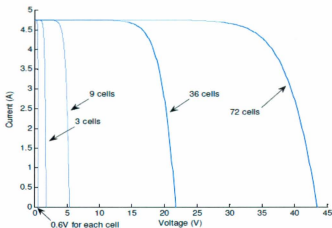


Figure 4.1-6: PV cells are connected in series to make up a PV module

#### 4.1.5 Modeling a PV Module by Matlab

Multiple modules can be wired together in series or parallel to deliver the voltage and current level needed. The group of modules is called an array.

**SG17524** (175W) PV module, pictured in Figure 4.1-7, is chosen for a Matlab simulation model. The module is made of 72 multi-crystalline silicon solar cells in series and provides 175W of nominal maximum power [<http://www.solardesigntool.com>]. Table 4.1-1 shows its electrical specification.

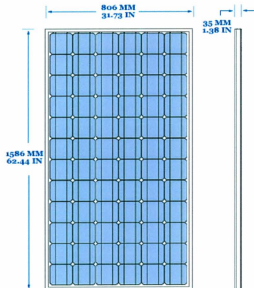


Figure 4.1-7: Picture of SG17524 (175W) PV module [<http://www.solardesigntool.com>]

Table 4.1 Specification of Solar Panel

Electrical Characteristics	Specification
Maximum Power ( $P_{max}$ )	175W
Voltage at $P_{max}$ ( $V_{mp}$ )	35.6V
Current at $P_{max}$ ( $I_{mp}$ )	4.77A
Open-circuit voltage ( $V_{oc}$ )	44V
Short-circuit current ( $I_{sc}$ )	5.1A
Temperature coefficient of $I_{sc}$	0.028% / °C
Temperature coefficient of $V_{oc}$	-0.344% / °C
Temperature coefficient of power	-0.482% / °C
NOCT	42°C +/- 1°C

The strategy of modeling a PV module is no different from modeling a PV cell. It uses the same PV cell model. The parameters are the same, but only a voltage parameter (such as the open-circuit voltage) is different and must be divided by the number of cells.

The study done by Walker [52] of University of Queensland, Australia, uses the electric model with moderate complexity, shown in Figure 4.1-9, and provides fairly accurate results. The model consists of a current source ( $I_{sc}$ ), a diode ( $D$ ), and a series resistance ( $R_s$ ). The effect of parallel resistance ( $R_p$ ) is very small in a single module; thus, the model does not include it. To make a better model, it also includes temperature effects

on the short-circuit current ( $I_{sc}$ ) and the reverse saturation current of diode ( $I_0$ ). It uses a single diode with the diode ideality factor ( $n$ ) set to achieve the best  $I$ - $V$  curve match.

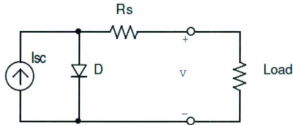


Figure 4.1.8: Equivalent circuit used in the Matlab simulations

Since it does not include the effect of parallel resistance ( $R_p$ ), letting  $R_p = \infty$  in the equation (4.1.8) gives the equation [52] that describes the current-voltage relationship of the PV cell, and it is shown below.

$$I = I_{sc} - I_0 \left[ e^{q \left( \frac{V + IR_s}{nkT} \right)} - 1 \right] \quad (4.1.10)$$

where,  $I$  is the cell current (the same as the module current),

$V$  is the cell voltage = {module voltage}  $\div$  {# of cells in series},

$T$  is the cell temperature in Kelvin (K).

First, calculate the short-circuit current ( $I_{sc}$ ) at a given cell temperature ( $T$ )

$$I_{sc|T} = I_{sc|T_{ref}} \left[ 1 + a(T - T_{ref}) \right] \quad (4.1.11)$$

where,  $I_{sc}$  at  $T_{ref}$  is given in the datasheet (measured under irradiance of 1000W/m<sup>2</sup>),

$T_{ref}$  is the reference temperature of PV cell in Kelvin (K), usually 298K (25°C),

$a$  is the temperature coefficient of  $I_{sc}$  in percent change per degree temperature, also given in the datasheet.

The short-circuit current ( $I_{sc}$ ) is proportional to the intensity of irradiance, thus  $I_{sc}$  at a given irradiance ( $G$ ) is:

$$I_{sc}I_G = \left(\frac{G}{G_0}\right) I_G I_{G0} \quad (4.1.12)$$

where,  $G_0$  is the nominal value of irradiance, which is normally  $1\text{ kW/m}^2$ .

The reverse saturation current of diode ( $I_0$ ) at the reference temperature ( $T_{ref}$ ) is given by the equation (2.6) with the diode ideality factor added:

$$I_0 = \frac{I_{sc}}{\left(e^{qV_{oc}/nkT} - 1\right)} \quad (4.1.13)$$

The reverse saturation current ( $I_0$ ) is temperature dependent and the  $I_0$  at a given temperature ( $T$ ) is calculated by the following equation [52]:

$$I_0I_T = I_0I_{Tref} \cdot \left(\frac{T}{T_{ref}}\right)^{\frac{3}{n}} \cdot e^{-\frac{qE_g}{nk} \left(\frac{1}{T} - \frac{1}{T_{ref}}\right)} \quad (4.1.14)$$

The diode ideality factor ( $n$ ) is unknown and must be estimated. It takes a value between one and two; the value of  $n=1$  (for the ideal diode) is used.

The series resistance ( $R_s$ ) of the PV module has a large impact on the slope of the  $I$ - $V$  curve near the open-circuit voltage ( $V_{oc}$ ); hence, the value of  $R_s$  is calculated by evaluating the slope  $dI/dV$  of the  $I$ - $V$  curve at the  $V_{oc}$  [52]. The equation for  $R_s$  is derived by differentiating the equation (4.1.10) and then rearranging it in terms of  $R_s$ .

$$I = I_{sc} - I_0 \left[ e^{q\left(\frac{V+IR_s}{nkT}\right)} - 1 \right] \quad (4.1.15)$$

$$dI = 0 - I_0 \cdot q \left( \frac{dV + R_s dI}{nkT} \right) \cdot e^{q\left(\frac{V+IR_s}{nkT}\right)} \quad (4.1.16)$$

$$R_s = -\frac{dI}{dV} - \frac{nkT/q}{I_o \cdot e^{q(V+IR_s)/nkT}} \quad (4.1.17)$$

Then, evaluate the equation (4.1.17) at the open circuit voltage that is  $V=V_{oc}$  (also let  $I=0$ ).

$$R_s = \left. \frac{dV}{dI} \right|_{V_{oc}} - \frac{nkT/q}{I_o \cdot e^{\frac{qV_{oc}}{nkT}}} \quad (4.1.18)$$

where,  $\left. \frac{dV}{dI} \right|_{V_{oc}}$  is the slope of the  $I$ - $V$  curve at the  $V_{oc}$  (use the  $I$ - $V$  curve in the datasheet then divide it by the number of cells in series),

$V_{oc}$  is the open-circuit voltage of the cell (found by dividing  $V_{oc}$  in the datasheet by the number of cells in the series).

#### 4.1.6 Maximum Power Point Tracker

A PV module can produce the power at a point, called an operating point, anywhere on the  $I$ - $V$  curve. The coordinates of the operating point are the operating voltage and current. There is a unique point near the knee of the  $I$ - $V$  curve, called a maximum power point (MPP), at which the module operates with the maximum efficiency and produces the maximum output power. It is possible to visualize the location of the MPP by fitting the largest possible rectangle inside of the  $I$ - $V$  curve, and its area equals to the output power, which is a product of voltage and current. The amount of power produced by the PV module varies greatly depending on its operating condition. It is important to operate the system at the MPP of the PV module in order to exploit the maximum power from the module.

When a PV module is directly coupled to a load, the PV module's operating point will be at the intersection of its  $I-V$  curve and the load line, which is the  $I-V$  relationship of load. In other words, the impedance of load dictates the operating condition of the PV module. In general, this operating point is seldom at the PV module's MPP; thus, it is not producing the maximum power. A study shows that a direct-coupled system utilizes a mere 31% of the PV capacity [53]. A PV array is usually oversized to compensate for a low power yield during winter months. This mismatching between a PV module and a load requires further over-sizing of the PV array and thus increases the overall system cost. To mitigate this problem, a maximum power point tracker (MPPT) can be used to maintain the PV module's operating point at the MPP. MPPTs can extract more than 97% of the PV power when properly optimized [54].

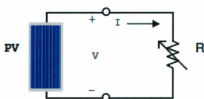


Figure4.1.9: PV module is directly connected to a (variable) resistive load [54]

In this work the solar panel is simulated with MPPT. To do so, first we have collected the information about the short circuit current, maximum power point current, open circuit voltage, maximum power point voltage, thermal coefficient of the short circuit current and the thermal coefficient of the open circuit voltage (table 4.1) from the data sheet. Then we modeled the solar panel using a function of the form  $I = f(V)$ . Some constants,

solar irradiance and ambient temperature play a role in the function. The inputs of the model are solar irradiance ( $G$ ), ambient temperature ( $T_a$ ) and voltage. By keeping solar irradiance and ambient temperature steady and changing voltage 0 to open circuit voltage, we get the  $I$ - $V$  characteristics of the solar panel. By connecting the model to a complex circuit we get the electrical behaviour of the solar panel. The following figure shows Simulink model of a solar panel.

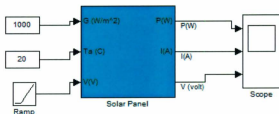
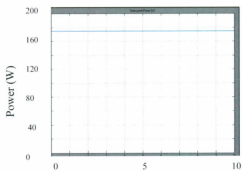


Figure 4.1.10: Solar panel model in Simulink

The subsystem model is included in appendix A (Figure A-5 to Figure A-6).

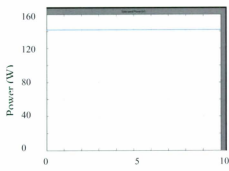
We have observed the effect of solar irradiance on output power of the module. The following (Figure 14.1.11) shows the effect of solar irradiance.

$G = 1000 \text{ W/m}^2$ ;  $P_{pv} = 175 \text{ W}$



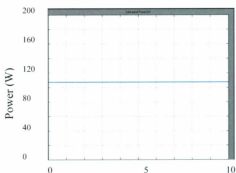
Time (sec)

$G = 800 \text{ W/m}^2$ ;  $P_{pv} = 142 \text{ W}$



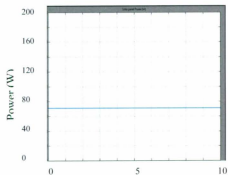
Time (sec)

$G = 600 \text{ W/m}^2$ ;  $P_{pv} = 108 \text{ W}$



Time (sec)

$G = 400 \text{ W/m}^2$ ;  $P_{pv} = 72 \text{ W}$



Time (sec)

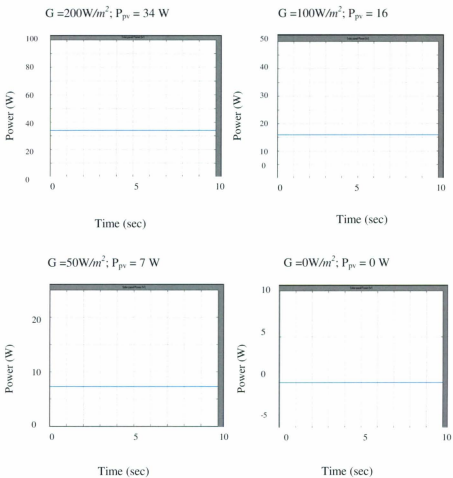


Figure 4.1.11: Power generation in a solar panel at different solar irradiances.

From the above figure it can be said that at zero irradiance the output power from the solar panel is zero. In the range above zero to  $500 \text{ W/m}^2$  the solar panel generates less power, but above  $500 \text{ W/m}^2$  the panel generates more power, and the rated power obtained at  $G = 1000 \text{ W/m}^2$ . From the above effect it is clear that if solar irradiance is low, the solar panel generates less power and it produces more power if there is high irradiance.

#### **4.1.7 DC-DC Converter**

The heart of MPPT hardware is a switch-mode DC-DC converter. It is widely used in DC power supplies and DC motor drives for the purpose of converting unregulated DC input into a controlled DC output at a desired voltage level [17]. MPPT uses a DC-DC converter for a different purpose: regulating the input voltage at the PV MPP and providing load matching for the maximum power transfer. In our system a DC-DC boost converter is used.

##### **4.1.7.1 Boost Converter Analysis**

A simple boost converter consists of an inductor, a switch, a diode, and a capacitor, as shown in Figure 4.1.12 [55]. The boost converter circuit can be divided into two modes. Mode 1 begins when the switch SW is turned on at  $t = T_{on}$  as shown in Figure 4.1.13. The input current which rises flows through inductor  $L$  and switch SW. During this mode, energy is stored in the inductor. Mode 2 begins when the switch is turned off at  $t = T_{off}$ . The current that was flowing through the switch would now flow through inductor  $L$ , diode  $D$ , capacitor  $C$ , and load  $R$  as shown in Figure 4.1.14. The inductor current falls

until the switch is turned on again in the next cycle. Energy stored in the inductor is then transferred to the load. Therefore, the output voltage is greater than the input voltage and is expressed as [56]:

$$V_{out} = \frac{1}{1-D} V_{in} \quad (4.1.19)$$

where,  $V_{out}$  is the output voltage,  $D$  is duty cycle, and  $V_{in}$  is input voltage which in this case will be the solar panel voltage.

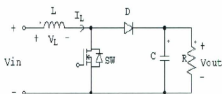


Figure 4.1.12: Circuit diagram of boost converter

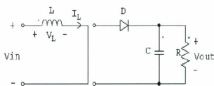


Figure 4.1.13: Mode 1-Circuit diagram of boost converter during  $T_{on}$

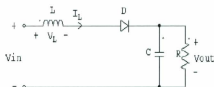


Figure 4.1.14: Mode 2-Circuit diagram of boost converter during  $T_{off}$

In order to operate the converter in continuous conduction mode (CCM), the inductance is calculated so that the inductor current  $I_L$  flows continuously and never falls to zero, as shown in Figure 4.1.15. Thus,  $L$  is given by [56]:

$$L_{min} = \frac{(1-D)^2 DR}{2f} \quad (4.1.20)$$

where  $L_{min}$  is the minimum inductance,  $D$  is duty cycle,  $R$  is output resistance, and  $f$  is the switching frequency of switch SW.

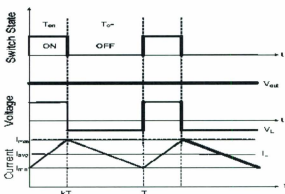


Figure 4.1.15: Waveforms for boost converter operating under CCM [56]

The output capacitance to give the desired output voltage ripple is given by [56]:

$$C_{min} = \frac{D}{RfV_r} \quad (4.1.21)$$

where  $C_{min}$  is the minimum capacitance,  $k$  is duty cycle,  $R$  is output resistance,  $f$  is switching frequency of switch SW, and  $V_r$  is output voltage ripple factor.  $V_r$  can be expressed as [56]:

$$V_r = \frac{\Delta V_{out}}{V_{out}} \quad (4.1.22)$$

## **4.2 Battery Bank**

Batteries convert the stored chemical energy into electrical energy. Battery applications are many; that is the reason that they are available in different sizes, voltage, amp-hour ratings, liquid or gel, vented or non-vented, etc. [47]. The battery bank is supposed to be designed so the batteries do not discharge more than 50% of their capacity on a regular basis. Discharging up to 80% is acceptable on a restricted basis, such as an extended utility outage. Completely discharging a battery can reduce its effective life or damage it [47].

The charged period of the battery bank could differ depending upon the availability of other charging sources, the nature of the load and other factors. If renewable energy (wind, solar, etc.) powers the system, the charged period of the battery depends on the resource variations among others. However, the batteries are not just used for storage; they are also a buffer for all the charging energy which is brought into them [47].

There are mainly four types of battery [57]: Lead-Acid, Lithium-Ion, Nickel-Cadmium and Nickel-Metal-Hydrid. A model of a Battery is shown in the figure 4.2.1 [57]:

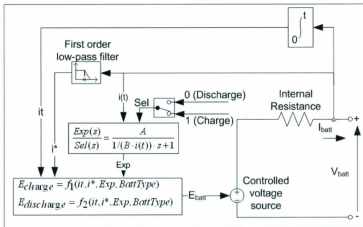


Figure 4.2.1 Model of a battery [57]

Based on its discharge characteristics, the parameters of the model can be modified to represent a particular battery type.

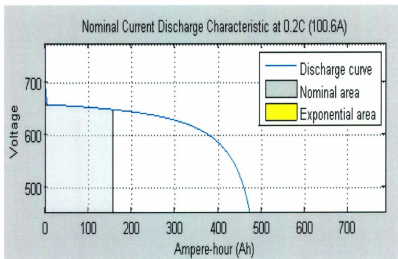


Figure 4.2.2 Discharge characteristics of Lead-Acid battery [57]

The first section represents the exponential voltage drop when the battery is charged. Depending on the battery type, this area is more or less a straight line. The second section represents the charge that can be extracted from the battery until the voltage drops below the battery nominal voltage. Finally, the third section represents the total discharge of the battery, when the voltage drops rapidly.

When the battery current is negative, the battery will recharge following a charge characteristic as shown in figure 4.2.3. The charge characteristics also depend upon battery type.

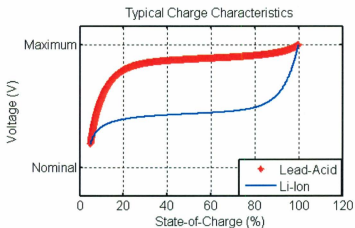


Figure 4.2.3: Charge characteristics of Li-Ion and lead acid battery [57]

The discharge and charge model of the Lead Acid battery can be characterized by the following two equations 4.2.1, 4.2.2 [57]:

Discharge model ( $i^* > 0$ )

$$f_1(it, i^*, i, Exp) = E_0 - K \frac{Q}{Q-it} \cdot i^* - K \frac{Q}{Q-it} \cdot it + L^{-1} \left( \frac{Exp(s)}{Sel(s)} \cdot 0 \right) \quad (4.2.1)$$

Charge model ( $i^* < 0$ )

$$f_2(it, i^*, i, Exp) = E_0 - K \cdot \frac{Q}{it+0.1 \cdot Q} \cdot i^* - K \cdot \frac{Q}{Q-it} \cdot it + L^{-1} \left( \frac{Exp(s)}{Sel(s)} \cdot \frac{1}{s} \right) \quad (4.2.2)$$

where,

$E_{Bat}$  = Nonlinear voltage (V)

$E_0$  = Constant voltage (V)

$Exp(s)$  = Exponential zone dynamics (V)

$Sel(s)$  = Represents the battery mode.  $Sel(s) = 0$  during battery discharge,  $Sel(s) = 1$  during battery charging.

$K$  = Polarization constant ( $Ah^{-1}$ ) or Polarization resistance (Ohms)

$i^*$  = Low frequency current dynamics (A)

$i$  = Battery current (A)

$i_t$  = Extracted capacity (Ah)

$Q$  = Maximum battery capacity (Ah)

The details of the battery is given in the following table 4.2.

Table 4.2: Specification of battery

Parameters	Specifications
Battery type	12 V, 6 cell Deep Cycle
Weight dry	100 kg
Weight wet	124 kg
Plates per cell	11
Cycles	3300
Capacity at 100 hr rate	503 AH
Capacity at 20 hr rate	357AH

### 4.3 Diesel Engine

Diesel engines are a common part of our everyday lives and are widely used in automobiles and other applications. Diesel prime-movers are attractive for applications requiring fast responding backups at the time of peak load demands, or where local demand for additional power necessitates augmentation of a power source. The dead time of the diesel engine is a non-linear function of the operating conditions, and also of the engine speed. This significantly degrades the performance of the prime mover under disturbances, although certain PID schemes presently in use give an acceptable performance [58].

### **4.3.1 Speed Control of Diesel Engine**

Speed control of power generation plants driven by diesel prime-movers is difficult because of the presence of a dead time and changes in parameters. A typical diesel engine model describes the fuel consumption rate as a function of speed, and mechanical power as the output of the engine. It is usually modeled by a simple first order relating the fuel consumption (fuel rack position) to the engine's mechanical power [14]. The task of the governor is to adjust the fuel flow and then regulate the input of the engine and the generator so as to provide the required power to meet any change in the load. The presence of dead-time between the actuator fuel injection and the production of mechanical torque is a very important characteristic of the diesel engine. There are also system parameter uncertainties which, together with the varying dead time, significantly degrade the performance of the prime mover, especially in case of a load. A diesel engine is a nonlinear system together with a nonlinear, time-varying dead time between the injection and production of the mechanical torque. It is commonly controlled with a PI controller to prevent steady-state error in speed.

#### **4.3.1.1 Modeling of Diesel Engines**

There are many methods for modeling a diesel engine. Desired and actual speeds are the two inputs to the engine block and the mechanical power is the output from the block which will further be coupled to the synchronous generator. The engine characteristics are based on two transfer functions as follows [57].

Controller transfer function,

$$H_c = \frac{(1+T_3s)K}{(1+T_1s+T_1T_2s^2)} \quad (4.3.1)$$

actuator transfer function,

$$H_a = \frac{(1+T_4s)}{[s(1+T_5s)(1+T_6s)]} \quad (4.3.2)$$

where,  $K$  is the regulator gain,  $T_1$ ,  $T_2$  and  $T_3$  are the regulator time constants and  $T_4$ ,  $T_5$  and  $T_6$  are the actuator time constants.

### 4.3.2 Diesel Generators

Diesel generators, also known as Gensets, provide reliable power when properly maintained. The initial cost of a complete diesel power system is also relatively low. They can be easily transported and are low-tech which aids in their reliability and ensures ease of operation. So far, they sound like the ideal solution for the given application, but where they fall down is in the environmental and running costs. Standard diesel generators are fitted with synchronous generators and consequently are controlled to run at a constant speed to guarantee constant electrical frequency. Due to the poor efficiency at low load, most engine manufacturers recommend their plants be operated at no lower than 40% of rated capacity in order to prolong the diesel engine lifetime.

#### 4.3.2.1 Modeling of Diesel Generator

Like the asynchronous machine, the synchronous machines operate in either generator or motor mode depending on the sign of the mechanical power applied. For negative mechanical power, this machine will run as a generator. The electrical part of the machine is represented by a sixth-order state-space model. This generator model takes the dynamics of the stator, field and damper winding into account. Moreover, all the rotor

parameters and electrical quantities are viewed from the stator, and the equivalent circuit of the model is expressed in rotor reference frame (d-q frame). The equivalent electrical part of this machine in d-q reference frame is depicted in figure 4.3.1 [57].

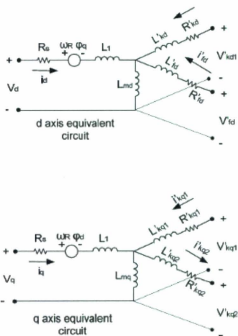


Figure 4.3.1: Diesel generator equivalent circuit

The emf expressions results from the d-q frame equivalent circuits can be shown below.

$$V_d = R_s i_d + \frac{d}{dt} \varphi_d - \omega_R \varphi_q \quad (4.3.3)$$

$$V_q = R_s i_q + \frac{d}{dt} \varphi_q + \omega_R \varphi_d \quad (4.3.4)$$

$$V'_{fd} = R'_{fd} i'_{fd} + \frac{d}{dt} \varphi'_{fd} \quad (4.3.5)$$

$$V'_{kd} = R'_{kd}i'_{kd} + \frac{d}{dt}\phi'_{kd} \quad (4.3.6)$$

$$V'_{kq1} = R'_{kq1}i'_{kq1} + \frac{d}{dt}\phi'_{kq1} \quad (4.3.7)$$

$$V'_{kq2} = R'_{kq2}i'_{kq2} + \frac{d}{dt}\phi'_{kq2} \quad (4.3.8)$$

where,  $V_d$  and  $V_q$  are d and q axis voltages,  $R_s$  is the stator resistance,  $i_d$  and  $i_q$  are d and q axis currents,  $\phi_d$  and  $\phi_q$  are d and q axis fluxes,  $\omega_r$  is the rotor rotational speed,  $V'_{fd}$ ,  $R'_{fd}$ ,  $i'_{fd}$  and  $\phi'_{fd}$  are d-axis field winding voltage, resistance, current and flux respectively. In the same way  $V'_{kd}$ ,  $R'_{kd}$ ,  $i'_{kd}$  and  $\phi'_{kd}$  are d-axis damper winding voltage, resistance, current and flux respectively. In q-axis there is no field quantity. Rather two damper quantities exist. Therefore,  $V'_{kq}$ ,  $R'_{kq}$ ,  $i'_{kq}$  and  $\phi'_{kq}$  are q-axis damper winding voltage, resistance, current and flux. Subscript 1 and 2 represent the first and second damper windings.

All the flux components depending on the d-q axis inductances and currents are expressed as follows.

$$\phi_d = L_d i_d + L_{md}(i'_{fd} + i'_{kd}) \quad (4.3.9)$$

$$\phi_q = L_q i_q + L_{mq} i'_{kq} \quad (4.3.10)$$

$$\phi'_{fd} = L'_{fd} i'_{fd} + L_{mq}(i_d + i'_{kd}) \quad (4.3.11)$$

$$\phi'_{kd} = L'_{kd} i'_{kd} + L_{mq}(i_d + i'_{fd}) \quad (4.3.12)$$

$$\phi'_{kq1} = L'_{kq1} i'_{kq1} + L_{mq} i_q \quad (4.3.13)$$

$$\phi'_{kq2} = L'_{kq2} i'_{kq2} + L_{mq} i_q \quad (4.3.14)$$

The synchronous machine block computes the mechanical characteristics described by the following equations:

$$\Delta\omega(t) = \frac{1}{2H} \int_0^t (T_m - T_e) dt - K_d \Delta\omega(t) \quad (4.3.15)$$

$$\omega(t) = \Delta\omega(t) + \omega_0 \quad (4.3.16)$$

where  $\Delta\omega$  is the speed variation with respect to the speed of operation,  $H$  is the inertia constant,  $T_m$  and  $T_e$  are the mechanical and electromagnetic torque respectively,  $K_d$  is the damping factor,  $\omega(t)$  is the mechanical speed of the rotor and  $\omega_0$  is the speed of operation.

In order to model the synchronous generator in the Simulink environment and to measure the active power from it, an excitation system, and a per unit fundamental synchronous machine block are coupled together. The arrangement is revealed in figure 4.3.2. The generator specifications are presented in table 4.3 and 4.4.

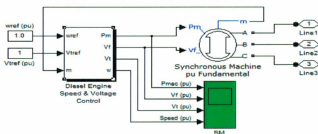


Figure 4.3.2: Simulink model of the Diesel Generator

The diesel engine and excitation system's parameters are specified in table 4.5 and table 4.6, and their SimPower subsystem model is depicted in figure 4.3.3. The subsystem model of the diesel engine are presented in appendix A.

Table 4.3 Diesel generator system parameters for 150 kW generator.

Parameters	Values	Parameters	Values
$R_s$	0.3516 pu	Lkd	1.5523 pu
$L_l$	0.07 pu	Rkq1	0.1134 pu
$L_{md}$	2.67 pu	Lkq1	1.7684 pu
$L_{mq}$	1.45 pu	H	0.2531 s
$R_f$	0.01012 pu	F	0.01245 pu
$L_{fd}$	0.1276 pu	P	2
$R_{kd}$	0.5612 pu		

Table 4.4 Diesel generator system parameters for 75 kW generator.

Parameters	Values	Parameters	Values
$R_s$	0.4561 pu	Lkd	0.7733 pu
$L_l$	0.08 pu	Rkq1	0.04402 pu
$L_{md}$	2.56 pu	Lkq1	0.04147 pu
$L_{mq}$	1.13 pu	H	0.1225 s
$R_f$	0.01901 pu	F	0.02352 pu
$L_{fd}$	0.2456 pu	P	2
$R_{kd}$	0.2708 pu		

Table 4.5 Diesel Engine System Parameters

Engine Parameters	Values
Regulator Gain, K	30
Regulator Time constants (T1, T2, T3)	0.01, 0.02, 0.2
Actuator Time Constants (T4, T5, T6)	0.25, 0.009, 0.384
Torque Limit	0 - 1.1
Engine Time Delay, Td	2.4 ms

Table 4.6 Diesel Excitation System Parameters

Engine Parameters	Values
Low Pass filter Time constant	10 ms
Regulator Gain	200
Regulator Time Constant	20 ms
Exciter Gain	1
Damping Filter Gain	0.1
Damping Filter Time Constant	1.5 s
Regulator Output Limits	0-6 pu

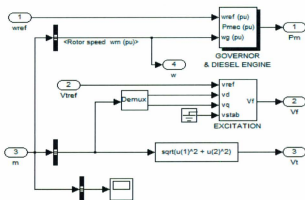


Figure 4.3.3: Engine and excitation system of Diesel generator.

#### 4.4 Summary

The simulation models for the photovoltaic system, diesel generators and battery bank have been presented in this chapter. Though the solar irradiance of St. John's area does not support installing photovoltaic system, the objective of utilizing PV is to design the system in a generalized way so that the model can be used some other place where sufficient solar irradiance is available. The battery bank is used to store energy. The objective of utilizing the diesel generator is to ensure a constant power supply to the consumer in case of no wind speed or solar irradiance, and when the energy stored in the battery bank is used up. The dynamic simulations of a combined system will be discussed in the next chapter.

## Chapter 5

### Simulation and Results of the Hybrid Power System

Both AC coupled and DC coupled Hybrid power systems have been simulated and analyzed with different input conditions using Matlab/Simulink. The Rosenbrock solver [57] has been chosen for the simulation. The simulation is allowed to run for 20 seconds. The simulation diagram for an AC coupled Hybrid system and a DC coupled hybrid system are given in Figure 5.1 and Figure 5.20. In the system, two 100 kW wind turbines are used instead of four 50kW wind turbines as four 50 kW wind turbines add more complexity to the model, and take a long time for simulation. All the cases studied have been discussed in the following subsection.

#### 5.1 Simulation for AC coupled Hybrid Power System

The complete block diagram of an AC coupled hybrid power system is presented in figure 5.1, and the corresponding simulation model of an AC coupled system is shown in figure 5.2. Details of various blocks can be found in Appendix A (Figure A-1 to Figure A-10). This simulation was tested for a number of conditions as described below.

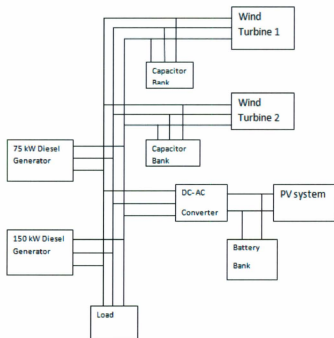


Figure 5.1: Overall block diagram of the AC coupled Hybrid System

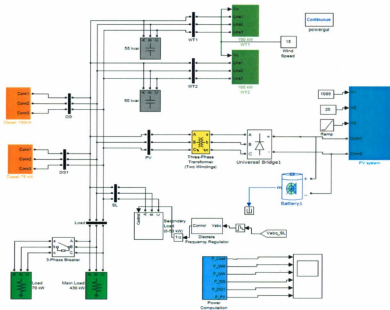


Figure 5.2: Simulink Model for the AC coupled Hybrid System

### 5.1.1 Case Study 1: Simulation of AC system with fixed wind speed and variable load

The community load has been changed after a certain period and the behaviours of all generating units have been observed. In this case, the wind speed and solar radiation have been kept to their rated values. Simulation results have been recorded for 10 seconds. At the 3<sup>rd</sup> second the load has been changed from 350 kW to 400kW and at the 6<sup>th</sup> second it has returned to the initial value of 350 kW. As the rated wind speed is set for this case, both 100 kW wind turbines generate maximum power. The wind turbines also ensure constant power generation ignoring small spikes regardless of the load fluctuations. The

diesel generators respond to the main load variations as expected. At the 3<sup>rd</sup> second both generators increased power generation as the load is increased and at the 6<sup>th</sup> second the generators decreased the power generation as the load is reduced by 50 kW. The photovoltaic system generated the rated power and there was no change due to load variation, which is expected. Figure 5.3 reveals the simulation results and system transience. Results show that the system is stable, and transience lasts for less than a second.

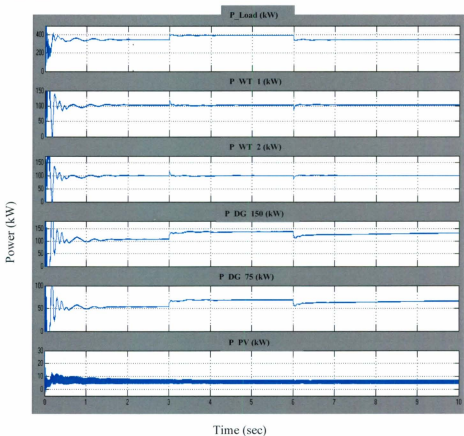


Figure 5.3: Simulation result fixed wind speed variable load

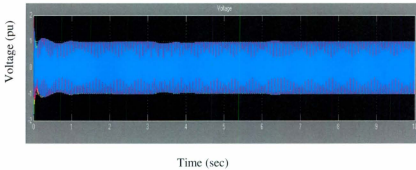


Figure 5.4: Effect of change of load on voltage

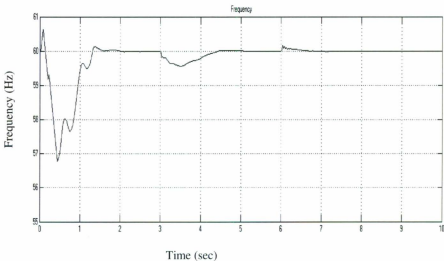


Figure 5.5: Effect of change of load on frequency.

The above two figures (Figure 5.4 and Figure 5.5) show the effect of change of load on system voltage and frequency. There is some initial transient in frequency and voltage but

but they go to stable position within one second. After 3 seconds, when the load changed from 350kW to 400kW, both the voltage and frequency dropped by a small amount; then it returned to the previous value within a second. Frequency dropped from 60 Hz to 59.5 Hz and then went to 60 Hz again. At the 6<sup>th</sup> second, when the load dropped from 400kW to 350kW, then there was a rising spike on the frequency curve but it only took a fraction of second to return to the previous constant value. There was no significant change in voltage when load dropped.

### **5.1.2 Case Study II: Simulation of AC system with Fixed Load Variable Wind Speed**

In this case the wind speed is allowed to vary but the main load remains constant. The main load has been kept at 300kW and the wind speed varies by 15m/s to 10m/s and back to 14 m/sec. Although that much sudden variation of wind speed is not realistic within a few seconds we simulate this wind speed variation in the system just to see what the power would be if such an exception happens. At the 3<sup>rd</sup> second the wind speed slumps from 15 m/s to 10 m/s and then at the 6<sup>th</sup> second is elevated to 14 m/s. Figure 5.6 shows the corresponding simulation results. The load power is almost constant and both types of wind turbines respond according to the wind speed change. As the wind generation drop during the 3<sup>rd</sup> second to the 6<sup>th</sup> second, the additional load is met up by the two diesel generators as shown in the results. After 6 second when wind speed rises the wind power increased and diesel generation returns to the previous value as the load is not increasing. Solar power remains unchanged as there is no variation in solar radiation. The effect of a two step change in wind speed on voltage and frequency are shown in Figure 5.7 and

Figure 5.8. Both voltage and frequency go down in small amounts when wind speed falls from 15 m/s to 10m/s, but they return to their steady state value within a minute. Again, when wind speed rises 10 m/s to 14 m/s, there is a spike on the frequency curve and it returns to steady state value in a fraction of a second. The same thing happens in the voltage curve.

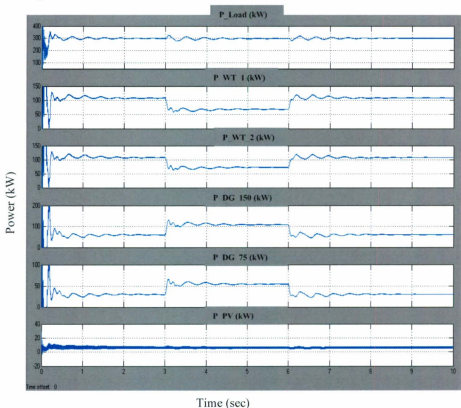


Figure 5.6: Simulation results for 300kW load and two step changes in the wind speed

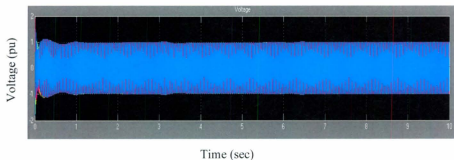


Figure 5.7: Effect of two step changes in the wind speed on voltage

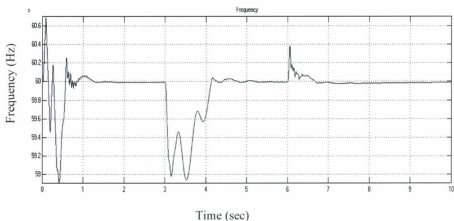


Figure 5.8: Effect of two step changes in the wind speed on frequency

Another scenario has been introduced with a 200 kW constant load and a wind speed elevation from 7ms/ to 9 m/s. The wind speed increment occurred in the 3<sup>rd</sup> second. Simulation results are shown in Figure 5.9 where the diesel engines provide the necessary power when wind generation is nearly zero.

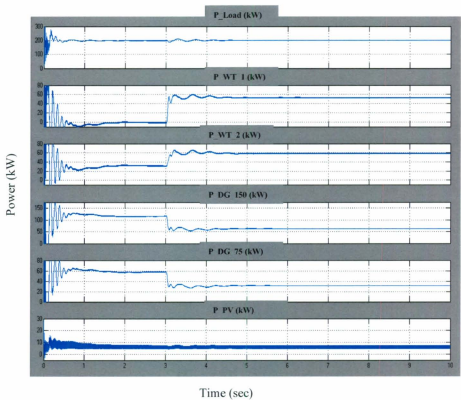


Figure 5.9: Simulation Results for 200kW load and wind speed elevation from 7 to 9m/s

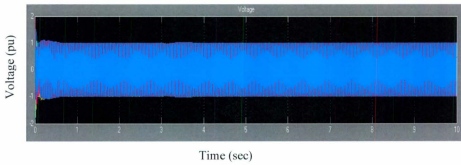


Figure 5.10: Voltage curve for 200kW load and wind speed elevation from 7 to 9m/s

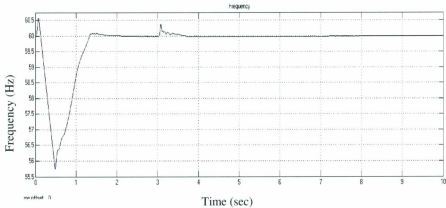


Figure 5.11: Frequency curve for 200kW load and wind speed elevation from 7 to 9m/s

The above figure 5.8 reveals that the wind generation distended significantly with the rise of wind speed. For a 7 m/s wind speed, although the wind turbine 1 power looks to be zero, it is actually around 5 kW. After 3 seconds it leaps to around 60 kW. Then the diesel generator decreases power generation. Figure 5.10 and Figure 5.11 represent the voltage and frequency curve in this condition respectively. There is little change on the voltage and frequency curve when wind speed goes from 7m/s to 9 m/s but it returns to the steady state condition soon.

In order to observe the function of the system, different transient circumstances have been considered. In this instance the wind speed is allowed to vary from 14m/s to 15m/s and the community load is steady at 350kW. Figure 5.12 shows the component behaviours of the system.

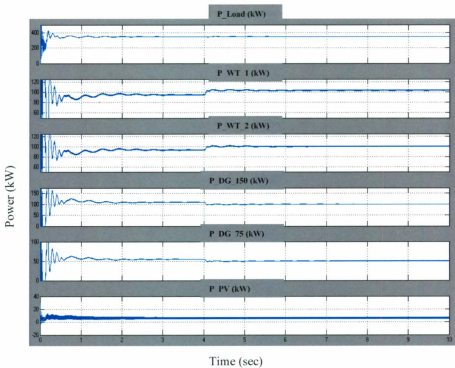


Figure 5.12: Simulation results for fixed load and wind speed 14ms to 15 m/s variation.

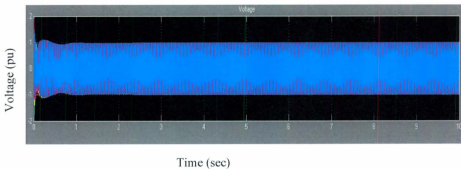


Figure 5.13: Voltage curve for fixed load and wind speed 14ms to 15 m/s variation.

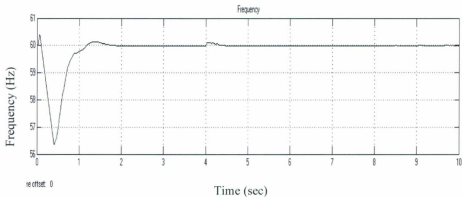


Figure 5.14: Frequency curve for fixed load and wind speed 14ms to 15 m/s variation.

Figure 5.12 shows that the load is fixed at 350 kW and the wind turbine responds appropriately to the change in the wind speed at the 4<sup>th</sup> second. It is important to realize that the high wind speed at low power keeps the diesel generator power significantly low. The effect of wind speed change on system voltage and frequency are shown in Figure 5.13 and Figure 5.14 respectively.

### 5.1.3 Case Study III: Simulation of AC system with diesel generators and Photovoltaic system in operation

The condition might occur when there is no wind and all the stored battery charge is used up. As the contribution of the photovoltaic system is very small, in this case the diesel generators are only the means to produce energy. Figure 5.15 illustrates the transience of diesel power with a 200kW load. As the load is not changing, the diesel generators give a

constant power supply throughout the period. The voltage and frequency in Figure 5.16 and Figure 5.17 goes to a steady state value in the first second and stays in that value as the load and wind speed are not changing.

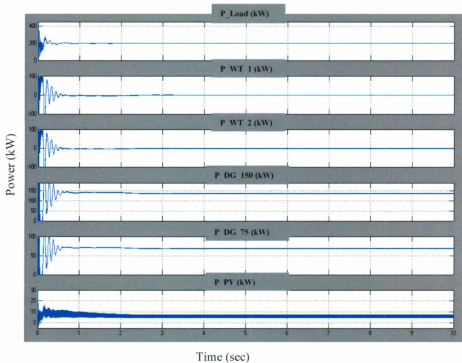


Figure 5.15: Simulation results for 200kW load with zero wind speed

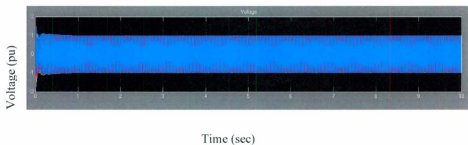


Figure 5.16: Voltage at 200kW load with zero wind speed

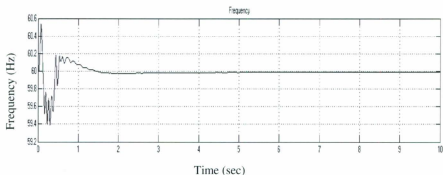


Figure 5.17: Frequency at 200kW load with zero wind speed

Another situation has been considered when there is no wind speed. We keep the wind speed zero but the load varies. From Figure 5.18 it can be observed that the load is initially 175 kW. At the 3<sup>rd</sup> second it goes up to 225kW and drops to 175 kW again at the 6<sup>th</sup> second. The diesel generators precisely follow the load. Figure 5.19 and Figure 5.20 show the effect on voltage and frequency. The photovoltaic system has no significant effect in that case as the solar irradiance is constant.

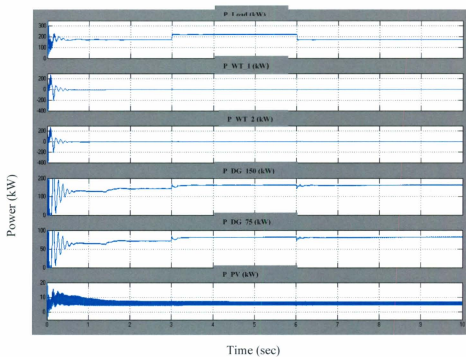


Figure 5.18: Simulation results for Variable load with Zero wind speed

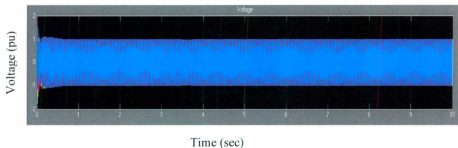


Figure 5.19: Voltage at Variable load with Zero wind speed

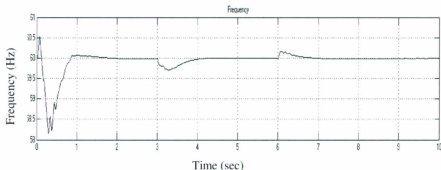


Figure 5.20: Frequency at Variable load with Zero wind speed

## 5.2 DC coupled system simulation and its results

After modeling the AC coupled hybrid system I have also modeled the DC coupled Hybrid system with a DC bus voltage of 648 volts. In the case of modeling of a wind turbine of a DC coupled system, I used a Permanent magnet DC generator instead of a synchronous generator, as the output of PMG is DC. The subsystem of wind turbine, PV, and diesel generators will be given in appendix A. The power of subsystems and load is calculated by multiplying the bus voltage by the current of the corresponding branch. In Figure 5.21 the overall block diagram is presented and the corresponding Simulink model of the DC coupled hybrid system is shown in Figure 5.22. Details of various blocks will be found in appendix A. As the main aim of the thesis work is the modeling and comparison of dynamics of the AC and DC coupled hybrid system, we consider the same case study for a DC coupled hybrid system that we have considered for an AC coupled hybrid system. All the cases studied have been discussed in the following subsection.

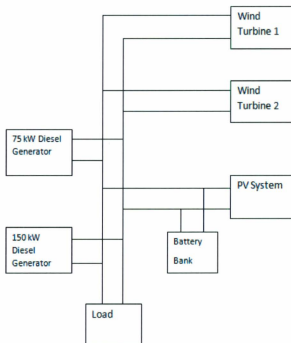


Figure 5.21: Complete block diagram of DC coupled hybrid system

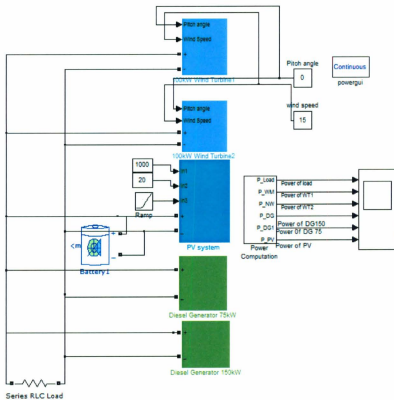


Figure 5.22: Simulink model for DC coupled hybrid system.

### 5.2.1 Case Study 1: Simulation of DC system with a fixed wind speed and variable load

Like case study I of an AC coupled system, the community load has been changed after a certain period and the behaviours of all generating units have been observed. In that case the wind speed has been kept to its rated value and solar radiation has been changed after 4 seconds. Simulation results have been recorded for 10 seconds. At the 3<sup>rd</sup> second the

load was changed from 550 kW to 600kW and at the 6<sup>th</sup> second it returned to the initial value 550 kW. As rated wind speed is set for the simulation, both 100 kW wind turbines generate the maximum power. The wind turbines also ensure constant power generation, ignoring small spikes regardless of the load fluctuations. The diesel generators respond to the main load variations as expected. At the 3<sup>rd</sup> second both generators increased generation as the load is increased, and at the 6<sup>th</sup> second they decrease the generation as the load is reduced by 50 kW. The photovoltaic system generated power rose after 4 seconds as we changed solar irradiance from 950 W/m<sup>2</sup> to 1000 W/m<sup>2</sup>. Figure 5.23 reveals the simulation results and system transience. Results show that system is stable and transience lasts for less than a second.

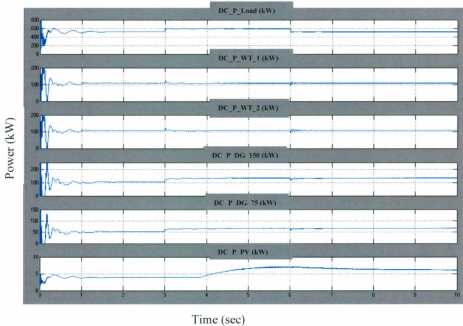


Figure 5.23: Simulation result for fixed wind speed variable load

## 5.2.2 Case Study II: Simulation of DC system with Fixed Load Variable Wind Speed

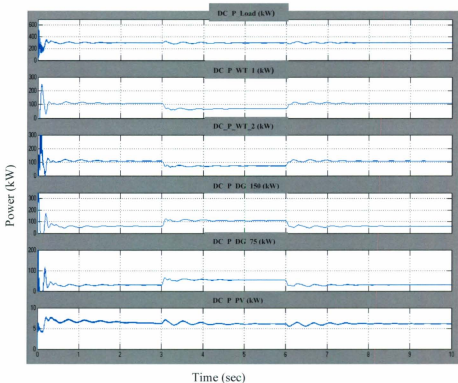


Figure 5.24: Simulation results of DC system for 300kW load and two step changes in the wind speed

In that case the main load remains constant but the wind speed is allowed to vary, just like in the AC system. The main load has been kept to 300kW and the wind speed is varied by 15m/s to 10m/s and back to 14 m/sec. At the 3<sup>rd</sup> second the wind speed slumps from 15 m/s to 10 m/s and then at the 6<sup>th</sup> second elevated to 14 m/s. Figure 5.24 shows the

corresponding simulation results and it is found that the result is almost the same as the result of the AC system at this condition except for the solar power. Solar power has less transience than an AC coupled system. The load power is almost constant and both types of wind turbines respond according to the wind speed change. As the wind generation drops during the 3<sup>rd</sup> second to the 6<sup>th</sup> second, the additional load is met by the two diesel generators, as shown in the results. After 6 seconds when wind speed rises, the wind power increases and diesel generation returns to the previous value, as the load is not increasing. Solar power is constant and remains unchanged as there is no variation in the solar radiation.

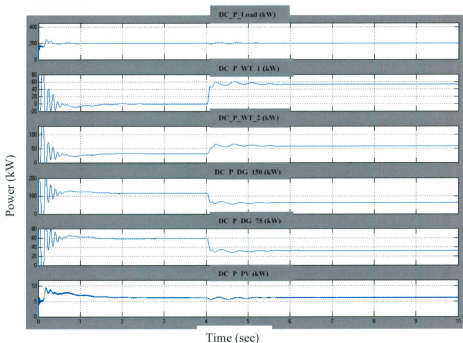


Figure 5.25: Simulation Results of DC coupled system for 200kW load and wind speed rise from 7 to 9m/s

The next scenario has been introduced with a 200 kW constant load and a wind speed rise from 7m/s to 9 m/s. The wind speed increment occurred in the 3<sup>rd</sup> second. Simulation results are shown in figure 5.25 where the diesel engines provide the necessary power when wind generation is nearly zero. The transience in PV system is less than in the AC system in this scenario.

Another transient circumstance is to allow the wind speed to vary from 14 m/s to 15 m/s (Figure 5.26). From the data, it is clear that the result is nearly the same as the results of the AC based hybrid system (Figure 5.11), but the initial transience of the DC based system is a little bit less than for the AC based system. The PV system shows better performance.

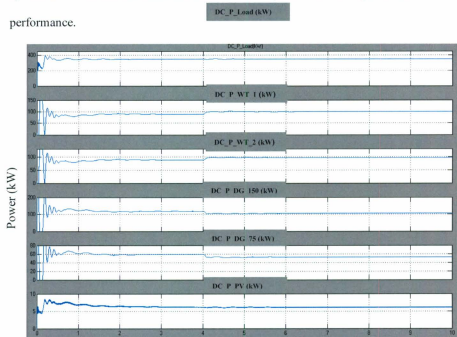


Figure 5.26: Simulation Results of DC Power (kW) vs Time (sec) for 350kW load and wind speed drop from 14 to 15m/s

### 5.2.3 Case Study III: Simulation of DC system with diesel generators and Photovoltaic system in operation

This condition appears when there is no wind and only the diesel generators and the PV system produce energy. Figure 5.27 shows the transient results of the total system. As there is no wind and the load is fixed, there is no transient in the whole period except for a small amount of initial transience.

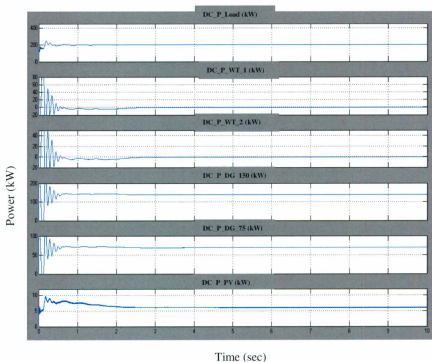


Figure 5.27: Simulation results of DC based system for 200kW load with zero wind speed

Finally I have considered another situation when there is no wind speed. We kept the wind speed at zero, but the load varies. From Figure 5.28 it can be observed that the load is initially 175 kW. At the 3<sup>rd</sup> second it goes up to 225kW and drops to 175 kW again at the 6<sup>th</sup> second. The diesel generators precisely follow the load, as in the AC coupled system.

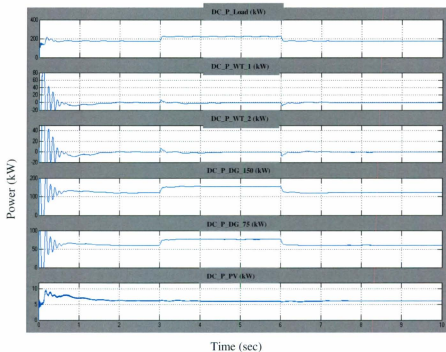


Figure 5.28: Simulation results of DC based system for Variable load with Zero wind speed

### 5.3 Summary

The AC based Wind-PV-Diesel-Battery hybrid power system and the DC based Wind-PV-Diesel-Battery hybrid power system have been simulated with three different stages. The simulations have been carried out for 10 seconds because of the size of model. The model is so complex that it is just about impossible to run for a longer period. Although it was not possible to carry out the simulations for a long time, it can easily be verified that the systems will work stable for hours of operation. From the simulation results shown in Figure 5.3 to Figure 5.20 and from Figure 5.23 to Figure 5.28 it can be said that the system goes to stability within one second and remains unchanged until the variable changes. If the variables (load, wind speed, solar irradiance) are changed, the system responds quickly and goes to a corresponding stable position. I have considered the same case studies for both systems to observe the power quality and transience. From the results of the transient analysis of both systems it can be said that they have almost the same characteristics. The only exception is that the PV system of the DC based system shows a better performance than the AC based system. The summary of all three case studies is shown in table 5.1

Table 5.1 Summary of Three Case Studies.

Case Study	AC Based HPS	DC Based HPS
CS1: Simulation With Fixed Wind Speed Variable Load	<ul style="list-style-type: none"> <li>➤ Load 350/400/350 kW</li> <li>➤ Wind Speed 15 m/s</li> <li>➤ No change in WT power</li> <li>➤ DGs respond with main load variation</li> <li>➤ Frequency goes down from 60 Hz to 59.6 Hz when load increases 350 kW to 400 kW, then returns to 60 Hz within a second.</li> <li>➤ Frequency rises from 60 Hz to 60.1 Hz when load changes from 400kW to 350 kW and returns to 60 Hz immediately.</li> <li>➤ Voltage goes down a very little amount when load goes up for a fraction of a second.</li> <li>➤ There is a small amount of voltage rise when load drops but it goes to a constant value immediately.</li> </ul>	<ul style="list-style-type: none"> <li>➤ Load 550/600/550 kW</li> <li>➤ Wind Speed 15 m/s</li> <li>➤ No change in WT power</li> <li>➤ DGs respond with main load variation</li> <li>➤ Power quality of PV is better than AC</li> <li>➤ There is no frequency variation</li> <li>➤ There is no voltage variation</li> </ul>
	<ul style="list-style-type: none"> <li>➤ Load 300kW</li> <li>➤ Wind Speed 15/10/14 m/s</li> <li>➤ WTs respond to wind speed change</li> <li>➤ When wind generation drops, DGs met additional load</li> <li>➤ At 3<sup>rd</sup> second f, goes down from 60 Hz to 58.9 Hz when wind</li> </ul>	<ul style="list-style-type: none"> <li>➤ Load 300kW</li> <li>➤ Wind Speed 15/10/14 m/s</li> <li>➤ WTs respond to wind speed change</li> <li>➤ When wind generation drop, DGs met additional load</li> <li>➤ PV system shows better power quality.</li> <li>➤ There is no voltage and</li> </ul>

CS2: Simulation With Fixed Load Variable Wind Speed	speed drops but immediately returns to previous value ➤ f, rises from 60 Hz to 60.4 Hz at 6 seconds but returns to steady state within a fraction of second ➤ Voltage has corresponding response like frequency.	Frequency variation.
	➤ Load 200kW ➤ Wind Speed 7/9 m/s ➤ WT's respond to wind speed change ➤ When wind generation rises, diesel generation drops automatically. ➤ f, rises from 60 Hz to 60.4 Hz when WS rises 7m/s to 9 m/s and returns to steady state within a second. ➤ There is also a small variation on Voltage	➤ Load 200kW ➤ Wind Speed 7/9 m/s ➤ WT's respond to wind speed change ➤ When wind generation rises, Diesel generation drops automatically. ➤ PV system shows better power quality. ➤ There is no voltage and Frequency variation.
	➤ Load 350kW ➤ Wind Speed 14/15 m/s ➤ WT's respond to wind speed change ➤ When wind generation rises, diesel generation drops automatically. ➤ f, rises from 60 Hz to 60.2 Hz with the rise of WS and returns to steady state within a second. ➤ No significant effect on voltage	➤ Load 350kW ➤ Wind Speed 14/15 m/s ➤ WT's respond to wind speed change ➤ When wind generation rises, diesel generation drops automatically. ➤ PV system shows better power quality. ➤ There is no voltage and Frequency variation.

CS3: Simulation With Diesel Generator and Photovoltaic System	<ul style="list-style-type: none"> <li>➤ Load 200kW</li> <li>➤ Zero Wind Speed</li> <li>➤ Load is met by DGS and PV.</li> <li>➤ There is no effect on voltage and frequency</li> </ul>	<ul style="list-style-type: none"> <li>➤ Load 200kW</li> <li>➤ Zero Wind Speed</li> <li>➤ Load is met by DGS and PV.</li> <li>➤ PV system shows better power quality.</li> <li>➤ There is no voltage and Frequency variation.</li> </ul>
	<ul style="list-style-type: none"> <li>➤ Load 175/225/175kW</li> <li>➤ Zero Wind Speed</li> <li>➤ Diesel generation follows the load</li> <li>➤ f, goes down from 60 Hz to 59.7 Hz when load increases but immediately returns to previous value</li> <li>➤ f, rises from 60 Hz to 60.2 Hz when load drops and returns to steady state within a second.</li> <li>➤ No significant effect on voltage.</li> </ul>	<ul style="list-style-type: none"> <li>➤ Load 175/225/175kW</li> <li>➤ Zero Wind Speed</li> <li>➤ Diesel generation follows the load</li> <li>➤ PV system shows better power quality.</li> <li>➤ There is no voltage and Frequency variation.</li> </ul>

## Chapter 6

### Conclusions and Recommendations

#### 6.1 Summary of Research

The main objective of this research is to design a cost effective power system for a small remote community near St. John's. Approximately 0.2 million people are living in 300 isolated communities around the Yukon, Nunavut and the Coastal islands [59]. Electric distribution grids have not reached those people because of difficulty in establishing and maintaining transmission and distribution lines. These detached communities are powered by diesel generators. However, because of the higher fuel transport cost and emission of tons of harmful gas, the diesel power system became less popular. As most remote communities are blessed by wind resource a wind-diesel hybrid system may be an option for power supply.

In this research I have decided to design a power system for a remote community with wind turbine, photovoltaic, diesel generator and batteries. I designed two systems. First I designed an AC-based Wind-diesel-PV-Battery system; then we designed a DC-based Wind-diesel-PV-Battery system using the same components, and finally we made a comparison to determine which one is perfect for the community.

For designing these two systems I used the FD13-50/12 wind turbine, SG17524 (175W) PV module, one 150kW and one 75 kW diesel generator, a Surrette 12-Cs-11-Ps 12 volts battery and a Solectria PVI60KW-480V inverter. The earlier chapters explicate the steady state models of individual constituents of this system. Finally they are coupled

together and simulated to examine their characteristics and dynamic behaviour. In the next section we will briefly adduce the contribution of this thesis.

A brief introduction of AC and DC coupled hybrid power systems has been presented. Some papers related to cost analysis, operation and performance of hybrid systems, performance of a photovoltaic system, the permanent magnet synchronous generator based wind turbines and squirrel case induction generator based wind turbines have been highlighted.

For sizing, economic and electrical aspects analysis of the AC and DC based hybrid power system, HOMER software has been used. Then a comparison has been made between these two systems. From the comparison it can be said that a DC based system is better than the AC based on cost, number of components required, amount of diesel used and corresponding greenhouse gas emission when 70 % of the load considered is DC and 30% of it is an AC load.

The details of wind energy conversion systems have been elucidated. The generators have been described by d-q reference frame. The Matlab/Simulink models of wind energy conversion systems have been simulated with different wind speeds to compute the energy production by them, and power curves have been validated by comparing them with those provided by the manufacturers.

The photovoltaic system, diesel generators and battery banks have been modeled and simulated in order to determine their characteristics. To compute the energy production of the PV system, a PV system has been simulated with different solar irradiance.

Finally the transient behaviour of the AC based system and the DC based system has been determined for different conditions. First the wind speed is kept constant and the load is varied. Then, keeping the load fixed, wind speed is allowed to vary. A step change and a two step change of wind speed is considered in that case. Another scenario has been considered with no wind and with only the diesel generators and PV operating. Both systems show almost the same dynamic behaviour for the above mentioned conditions, except for the PV system. The PV shows better performance in a DC based system than in the AC based System

The three case studies of both systems are summarized in table 5.1 in chapter 5. The voltage and frequency variation have also been presented in that table. From the table it is clear that there is some variation in voltage and frequency in the AC coupled system with the variation of load and wind speed, but no such type of variation in the DC coupled system.

In conclusion, it can be said that the DC based hybrid power system would be a better power generation option for a remote community. The contribution of this research can be summarized by the following points.

1. Wind data, solar data and load data of St.John's Newfoundland have been collected and studied.
2. Economical and feasible components of the hybrid power system have been selected so that minimized system cost can be achieved.
3. AC coupled and DC coupled hybrid systems have been designed using HOMER.

4. Comparison has been made between these two systems based on components required, system cost, the fraction of renewable resources in use, the diesel used and corresponding emissions.
5. Modeling of individual components has been done using Matlab /Simulink.
6. Individual models have been combined to form the complete system.
7. Three different case studies have been considered for transient analysis.
8. A comparison table has been made including the results from the case studies and voltage and frequency variation.
9. Finally it can be said that for remote hybrid power systems the DC bus system would be a better power system option.

## **6.2 Future Work**

The short 10 second simulation time is too small to comprehend all the transient characteristics of the constituents of this power system. Because of the limitation of available computers and software, we were not able to simulate for more than 10s. Some other competitive software might be put to use for a longer duration of simulation to obtain better results.

Although this research employs some extent of control during the modeling of wind energy conversion systems, it does not aim at precise control of the whole power system. The energy generation from some components was computed without controlling. For better results it is possible to control them individually and set the threshold. Therefore addition of system controllers is highly recommended for simulation.

Although the effect of solar irradiation on energy production in PV has been observed in chapter 4, it kept constant while simulating the combined system as discussed in chapter 5. The reason is that the contribution of PV is relatively very small for the selected location. It is possible to include the effect of solar irradiance by selecting a location with a higher solar radiation capability.

The performance of the battery bank has not been included in this work. It was of no use to study that for 10 seconds. It could be studied thoroughly in future if longer duration dynamic simulations are done.

The work done in this research is not for an existing system. The results would be more accurate if it were possible to build practical systems according to design. There would be more of a challenge in building a completely AC based system and DC based system, and comparing their performance. Also the power distribution of a DC based system would be an interesting aspect of further work.

## Publications

1. Tanjila Haque, M. T. Iqbal, "A Comparison of AC and DC Coupled Hybrid Power Systems," presented in WESNet Poster Presentation, CanWEA, 2010, Montreal, Quebec
2. Tanjila Haque, M. T. Iqbal, "A Comparison of AC and DC Coupled Remote Hybrid Power Systems," presented at 19th IEEE-NECEC Conference 2010, St. John's, NL
3. Tanjila Haque, M. T. Iqbal, "A Comparison of Dynamics and Control of AC and DC Coupled Hybrid Power Systems," presented at WESNet Workshop, February 24-25, Ryerson University, Toronto, ON, Canada 2011
4. Tanjila Haque, M. T. Iqbal, Modeling and Comparison of Dynamics of AC and DC Coupled Remote Hybrid Power Systems. *Presented at CanWEA 2011 Conference and Exhibition held on October 3rd to 6th, 2011 in Vancouver, British Columbia*
5. Tanjila Haque, M. T. Iqbal, Modeling and Dynamics of DC Coupled Remote Hybrid Power System. *Accepted for 20th IEEE-NECEC Conference 2011, St. John's, Canada*
6. Tanjila Haque, M. T. Iqbal, Comparison of Dynamics and Modeling of AC and DC Coupled Remote Hybrid Power Systems. *Accepted for 20th IEEE-NECEC Conference 2011, St. John's, Canada*

7. Tanjila Haque, M. T. Iqbal, Modeling and comparison of Dynamics of DC Coupled Remote Hybrid Energy System. *Will be submitted for Journal publication in Renewable Energy, 2011.*

## References

- [1] IEA, "World Energy Outlook 2004," 2004.
- [2] K. Reiche, A. Covarrubias, and E. Martinot, "Expanding Electricity Access to Remote Areas: Off-Grid Rural Electrification in Developing Countries," *World Bank* 2000.
- [3] Azbe V, Mihalic R, Distributed generation from renewable sources in an isolated DC network. *Renewable Energy* 2006; 31(14):2370-84.
- [4] Agustoni A, Brenna M, Tironi E. Proposal for high quality DC network with distributed generation. In *CIREN, 17<sup>th</sup> international conference on electricity distribution, Barcelona; 2003*.
- [5] R. Noroozian, M. Abedi, G.B. Gharehpetian, S.H. Hosseini. Combined operation of DC isolated distribution and PV system for supplying unbalanced AC loads. *Renewable Energy* 2009; 34:899-908.
- [6] G.P. Giatrakors, T.D. Tsoutsos, P.G. Mouchtaropoulos, G.D. Naxakis, G. Stavrakakis. Sustainable energy planning based on a standalone hybrid renewable energy/ hydrogen power system: Application in karpathos island Greece. *Renewable Energy* 2009; 34:2562-2570.
- [7] S.M. Hakimi, S.M. Moghaddas-Tafreshi. Optimal sizing of a stand-alone hybrid power system via particle swarm optimization for Kahnouj area in south east-east of Iran. *Renewable Energy* 2009; 34:1855-1862.
- [8] M. Uzunoglu, O.C. Onar, M.S. Alam. Modeling control and simulation of a PV/FC/UC based hybrid power generation system for stand-alone applications. *Renewable Energy* 2009; 34:509-520

- [9] Eftichios Koutroulis, Dionissia Kolokkotsa, Antonis Potirakis, Kostas Kalaitzakis. Methodology for optimal sizing of stand-alone photovoltaic/ wind-generator systems using genetic algorithms. *Solar energy*2006; 80: 1072-1088.
- [10] Rodolfo Dufo-Lopez, José L. Bernal-Agustín. Multi-objective design of PV-wind-diesel-hydrogen-battery systems. *Renewable Energy* 2008; 33:2559-2572
- [11] Coello CA, Veldhuizen DAV, Lamont GB. Evolutionary algorithms for solving multi-objective problems. *New York: Kluwer Academic/Plenum Publishers; 2002.*
- [12] M.Little, D.Infield, M.Thomson, "Electrical Integration of Renewable Energy into Stand-Alone Power Supplies with a Central DC Bus", *Loughborough University Division Conference, Sutton Bonnington, Nottinghamshire, 2005.*
- [13] S.R. Vosen and J.O. Keller, "Hybrid energy storage Systems for Stand-alone electric power systems: optimization of system performance and cost through control strategies", *International Journal of Hydrogen energy*, 24(1999), pp.1139-1156.
- [14] Mohammad Saad Alam and David W. Gao, "Modeling and Analysis of a Wind/PV/Fuel Cell Hybrid power System in HOMER", *Second IEEE Conference on Industrial Electronics and Applications, 2007*, pp.1594-1599.
- [15] Tomonobu Senjyu, Eitaro Omine, Daisuke Hayashi, Hideomi Sekine and Toshihisa Funabashi, " Application of Decentralized Control for remote Power System Stabilization by Installing renewable energy Power Plant" *IEEJ trans* 2008, Vol 3, pp.473-481.
- [16] A. Bilodeau and K. Agbossou, " Control analysis of renewable energy system with hydrogen storage for residential applications", *Journal of Power Sources*, 162(2006), pp. 757-764.

- [17] M.T. Iqbal, "Simulation of small wind fuel cell hybrid energy system", *Renewable Energy*, 28 (2003), pp.511-522.
- [18] O.C. Onar, M. Uzunoglu and M.S. Alam, "Dynamic modeling, design and simulation of wind/fuel cell/ultra capacitor based hybrid power generation system", *Journal of Power Sources*, 161 (2006), pp. 707-722.
- [19] Chun-Hua Li, Xin-jian Zhu, Guang -Yi Cao, Sheng Sui and Ming-Ruo Hu, "Dynamic modeling and sizing optimization of stand-alone photovoltaic power systems using hybrid energy storage technology", *Renewable Energy*, 34(2009), pp. 815-826.
- [20] Alejandro J. del real, Alicia Arce and Carlos Bordons, "Hybrid model predictive control of a two- generator power plant integrating photovoltaic panels and fuel cell", 46<sup>th</sup> *IEEE conference on Decision and Control, New Orleans, LA, USA, Dec.12-14, 2007*, pp. 5447-5452.
- [21] M.J. Khan and M.T. Iqbal, "Dynamic modeling and simulation of a small wind-fuel cell hybrid energy system", *Renewable energy*, vol.30, 2005, pp.421-439.
- [22] R. Chedid, F.B. Chaaban and R. Shihab, "A Simplified Electric Circuit Model for the Analysis of hybrid Wind-Fuel cell Systems", *Power Engineering Society general Meeting 2007, IEEE, Tampa, FL, June 24-28, 2007*, pp.1-6
- [23] T. Tafticht, K. Agbossou, A. Cheriti and M.L. Dombia, "Output Power Maximization of a Permanent Magnet Synchronous Generator Based Stand-alone Wind Turbine", *IEEE ISIE 2006*, pp.2412-2416, July 9-12, 2006, Montreal, Quebec, Canada.
- [24] Xibo Yuan, Fred Wang, Rolando Burgos, Yongdong Li and Dushan Boroyevich, "DC-link voltage Control of Full Power Converter for Wind Generator operating in Weak

grid Systems". This work made use of ERC Shared Facilities supported by the National Science Foundation under Award Number EEC-9731677, *Applied Power Electronics Conferences and Exposition*, pp. 761-767, Feb 24-28, 2008.

[25] Md. Arifujjaman, M. Tariq Iqbal, John E. Quicoe and M. Jahangir Khan, "Modeling and Control of a Small Wind turbine", *CCECE/CCGEI, Saskatoon*, pp. 778-781, May 2005.

[26] Loraind Szabo, Kairoly Agoston Biro, Cosmina Nicula and Florin Jurca, "Simulation of Wind turbine Driven Autonomous Squirrel Cage Induction Generators", *INES 2007-11<sup>th</sup> International Conference on Intelligent Engineering Systems-29 June-1 July 2007-Budapest, Hungary*, pp. 213-218.

[27] Alexander Hamlyn, Helen Cheung, Lin Wang, Cungang Yang and Richard Cheung, "Adaptive Protection and Control Strategy for Interfacing Wind-Power Electricity Generators to Distribution Grids", *IEEE conference 2008*, pp. 1-8.

[28] Tarek Ahmed, Osamu Noro, Eiji Hiraki and Mutsuo Nakaoka, "terminal Voltage Regulation Characteristics by Static Var Compensator for a Three-ohase Self-Excited induction Generator", *IEEE Transaction on Industry Applications, Vol.40, No.4*, pp. 978-988, July/August2004.

[29] I. Dincer, "Renewable energy and sustainable development: a crucial review." *Renewable and Sustainable Energy Reviews*, vol. 4, pp. 157-175, 2000.

[31] M. Little, M. Thomson and D. Infield "Electrical integration of renewable energy into stand-alone power supplies incorporating hydrogen storage" *presented at the Second European Hydrogen Energy Conference, Zaragoza, 2005*.

- [32] E. Ortjohann, O. Omari, M. Lingemann, N. Hamsic, W. Sinsukthavorn, and D. Morton. An Online Control Strategy for Modular DC Coupled Hybrid Power Systems. *12th European Conference on Power Electronics and Applications*, Aalborg, Denmark, September, 2007.
- [33] Karim Moutawakkil and Steffen Elster, "Coupling of Renewable Energy Sources on the AC and DC Side of the Inverter" *Conergy report*.
- [34] US. Energy Information Administration, *International Energy Outlook 2001*, May 2001.
- [35] Kilian Reiche, Alvaro Covarrubias, and Eric Martinot. "Expanding Electricity Access to Remote Areas: Off-Grid Rural Electrification in Developing Countries" *Several World Bank Group projects report 2000*.
- [36] Henrik Stiesdal "The wind turbine components and operation" *the special issue of the Bonus-Info 1998 newsletter, autumn 1999*.
- [37] Erich, Hau, "Wind Turbines: Fundamentals, Technologies, application, Economics", *Springer Verlag Berlin Heidelberg New York, ISBN: 3-540-57064-0, 2000*.
- [38] MATLAB/SIMULINK and MATLAB/ SimPower System are the products of the MathWorks, 3 Apple Hill Drive, Natick, MA 017602098, USA.
- [39] Bogdan S. Borowy and Ziyad M. Salameh, "Dynamic Response of a Stand-Alone Wind Energy Conversion System with Battery Energy Storage to a Wind Gust", *IEE Transactions on Energy Conversion, Vol.12, No.1, pp.73-78, March 1997*.

- [40] Mohd. Abdus Salam, " Fundamentals of Electric Machines", *Alpha Science International Ltd., 7200 The Quorum, Oxford Business Park North, Garsington Road, oxford, OX4 2JZ, U.K., ISBN: 1-84265-275-3, 2005.*
- [41] Seyoum, D., Rahman, M.F. and Grantham, C., " Terminal Voltage control of a wind turbine driven isolated induction generator using stator oriented field control," *Proceeding of the Eighteenth Annual IEEE Applied Power Electronics Conference and Exposition (APEC'03), Miami Beach (FL, USA), Vol.2, 2003, pp. 846-852.*
- [42] S.N. Bhadra, D. Kastha, S. Banerjee, " Wind Electrical Systems" , *Oxford University Press, YMCA Library building, jai Singh Road, New Delhi 110001, ISBN-10: 0-19-567093-0, 2005.*
- [43] Newfoundland and Labrador Hydro ([www.nlh.nl.ca](http://www.nlh.nl.ca))
- [44] Frontier Power Systems, *Carl Brothers, 392 Church Street, Alberton, PEI C0B1B0, Canada.*
- [45] Muselli, M. Notton, G.Louche, A. "Design of Hybrid Photovoltaic power generator with Optimization of Energy Management". *Solar Energy Vol 65, No. 3. pp.143-157. 1999.*
- [46] Wies, R. W., Johnson, R.A, Agrawal, A.N. and Chubb, T. J, "Economic Analysis and Environmental impacts of a PV with Diesel Battery System for Remote villages", *IEEE General meeting of Power Engineering June 2004, Denver Colorado (USA).*
- [47] Masters, Gilbert M. *Renewable and Efficient Electric Power Systems. John Wiley & Sons Ltd, 2004*

- [48] Chapin, D. M., C. S. Fuller, & G. L. Pearson, Bell Telephone Laboratories, Inc., Murray Hill, New Jersey "A New Silicon p-n Junction Photocell for Converting Solar Radiation into Electrical Power" *Journal of Applied Physics*, Volume 25, Issue 5, p.p 676-677, May 1954.
- [49] Messenger, Roger & Jerry Ventre Photovoltaic Systems Engineering, 2nd Edition CRC Press, 2003.
- [50] Castañer, Luis & Santiago Silvestre Modelling Photovoltaic Systems, Using PSpice John Wiley & Sons Ltd, 2002.
- [51] Green, Martin A. Solar Cells; Operating Principles, Technology, and System Applications Prentice Hall Inc., 1982.
- [52] Walker, Geoff R. "Evaluating MPPT converter topologies using a MATLAB PV Model" *Australasian Universities Power Engineering Conference, AUPEC '00, Brisbane, 2000*.
- [53] Hussein, K. H., I. Muta, T. Hoshino, & M. Osakada "Maximum Photovoltaic Power Tracking: an Algorithm for Rapidly Changing Atmospheric Conditions" *IEEE Proceedings - Generation, Transmission and Distribution - v. 142, pp. 59-64, January 1995*.
- [54] Hohm, D. P. & M. E. Ropp "Comparative Study of Maximum Power Point Tracking Algorithms" *Progress in Photovoltaics: Research and Applications*, pp. 47-62, November 2002.
- [55] T.F. Wu, and Y.K. Chen, "Modeling of PWM DC/DC Converter Out of Basic Converter Units", *IEEE Transaction, Power Electronics, Vol.13, no.5 pp. 870-881, 1998*.

- [56] N. Mohan, T.M. Undeland and W.P. Robbins, 2003. *Power Electronics. USA: John Wiley & Sons, pp. 172-178.*
- [57] MATLAB/SIMULINK and MATLAB/ SimPower System are the products of the MathWorks, 3 Apple Hill Drive, Natick, MA017602098, USA  
URL: [http:// www.mathworks.com](http://www.mathworks.com)
- [58] Shunhui Li and Tim A. Haskew, " Characteristic Study of Vector- Controlled Direct Driven Parmanent Synchronous Generator in Wind Power Generation", *Power and Energy Society General Meeting- Conversion and Delivery of Electrical Energy in the 21<sup>st</sup> Century, 2008 IEEE, pp. 1-9 July 20-24,2008.*
- [59] C. V. Nayar, "Recent Developments in Decentralised Mini-Grid Diesel Power Systems in Australia," *Applied Energy, vol. 52, pp. 229-242, 1995.*
- [60] W. S. Isherwood, R; Aceves, S; Berry, G; Clark, W; Johnson, R; Das, D; Goering, D; Seifert, R, "Remote power systems with advanced storage technologies for Alaskan villages," *Energy, vol. 25, pp. 1005-1020, 2000.*
- [61] I. Dincer, "Renewable energy and sustainable development: a crucial review," *Renewable and Sustainable Energy Reviews, vol. 4, pp. 157-175, 2000.*
- [62] G. Boyle, B. Everett, and J. Ramage, *Energy Systems and Sustainability: Power for a Sustainable Future: Oxford University Press, 2003.*
- [63] D. Weisser and R. Garcia, "Instantaneous wind energy penetration in isolated electricity grids: concepts and review," *Renewable Energy, vol. 30, pp. 1299-1308, 2005.*
- [64] Michael Boxwell, *Solar Electricity Handbook, 2011 Edition*

## Appendix A

### MATLAB/SIMULINK Subsystem Blocks

The Appendix comprise of a number of Simulink and Simpower subsystem blocks which are the illustration of corresponding blocks in Chapter 3, Chapter 4 and Chapter 5. Most of the input and output parameters are denoted by the similar symbols as expressed in those chapters. It is important to note that, some of the inputs are linked with the preceding blocks and rests are constant values or coefficients. In order to provide a better idea about the subsystem blocks, the corresponding units are also given in the diagrams.

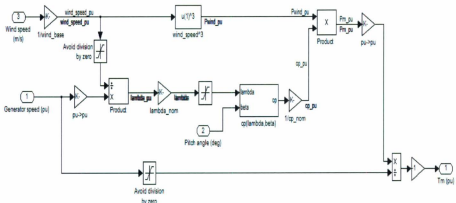


Figure A-1 Subsystem of the Wind Turbine.

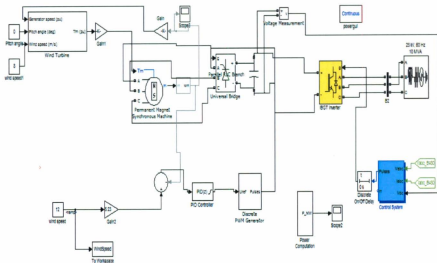


Figure A-2 Subsystem Model of a PMG based WECS for the AC System

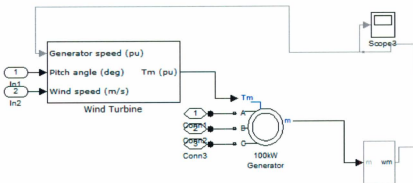


Figure A-3 Subsystem model of an induction generator based WECS for the AC system.

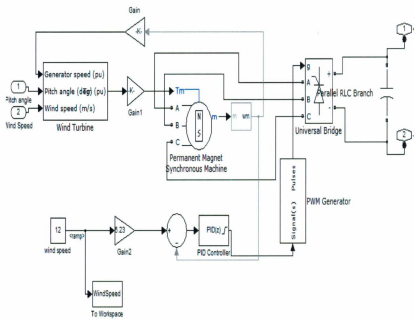


Figure A-4 The subsystem model of a PMG based WECS for the DC System.

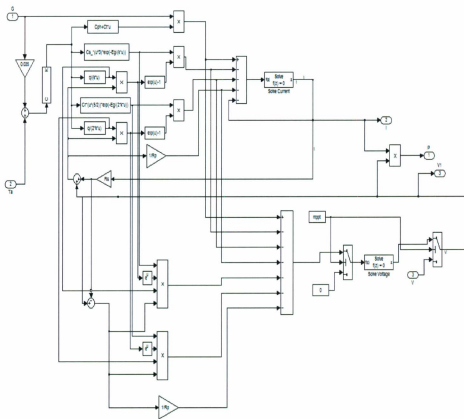


Figure A-5 The subsystem model of the Solar cell.

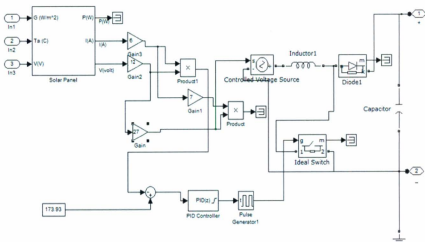


Figure A-6 The subsystem model of the PV system.

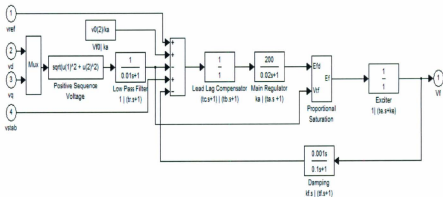


Figure A-7 The Simulink Model of the Excitation System.

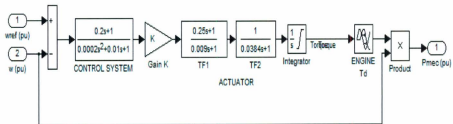


Figure A-8 The Simulink Model of the Governor and Diesel Engine.

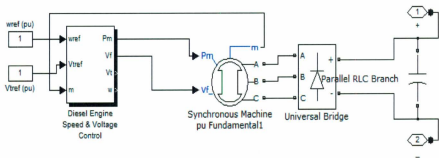


Figure A-9 Diesel generator Subsystem model for the DC system.

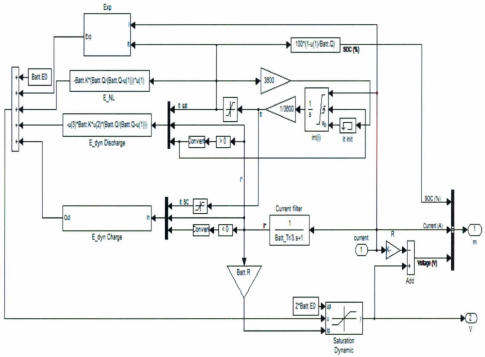


Figure A-10 Battery Subsystem Model.







